

Micro-macro analysis of creep behavior in a multi-pass weld

Dissertation

zur Erlangung des akademischen Grades

Doktoringenieur

(Dr.-Ing.)

von M.Sc. Ivan Lvov

geb. am 20.06.1987 in Kharkiv

genehmigt durch die Fakultät für Maschinenbau
der Otto-von-Guericke-Universität Magdeburg

Gutachter:

apl. Prof. Dr.-Ing. habil. Konstantin Naumenko

Prof. Dr.-Ing. S. Jüttner

Promotionskolloquium am 05.12.2014

Abstract

Currently welding is the most common way to create permanent connections in various constructions, operating at elevated temperatures. Power machinery is one of the industries in which the welds used in particularly critical structural elements. Large parts and components of steam generators, steam and gas turbines and nuclear reactors all operate at high mechanical stress, heat and radiation effects. In the welded joints of these structures creep deformation appears and creep rupture strength of welded joints often determines the strength of the assembly. In welding of nuclear reactor vessels, turbine rotors and heat transfer components in power plants multipass welds are widely used. Different zones of welded joints are subjected to different temperature fields during the process of welding. Furthermore, in multi-pass welding heating and cooling cycles, which occur due to the overlap of the pass beads, form complex microstructure. Metallographic examination reveals the following constituents of the welded joints: Weld Metal, Heat Affected Zone and Parent Material. These zones have different mechanical properties and differ significantly in their size, that is why in creep and long-term strength analysis is necessary to use a multi scaled approach. Current work is devoted to the development of such approach. On the micro scale level creep and damage is modeled in separate areas of multi-pass weld metal, on meso scale level welded joint altogether is modeled, and on the macro scale level analysis of the whole welded structure is performed. Multipass weld metal is structurally heterogeneous and has a distinct anisotropy of the creep properties and long-term strength. For modeling of the weld metal creep-damage model of orthotropic material is used as an equivalent homogeneous medium. The model is based on the hypothesis of the existence of creep potential and uses the concept of effective stress of modern continuum mechanics of creep damage that allows to build a thermodynamically consistent constitutive relations.

Creep-damage model of orthotropic material contains a large number of material parameters. To identify them, a special technique is introduced. It includes a procedure for finding the parameters of the isotropic model for multi-pass weld of separate zones based on the results of physical experiments. Identification of the parameters of the equivalent homogeneous orthotropic material model for weld metal performed numerically. Geometrical model of representative volume comprising a sufficient amount of recurring elements (individual passes) is made, and the finite element method is used to analyze creep and damage processes in it. Through a series of numerical experiments simulating all the necessary basic physical experiments, averaged

parameters of creep-damage model of weld metal are calculated. Reliability of the averaging results was checked by calculations with different numbers of passes in representative volume. Anisotropic creep-damage model is applied to the numerical structural analysis using FEM-based software ABAQUS. These models are incorporated into the finite element code by means of a user-defined material subroutines. As an example of macro scale structural analysis on a welded construction a three-dimensional creep-damage analysis was performed on a welded branched pressure vessel, under a constant inner pressure and an axial boundary loading at uniform temperature.

Zusammenfassung

Derzeit Schweißen ist der häufigste Weg, um dauerhafte Verbindungen in verschiedenen Ausführungen zu erstellen, die bei erhöhten Temperaturen arbeiten. Kraftmaschinen gehören zu einer der Branchen, wo die Schweißnähte in besonders kritischen Strukturelemente verwendet werden. Große Teile und Komponenten von Dampferzeugern, Dampf- und Gas Turbinen und Reaktoren alle arbeiten unter hohen mechanischen Spannung, Wärme und Strahlung Effekte. In der Schweißverbindungen von diesen Strukturen Kriechdeformation wird angezeigt und Zeitstandfestigkeit der Schweißverbindungen beschließt oft die Festigkeit des Aufbaus. In Schweißen des Kernreaktorbehälters, Turbinenrotoren und Wärmeübertragungskomponenten der Kraftwerken werden Mehrlagenschweißnähte weit verbreitet. Die verschiedenen Zonen der Schweißverbindungen werden an unterschiedlichen Temperaturfelder während des Schweißverfahrens unterworfen. Ferner, in Mehrlagenschweißung Heiz- und Kühlzyklen, die durch die Überlappung der Pass Perlen auftreten, bilden komplexe Mikrostruktur. Metallographische Untersuchung zeigt die folgenden Bestandteile des Schweißverbindungen: Schweiß Metall, Wärmeeinflusszone und Grundwerkstoff. Diese Zonen weisen unterschiedliche mechanische Eigenschaften nach und unterscheiden sich deutlich in ihrer Größe, deshalb in Kriech- und langfristige Festigkeitsanalyse notwendig ist, eine Mehr skaliert Ansatz zu verwenden. Aktuelle Arbeit wird der Entwicklung solcher Ansatz gewidmet. Auf der Mikroebene Kriechen und Schädigung werden in getrennten Bereichen des Mehrfachdurchlaufschweißgutes modelliert, auf Mesoebene wird insgesamt die Schweißverbindung modelliert, und auf der Makroebene wird der Analyse der gesamte Schweißkonstruktion ausgeführt. Mehrlagenschweißmetall ist strukturell heterogenen und hat eine unterschiedliche Anisotropie der Kriecheigenschaften und Dauerfestigkeit. Für Modellierung des Schweißmetalles Kriechschädensmodell der orthotropen Material als äquivalenten homogenen Medium verwendet wird. Das Modell basiert sich auf der Hypothes der Existenz des Schleichpotential und verwendet das Konzept der effektive Stress des modernen Kontinuumsmechanik von Kriechschädigung, dass Aufbau der thermodynamisch konsistente konstitutive Beziehungen ermöglicht.

Kriechschädensmodell der orthotropen Material enthält eine große Anzahl von Materialparametern. Um sie zu identifizieren, wird eine spezielle Technik eingeführt. Es enthält ein Verfahren zur Ermittlung der Parameter der isotrope Modell für Mehrlagenschweißnaht der getrennten Zonen, auf Grund die Ergebnisse der physikalischen Experimenten. Identifizierung des Pa-

rameters der äquivalenten homogenen orthotropen Materialmodell wird für Schweißnahtmaterial numerisch durchgeführt. Geometrisches Modell der repräsentative Volumen aus eine ausreichende Menge von wiederkehrenden Elemente (Einzelkarten) besteht, und der Finite-Elemente-Methode wird verwendet, um Kriechen und Schädigungsprozesse in das Model zu analysieren. Durch eine Serie von numerischen Experimenten, die alle notwendige grundlegende physikalische Experimente simulieren, die gemittelte Parameter von Kriechschädensmodell der Schweißmetall berechnet werden. Zuverlässigkeit der gemittelte Ergebnisse wurde durch die Berechnungen mit einer unterschiedlichen Anzahl von Durchläufen in Vertreter Volumen. Anisotrope Kriechschädensmodell wird in die numerische Strukturanalyse mit FEM-basierte Software ABAQUS angewendet. Diese Modelle werden mittels einer benutzerdefinierten Material Subroutinen in die Finite-Elemente-Code integriert. Als Beispiel des Strukturanalyse einer Schweißkonstruktion auf Makroebene, ein dreidimensionaler Kriechschädens Analyse wurde auf einem geschweißten verzweigten Druckbehälter ausgeführt, unter konstantem Innendruck und einer axialen Begrenzungsbelastung bei gleichmäßiger Temperatur.



Contents

1	Introduction	1
1.1	Welded constructions, operating under high temperatures . . .	1
1.2	Modeling creep and damage of metals	6
1.2.1	Isotropic creep-damage	9
1.2.2	Orthotropic creep damage	17
1.3	Experimental investigation of creep and damage of welded joints	18
1.4	Modeling of welded structures operating at high temperatures	25
1.5	A micro-macro approach to continuum mechanics	31
1.6	Scope and Motivation	35
2	Constitutive equations	39
2.1	Creep and damage of isotropic weld zones	39
2.1.1	Coupled creep-damage governing equations	40
2.1.2	Parameter identification technique	41
2.1.3	Parameters in damage evolution equations	42
2.2	Anisotropic creep damage model for multi-pass welds	43
2.2.1	Constitutive equations of anisotropic creep	45
2.2.2	Parameter identification technique	47
2.2.3	Damage evolution equation	48
2.2.4	Parameters of the anisotropic damage model	49
3	Numerical Procedure of Homogenization for Multipass Weld	51
3.1	Parameters of steady state creep equivalent continuum	51
3.1.1	Numerical experiments for in-plane tension	54

3.1.2	Numerical experiments for in-plane shear	58
3.1.3	Numerical experiments for longitudinal tension	60
3.1.4	Numerical experiments for longitudinal shear	62
3.2	Parameters of creep damage equivalent continuum	64
4	Macroscale	69
5	Conclusions	77
	Bibliography	81

CHAPTER

1

Introduction

1.1 Welded constructions, operating under high temperatures

Currently welding is the most used way to create indecomposable joinings in different branches of manufacturing and building. Appliance of welding for composing of the various metal constructional components has several advantages over the other types of connection. They include efficient material usage through the applying of the full cut surface for coupling; lower weight of components joined by welding; reducing the amount of failures and lowering the level of overmeasuring for additional processing when substituting casting with welding. Welding allows applying modern materials in constructions: highly durable and heat resistant steels, light alloys, pure metals etc. Welded joints have higher strength and reliability for constructional elements working under high temperatures. Application of welding has a number of economic advantages: reducing net cost due to lower labor input, lower resource costs and reduced production terms and as a result - high efficiency of manufacturing. High quality of joining and efficient usage of resources provides advantage to the welding for its usage in manufacturing of various metallic constructions, including industrial. In power plant industry welded joints are used in the extremely important constructional elements. Large details and junctions of steam generators, steam and gas turbines, nuclear reactors are all operating under high thermal and mechanical loads, and under influence of radiation. Creep deformation occurs and is observed in weldings of these constructions, and long-term durability of welded joints often defines the life-

time of the construction itself. Steam and gas turbines are high temperature appliances. In modern steam turbines the temperature of steam can reach more than 560°C , and for the stationary gas turbines can exceed 850°C . For steam turbines it is common to use thick walled massive constructions made by casting and forging. Operation at high temperatures requires a broad application of heat-resistant alloy steels in junctions of turbines. The use of welding can dramatically reduce the weight limit of forgings and castings to provide them better quality and lower the necessity of processing large workpieces on unique machines. The most critical turbine constructions are manufactured using welding: rotors, diaphragms, blading, body cylinders and valves and other components of alloy steels. Combined welding is widely used in constructions of dissimilar steels. Accuracy requirements for welded junctions in turbines are the most demanding among other welded construction. The world's leading manufacturers of power turbines in an effort to increase the power of their aggregates are producing welded rotors. In a review of Janssen [4] features of the welded rotor in steam turbines are considered. The combined intermediate and low pressure sections (IP/LP) of turbine rotor design 1.1 are based on the premise that steam pressure and temperature vary along its length.

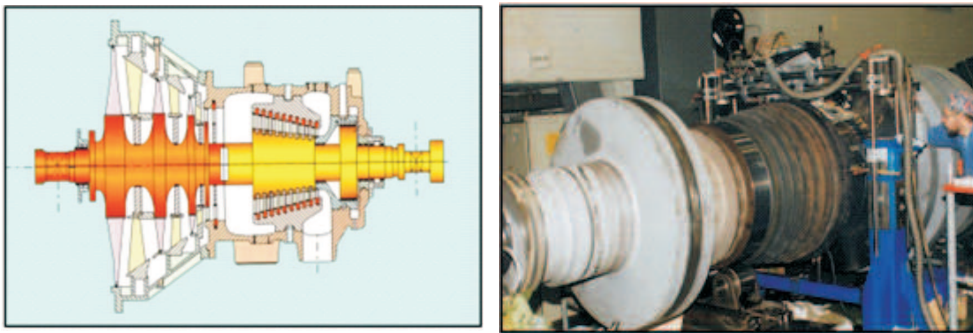


Figure 1.1 Welded rotor: schematic view and picture. After [7]

In the intermediate pressure inlet blades are operating under the temperatures up to 600°C which require to use creep resistant steel alloys, for example widely used CrMoV combinations. However in the low pressure area of the rotor one can say that creep is not of a significant importance. But since the length of the blades is substantial, it's more important to use materials with a high yield. For these applications forging NiCrMoV alloys are suitable. The 3.5% Ni steel forging has become the standard in industry for applications involving low pressure components. The joint welds are made with the multi-pass gas arc welding process in the narrow gap version. This process repre-

sents a variation of the conventional one, where the low weld metal sludge is offset by very narrow gap. Even for the wall of 180 mm thick the gap width in the base area is in the range of 9mm and at the top only 11mm. As an example in junction of thick walled components, this multipass technology is very efficient compared to other welding processes due to the very high depth-width ratio. Two parts of IP/LP turbine rotor are welded in overhead position to increase productivity, Fig. 1.1. Each part of a rotor is processed in a lathe to avoid unnecessary machine waste. After attachment welding, the gap is slowly filled by turning the rotor. After welding, various heat treatment procedures to handle the heat affected zones of IP and LP rotor parts without affecting the strength of both base metals.

Alstom's steam turbines for nuclear power plants are used in 30% of power plants worldwide [7]. Welded rotor technology is a key Alstom turbine innovation, which has been continuously improved over the past 80 years to serve larger and larger units. Welded rotors feature smaller forged pieces (which are welded together), meaning that sourcing and delivery are easier and more secure.

Welded HP and IP turbine rotors large-diameter Alstom's rotors are manufactured by welding together separate smaller forgings. The material designed to last is selected according to the mechanical requirements of the respective rotor section, with special advantages in case of very high temperature applications. A further gain lies in the fact that the stress levels of welded rotors are significantly lower compared to monoblock rotors - in particular during thermal transients. Welded rotors either allow faster start-up and load cycling or consume less life rate than mono-block rotors.

Welded rotors in steam turbines are used in the in power plants in Russia and Ukraine [137]. Weldments rotors LMZ are made of individual forgings and their subsequent welding with circumferential beads. Large rolls are welded from work pieces of relatively small size . High requirements for durability are set for welded joints, working at high temperature. A reliable solidification throughout the thickness of the weld must be ensured. Single-pass welding cannot provide symmetry of welding deformation in a circular seam due to non-uniformity of the transverse shrinkage. Therefore, for the thick-walled compounds multi-pass welding is used. Much attention is paid to a cutting of the joint before welding. One option of cutting for multi-pass weld is shown in 1.2b.

Ukrainian JSC TURBOATOM produces steam turbines for thermal and nuclear power plants with unit capacity that is up to 1000 MW. Welding of the rotors that weight up to 200 tons is performed on an automatic equipment in

narrow arc submerged in flux 1.2a. Much attention is paid to the design of butt parts of a complex rotor and cutting space for multi-pass welding. Developers patented original design of the welded rotor which provides an exclusion of axial tensile stresses in the root of the weld passes and the creation of compressive residual stresses [33]. This leads to the exclusion of evolution of cracks created by hidden defects in welded joints during operation of the rotor, which increases the reliability and durability and as a result security of the whole turbine machinery. When designing the interface of a joint one must take into account the complex technological factors, the conditions of heating and cooling when laying multiple passes, shrinkage and thermal deformation. One option of a butt junction is shown on Fig.1.2.

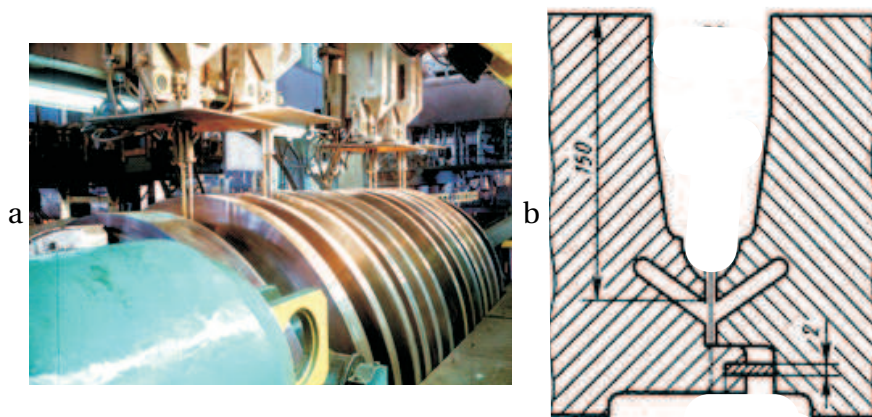


Figure 1.2 Welded rotor (a) and butt joint scheme (b). After [137]

Multipass welds are used in the manufacturing of such crucial constructions as the body of nuclear reactors. A typical example is a unified body of the nuclear reactor WWER-1000 produced in Russia. The body serves to contain the housing internal equipment and the active zone of the reactor core. It is a welded cylindrical pressure vessel with an elliptical bottom and it consists of a flange, area of nozzles, support shell, and cylindrical part and elliptic bottom. The main parts of the reactor pressure vessel are made of steel 15Cr2NiV, the thickness of the cylindrical shell - 192.5 mm, 324.4 tons of body weight. A general view of the reactor and the sketch of the body with welded seams is shown on Fig.1.3.

Additional shell (1) with nozzles (2), a top shell (3) with a flange (4) and the nozzles (2) are manufactured in one piece without welding from an ingot using forging, reeled into cylinder, followed by crimping of nozzles. The support shell (11) adapted for positioning of the reactor vessel is also produced from the ingot with forging and reeling. A cylindrical shell (5) of the core (13) made

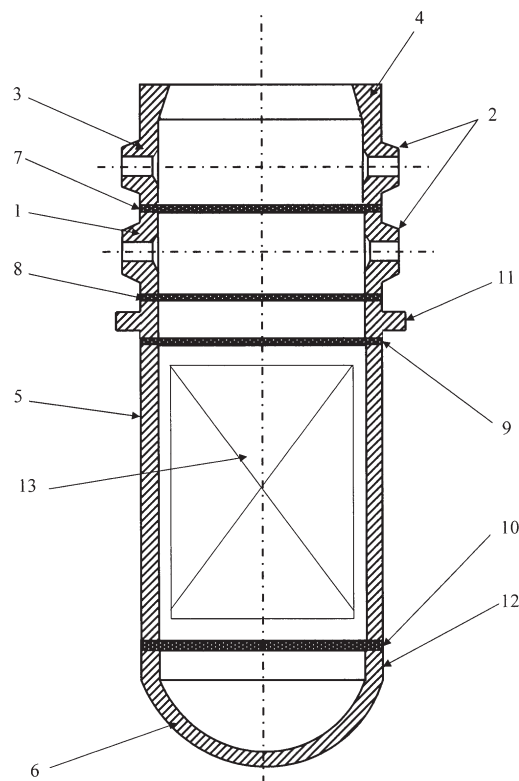


Figure 1.3 Body of the nuclear reactor. After [83]

of solid ingot weighing 200-350 tons by extrusion of an ingot followed reeling, and a convex bottom (6) with a cylindrical ring (12) is made of the solid ingot followed by forging and stamping.

After fabrication of the reactor body parts successively joined by annular welds, wherein the first seal (7) is disposed between the upper shell (3) from the flange (4) and the nozzles (2) and the additional shell (1) with nozzles (2), second (8) joint - between the additional sidewall (1) and the support sidewall (11), third (9) joint - between the support sidewall (11) and shell (5) of the core (13) and fourth (10) joint - between the shell (5) the core and the bottom (6), including in its cylindrical part (12). In the process of welding of circumferential joints of the reactor equipment for welding in narrow-gap cutting is used. Minimum cutting angle for welding on equipment for automatic flux submerged arc welding is 8° . As a result of applying multi-pass welds in the joint area residual stresses occur affecting the long-term strength of the reactor vessel. Study of residual stresses in the reactor vessel has received significant attention [77], [83], [153]. Welded joints during operation of nuclear reactors are subjected to mechanical, thermal and radiation effects. This makes it necessary to monitor their condition while in service [102]. Multi-pass welds

were widely used from the beginning of construction of nuclear power plants. The first nuclear power station in Japan is being constructed at Tokai-mura in Ibaraki Prefecture. The electrical output is 166 MW. The pressure vessel was fabricated using 80 mm and 92 mm thick aluminum steel made in Japan [132].

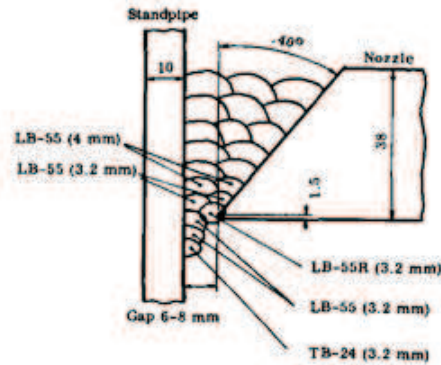


Figure 1.4 Multipass welded vessel. After [132]

Each part of pressure vessel, bottom cap, belt 1, 2, 3, 4 and top cap were prefabricated, then lifted into the reactor building and assembled. Multipass welds were used also for welding of charge and discharge nozzles Fig.1.4. They were installed and welded through the top cap shell of the pressure vessel.

1.2 Modeling creep and damage of metals

In modern solid mechanics theories that feature time dependence (explicitly or implicitly) of constitutive equations gained significant importance. A big number of phenomena that can be explained by taking time into account in the relations between strains and stresses are called creep. The feature of creep theory is that it takes into account the time of slow processes when the inertial forces are negligible. Creep can occur in a variety of materials: metals, plastics, concrete, etc. The physical mechanisms of creep processes can greatly differ in different materials. Even at the macro-level, observations show that different materials require specific ways for a phenomenological description of the creep processes.

In metals creep occurs mainly at high temperatures. For carbon steels creep is observed at temperatures of 450°C and higher. For nickel - chromium austenitic steels with high content of alloying elements allowable creep rate evolves at temperatures up to 600°C.

In constructions with higher operating temperatures in order to avoid a catastrophic accumulation of creep strains commonly cobalt and nickel based super alloys are used.

Creep theory for metals needed for the strength calculations in various industries. Consideration of creep in turbine constructions, nuclear power engineering, chemical engineering, aviation and space technology is particularly relevant.

Constitutive equations in the mechanics of deformable bodies are based on physical experiments. Due to the complexity of the creep processes in metals formulating of the phenomenological models requires a large variety of long and expensive experiments. The simplest and the minimum required are experiments on uniaxial tension of samples at a constant load and temperature. In the course of the experiment is strain is read as a function of time. The corresponding graph is called the creep curve.

Typical creep curve is shown in Fig.1.5 The first part of the curve shows increase of strain over time under constant load, and it is clear that the strain rate decreases in the first section. The first section is primary creep, then the second stage is the steady-state creep at a constant rate, which essentially depends on the applied loading. The third section, called tertiary creep is characterized by an increase in rate and fracture of the sample in the end.

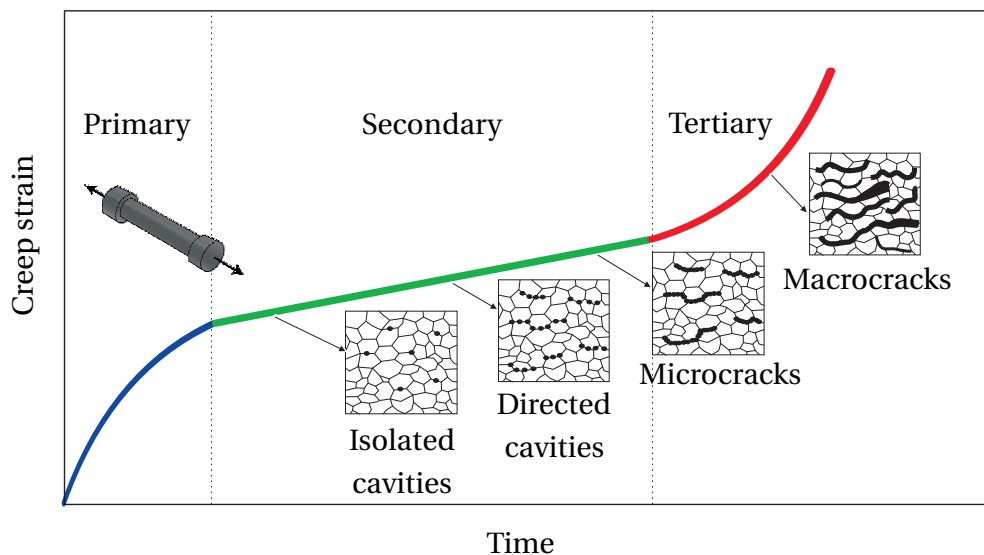


Figure 1.5 Typical creep curve. After [95]

To establish the dependence of strain rate on the stress during the steady-state creep stage one must have creep curves for different values of tensile stress. Also the influence of temperature on the creep behavior requires exper-

imental data for various temperatures. An experiment on simple relaxation is not widely used. Stress relaxation is the process of reduction of stress in the body in time. Classic experiment on simple relaxation is the following: sample is rapidly stretched to strain and fixed in this state. If the temperature is high enough for the material to undergo a process of creep, then eventually a decrease of stress is observed. The first step in formulating a phenomenological creep model is an analytical description of creep curves. This description should approximate with sufficient accuracy the original experimental data. Creep models under uniaxial stress state should adequately predict the behavior of materials under varying stresses and temperatures. To date, significant experience is gained in formulating of the theoretical models for uniaxial creep. A higher number of such models, that have become classical, is contained in the monographs [14], [16], [81], [105], [98] and review papers [94], [87], [99].

The next step in the phenomenological modeling of creep is the formulation of constitutive equations for complex stress states. At this stage, even for isotropic materials some mathematical correctness is required for description of invariant relations using tensor algebra and tensor analysis. In addition, the defining relations for the complex stress state must be physically consistent, comply with the laws of thermodynamics of irreversible processes. And of course, the proposed models should be validated by the experimental data on creep under complex stress state. This chapter of mechanics of deformable bodies gained significant attention and is well presented in literature [36].

Metallographic studies of samples indicate structural changes at different stages of creep. This is the result of a complex of multiple mechanisms that operate independently, such as strain hardening, relaxation, formation of cavities, carbides precipitation and others. Catchall reviews of the extensive literature on power plant steels can be found for example in [36], [78], [69], [113], [139], [143] and [62]. For the operating stress and temperature ranges, the most significant creep mechanism at a microstructural level is the dislocation motion, alongside with the diffusion of vacancies [69]. It is assumed that micro-voids nucleated from cavities due to dislocations, as a result of grain boundary sliding, mainly tend to align orthogonally with respect to the direction of the applied stress [69],[69], subsequently propagating into micro-cracks and then cracks which leads to fracture [95],[124]. The typical pattern of changing of the steel microstructure on different stages of creep is shown in Fig.1.5.

From a practical point of view, the most important result of the analysis of creep in structural elements is the evaluation the long-term strength.

The physical background of the processes occurring in metals and alloys under long-term loading at high temperatures is extremely complex and diverse. Methods of physics of metals allow to identify qualitative features of behavior of materials, but do not allow quantitatively predict evolution of macrostresses and strains over time and to define the time to rupture of components. Aspirations to merge phenomenological approaches with the results of microstructural analysis caused the development of non-classical models of creep and damage of metals. Pioneering work in this direction were made by Rabotnov [111] and Kachanov [61]. They proposed to add scalar internal structural parameters that characterize the degree of damage to the material in constitutive equations. These studies served as a starting point for the formation of a new direction in the mechanics of deformable bodies, which became known as Continuum Damage Mechanics (CDM).

Damage mechanics which at first started as a phenomenological theory has been supplemented by theoretical frameworks of material science, thermodynamics of irreversible processes, computational mechanics, and others. And now has been established as an accurate tool for damage and fracture analysis.

In the phenomenological approach the measure of damage can be considered as a formal structure parameter. However, the development of CDM results in correlation of the structural parameters with changes in microstructure. An example is the classification proposed by Neubauer and Wedel (Table 1.1)

1.2.1 Isotropic creep-damage

For the formulation of constitutive relations, taking into account the influence of damage on the creep process Rabotnov [110] introduced a scalar parameter of damage. Physical interpretation of damage parameter ω was accepted as a ratio of the area of the undamaged cross-section which is not covered with voids to the area of micro-cracks and micro-voids. The constitutive equation for uni-axial stress state should have the form:

$$\dot{\epsilon}^{cr} = \dot{\epsilon}_{cr}(\sigma, \omega), \quad (1.1)$$

Damage process can be described with the evolution equation:

$$\begin{aligned} \dot{\omega} &= \dot{\omega}(\sigma, \omega) \\ \omega|_{t=0} &= 0, \quad \omega|_{t=t^*} = \omega^* = 1 \end{aligned} \quad (1.2)$$

Table 1.1 Neubauer schematic assessment of the microstructure. After [95]

Damage grade	Microstructural conditions	Expected Spent Life Fraction	Expected Residual Life Fraction
0	Normal microstructure for new component	0	1
1	Normal microstructure for service conditions	0.181	0.819
2	Advanced creep load	0.442	0.558
3	Incipient creep damage	0.691	0.309
4	Advanced creep damage	0.889	0.111
5	Structural loosening	1	0

where ω^* is the critical value of the damage parameter for which the material fails. Assuming power laws for creep and damage constitutive equation for isotropic materials can be written as generalization of the Norton-Bailey-Odqvist [14] creep potential and the flow rule:

$$\dot{\epsilon}^{cr} = a \frac{\sigma^n}{(1-\omega)^m} \quad (1.3)$$

And the damage rate can be expressed by:

$$\dot{\omega} = b \frac{\sigma^k}{(1-\omega)^l} \quad (1.4)$$

These equations contain the material dependent parameters a, b, n, m, l, k . Often one can assume $n = m$ and $k = l$. It can be proven that for the damage free state ($\omega = 0$), the first equation results in the power law creep constitutive equation. A convenient interpretation of this type of models was introduced by Lemaitre and Chaboche [57]. They proposed the effective stress concept to formulate constitutive equations for damaged materials based on available constitutive equation for undamaged materials.

The modeling of creep-damage under multi-axial stress states is very important for the adequate prediction of the long term structural behavior. Such a modeling requires the introduction of tensors of stress, strain rate and corre-

sponding creep parts. Constitutive equations of multi-axial creep-damage are based on the concept of the creep potential and the flow rule. To generalize (1.3) and (1.4) to the multi-axial stress states Rabotnov [110] assumed that the creep process is determined by the effective stress tensor. In case of Norton-Bailey-Odqvist creep potential for the damaged material:

$$W(\tilde{\boldsymbol{\sigma}}) = \frac{\sigma_0}{n+1} \left(\frac{\tilde{\sigma}_{\text{vM}}}{\sigma_0} \right)^{n+1} \quad (1.5)$$

$$\sigma_{\text{vM}}^2 = \frac{3}{2} \tilde{\mathbf{s}} \cdot \tilde{\mathbf{s}} \quad (1.6)$$

$$\tilde{\mathbf{s}} = \tilde{\boldsymbol{\sigma}} - \frac{1}{3} \text{tr} \tilde{\boldsymbol{\sigma}} \mathbf{I} \quad (1.7)$$

formed by replacing the actual stress with effective one. Associating flow rule leads to the following equation for the creep strain rate:

$$\dot{\boldsymbol{\epsilon}} = \frac{3}{2} \frac{\dot{\epsilon}_{eq}^{cr}}{\sigma_{\text{vM}}} \mathbf{S} \quad (1.8)$$

where the equivalent creep strain rate have following form:

$$\dot{\epsilon}_{eq}^{cr} = A \left(\frac{\sigma_{\text{vM}}}{1-\omega} \right)^n \quad (1.9)$$

Consistent application of the basic concepts of CDM in the development of creep models for metals is made if works of Hayhurst [44], [41], [43]. These models include specific forms of the constitutive equation for the creep rate tensor and evolution equations for internal state variables. Leckie and Hayhurst [71] proposed to generalize the von Mises type secondary creep equation as follows:

$$\dot{\boldsymbol{\epsilon}}^{cr} = \frac{3}{2} a \left(\frac{\sigma_{\text{vM}}}{1-\omega} \right)^n \frac{\mathbf{s}}{\sigma_{\text{vM}}} \quad (1.10)$$

The next step is the formulation of the damage evolution equation. By analogy with the uni-axial case, the damage rate should have a form:

$$\dot{\omega} = \dot{\omega}(\sigma, \omega) \quad (1.11)$$

The dependence on the stress tensor can be expressed by means of the "damage equivalent stress $\sigma_{eq}^\omega(\boldsymbol{\sigma})$ " which allows to compare tertiary creep and long term strength under different stress states. With the damage equivalent stress, the uniaxial equation (1.4) can be generalized as follows:

$$\dot{\omega} = b \frac{(\sigma_{eq}^\omega)^k}{(1-\omega)^l}, \quad (1.12)$$

where the material constants a , b , n , k and l can be identified from uni-axial creep curves. In order to find a suitable expression for the damage equivalent stress, the data from multi-axial creep tests up to rupture are required. In general $\sigma_{eq}^\omega(\boldsymbol{\sigma})$ can be formulated in terms of three invariants of the stress tensor. One variant of the damage equivalent stress was proposed by Leckie and Hayhurst in [71]:

$$\sigma_{eq}^\omega = \alpha \sigma_I + (1-\alpha) \sigma_{vM} \quad (1.13)$$

Leckie and Hayhurst model reflects the fact that damage is not developing during compression. This is done by accepting following restrictions:

$$\sigma_{eq}^\omega = \langle \alpha \sigma_I + (1-\alpha) \sigma_{vM} \rangle, \quad (1.14)$$

where $\langle \sigma_{eq}^\omega \rangle = \sigma_{eq}^\omega$ when $\sigma_{eq}^\omega > 0$ and $\langle \sigma_{eq}^\omega \rangle = 0$ for $\sigma_{eq}^\omega \leq 0$

In (1.10) and (1.11), there is only one damage variable and no consideration is given to the physical nature of damage parameter. However, studies on metal physics and void growth theory show that the deterioration of high temperature material results from different mechanisms, e.g. grain boundary sliding, ductile void growth, diffusion of vacancies along the boundary and carbide precipitate coarsening, etc. To take into consideration the effects of these different damage mechanisms, multi-variable constitutive equations were thus developed, which can be described by the following general form [47]:

$$\begin{aligned} \dot{\varepsilon}_{ij} &= f(\sigma_{ij}, \omega_1, \omega_2, \dots, \omega_n, T) \\ \dot{\omega}_1 &= g_1(\sigma_{ij}, \omega_1, \omega_2, \dots, \omega_n, T) \\ \dot{\omega}_2 &= g_2(\sigma_{ij}, \omega_1, \omega_2, \dots, \omega_n, T) \\ &\cdot \\ &\cdot \\ \dot{\omega}_n &= g_n(\sigma_{ij}, \omega_1, \omega_2, \dots, \omega_n, T) \end{aligned} \quad (1.15)$$

where ε_{ij} is the creep strain tensor, σ_{ij} the stress tensor; ω_i ($i = 1, 2, \dots, n$) is the i -th damage variable; and g_i ($i = 1, 2, \dots, n$) is the i -th damage rate function. By selecting the appropriate strain rate function f and damage rate function g_i , the creep behavior of materials can be accurately described.

Further investigations were made in [72], [49], [24] and, who introduced a method to derive constitutive equations based on the framework of thermodynamics of irreversible processes and the principle of equivalence of strains.

In addition, tensor representations of damage variables were introduced in order to take damage-induced material anisotropy into account [26], [25], [87], [88], [67]. The rapid increase of interest and development in this field is observed from a large number of articles, monographs and reviews, for example by [45],[63], [60], [68], [74], [73], [126], [76].

Anisotropic damage of isotropic materials Because of its microscopic nature damage has, in general, an anisotropic character even if the material is originally isotropic. The orientation of fissures and their length result in an anisotropic macroscopic behavior. It is well known that the creep process of a metal in its tertiary stage and the ensuing creep rupture is accompanied by the formation of microscopic cracks on the grain boundaries and that damage accumulation occurs. In some cases voids are caused by a given stress history and, therefore, they are distributed anisotropically among the grain boundaries. Thus, the mechanical behavior will be anisotropic and it is necessary to consider this kind of anisotropy by introducing appropriately defined anisotropic damage tensors into constitutive equations. Problems of creep damage were investigated by many authors, for instance by Odquist and Hult, Martin and Leckie, Hayhurst and Leckie, Dyson and McLean, Parmar and Mellor, Millor and Langdon, and many other scientists.

Murakami and Ohno [91], [87] described the damage state by means of a second rank symmetric damage tensor specified by the three dimensional cavity-area density, and developed a continuum theory of creep and creep-damage of metals and alloys. The stress tensor \mathbf{s} is magnified to the following effective stress tensor:

$$\tilde{\boldsymbol{\sigma}} = \frac{1}{2}(\boldsymbol{\sigma} \cdot \boldsymbol{\Phi} + \boldsymbol{\Phi} \cdot \boldsymbol{\sigma}) \quad (1.16)$$

with $\boldsymbol{\Phi} = [\mathbf{I} - \boldsymbol{\omega}]^{-1}$

Above, \mathbf{I} is a second rank identity tensor and $\boldsymbol{\omega}$ is a second rank symmetric damage tensor. The evolution equation the damage tensor can be formulated as follows:

$$\dot{\boldsymbol{\omega}} = \mathbf{B} \left[\sigma_{eq}^{\boldsymbol{\omega}} \right]^l [\text{tr}(\boldsymbol{\Phi} \cdot \mathbf{n}_I \otimes \mathbf{n}_I)]^{k-1} \mathbf{n}_I \otimes \mathbf{n}_I \quad (1.17)$$

The creep constitutive equation on base Norton's law with respect to the damage-induced anisotropy may be written as proposed in [94] in following form:

$$\dot{\boldsymbol{\epsilon}} = \frac{3}{2} \frac{\dot{\boldsymbol{\epsilon}}_{eq}^{cr}}{\sigma_{vM}} \mathbf{S} \quad (1.18)$$

$$\dot{\boldsymbol{\epsilon}}_{eq}^{cr} = A(\hat{\sigma}_{vM})^n \quad (1.19)$$

where the modified von Mises effective stress is:

$$\sigma_{\text{vM}}^2 = \frac{3}{2} \tilde{\mathbf{s}} \cdot \tilde{\mathbf{s}} \quad (1.20)$$

One possibility of anisotropic creep damage model during creep of isotropic materials with the introduction of 4th order tensor is considered in [89]. Comparison between theories of anisotropic damage with using one fourth order damage tensor and two fourth order damage tensors is also described. It is stated, the essential difference between the above two anisotropic damage theories exists in the definition of the effective stresses and the equivalence hypotheses between damaged and undamaged materials. Systematic experimental results applicable to the validation of the above anisotropic creep damage theories have been hardly available. Series of model tests of Murakami and Imaizumi [90] shown that significant difference was not observed between two anisotropic damage theories. A more flexible model of anisotropic damage considered in [92].

Discussion of a local approach to the analysis of crack growth in a creep-orthotropic damaged material when the principal axes of the stress and damage tensors coincide (no rotation allowed) is due to [92]. Assuming that: (a) the damage rate is described by the combined net area reduction on the planes perpendicular to the direction \mathbf{n}_I of the maximum principal stress σ_I and the isotropic area reduction, the authors postulated the following form of the damage evolution equation:

$$\dot{\boldsymbol{\omega}} = B f(\boldsymbol{\sigma}) \text{tr}(\mathbf{I} - \boldsymbol{\omega})^{-1} (\mathbf{n}_I \otimes \mathbf{n}_I)^l [(1 - \eta) \mathbf{I} + \eta \mathbf{n}^1 \otimes \mathbf{n}^1], \quad (1.21)$$

where $f(\boldsymbol{\sigma}) = \xi \sigma_I + \zeta \sigma_{\text{vM}} + \frac{1-\xi-\zeta}{3} \text{tr}(\boldsymbol{\sigma})$ and B, ξ, ζ, η, k and l are material properties. Let us mention that, for particular cases of $\eta = 0$ and $\eta = 1$ (1.21) reduces to purely isotropic damage evolution. For $\eta = 1$ the damage growth is transversally isotropic due to micro crack growth in planes perpendicular to the maximum tensile stress, respectively. For $0 < \eta < 1$ a mixed isotropic/maximum principal stress controlled damage growth mechanism occurs. A combined the McVetty and the Mises type creep flow rules together with the strain hardening hypothesis was selected as the isotropic constitutive law:

$$\dot{\boldsymbol{\epsilon}}^c = \frac{3}{2} \left[A_1 \sigma_{eq}^{n_1-1} \alpha \exp(-\alpha t) \mathbf{S} + A_2 \tilde{\sigma}_{eq}^{n_2-1} \tilde{\mathbf{S}} \right] \quad (1.22)$$

where:

$$\sigma_I = \max[\sigma_i] \quad (1.23)$$

$$\sigma_{\text{vM}}^2 = \frac{3}{2} \mathbf{S} \cdot \mathbf{S} \quad (1.24)$$

$$\dot{\boldsymbol{\varepsilon}}_{eq}^c = \sqrt{\frac{2}{3} \dot{\boldsymbol{\varepsilon}}^c \cdot \dot{\boldsymbol{\varepsilon}}^c} \quad (1.25)$$

$$\tilde{\boldsymbol{\sigma}} = \frac{1}{2} [\boldsymbol{\sigma} \cdot (1 - \boldsymbol{\omega})^{-1} + (1 - \boldsymbol{\omega})^{-1} \cdot \boldsymbol{\sigma}] \quad (1.26)$$

$$\tilde{\boldsymbol{\sigma}}_{eq}^2 = \frac{3}{2} \tilde{\mathbf{S}} \cdot \tilde{\mathbf{S}} \quad (1.27)$$

$$\mathbf{S} = \boldsymbol{\sigma} - \frac{1}{3} (\text{tr} \boldsymbol{\sigma}) \mathbf{I} \quad \tilde{\mathbf{S}} = \tilde{\boldsymbol{\sigma}} - \frac{1}{3} (\text{tr} \tilde{\boldsymbol{\sigma}}) \mathbf{I} \quad (1.28)$$

whereas $A_1, A_2, n_1, n_2, \alpha$ are material constants.

Good agreement with the experimental data is achieved using the Chaboche-type model [27] for the analysis of anisotropic damage of initially isotropic materials. In the study [108] such a model is used in finite element analysis of circumferentially notched bar under creep loads. In the damage model, a second-order symmetric tensor is chosen as the thermodynamic state variable describing the anisotropic damage. It was assumed that the tensile principal stresses are responsible for the damage growth, and the anisotropy of the damage evolution depends on the principal directions of the stress and damage tensor. The damage law was established within the framework of thermodynamics. According to the effective stress concept of CDM, the suggested anisotropic damage model is coupled with the unified model proposed by Chaboche, by replacing the stress tensor by an effective stress tensor. The resulting creep- damage model includes flow rule:

$$\dot{\boldsymbol{\varepsilon}}^i = \frac{3}{2} \dot{p} \frac{\tilde{\mathbf{S}} - \mathbf{X}}{J_2(\tilde{\mathbf{S}} - \mathbf{X})} \quad (1.29)$$

$$\dot{p} = \left\langle \frac{J_2(\tilde{\mathbf{S}} - \mathbf{X}) - R_y}{K} \right\rangle^n, \quad (1.30)$$

the isotropic hardening rule:

$$\dot{R} = b(R_\infty - R) \dot{p}, \quad R(p=0) = R_0, \quad (1.31)$$

the effective stress:

$$\tilde{\mathbf{S}} = (\mathbf{I} - \mathbf{B})^{-\frac{1}{2}} \cdot \mathbf{S} \cdot (\mathbf{I} - \mathbf{B})^{-\frac{1}{2}}, \quad (1.32)$$

and the damage evolution law:

$$\dot{\boldsymbol{\omega}} = (\beta \mathbf{I} \otimes \mathbf{I} + (1 - \beta) \mathbf{I}) \cdot \left\langle \frac{\hat{\mathbf{S}}}{B_0} \right\rangle^m \quad (1.33)$$

$$\hat{\mathbf{S}} = \sum_{i=1}^3 \hat{\sigma}_i \hat{\mathbf{n}}_i^\sigma \otimes \hat{\mathbf{n}}_i^\sigma. \quad (1.34)$$

Special cases are isotropic materials with different properties in tension and compression. A creep damage model for initially isotropic materials with different properties in tension and compression was designed in [17], [18].

Anisotropy of creep mechanical properties shows itself much more significant in metals than elastic or elastic-plastic characteristics [110]. Samples cut from the rolling or forging material usually exhibit quite small anisotropy of the elastic properties. Anisotropy of the standard characteristics of plasticity show more noticeable difference in yield strength for samples of rolled steel, cut along and across the rolling direction, may be ten to fifteen percent. The discrepancy in the creep curves at the same stress and the same temperature can sometimes be huge, elongation at the same time moment can differ in two or three times depending on the orientation of the sample. When an anisotropic material is subject to creep conditions and a complex state of stress, an anisotropic creep damage behavior is observed. Some general considerations on the damage modeling of initially anisotropic media are given in the review of [15]. Because of its microscopic nature, damage generally has an anisotropic character even if the material was originally isotropic. The fissure orientation and length cause anisotropic macroscopic behavior. Therefore, damage in an isotropic or anisotropic material which is in a state of multiaxial stress can only be described in a tensorial form. When generalizing the uniaxial concept, constitutive equations for strain rates \mathbf{d}^p and anisotropic growth equations are expressed as the tensor-valued functions

$$\mathbf{d}^p = \mathbf{f}(\boldsymbol{\sigma}, \boldsymbol{\omega}), \quad \check{\boldsymbol{\omega}} = \mathbf{g}(\boldsymbol{\sigma}, \boldsymbol{\omega}) \quad (1.35)$$

Respectively, where $\check{(\)}$ denotes the Jaumann derivative, $\boldsymbol{\sigma}$ is a Cauchy stress tensor and $\boldsymbol{\omega}$ represents an appropriately defined damage tensor. Damage tensors have been constructed, for instance, in [94], where it has been proven that damage accumulating in the process of creep can be expressed through a symmetric tensor of rank two. The symmetric tensor-valued functions are valid for an isotropic material in anisotropic damage state. Furthermore, one must distinguish between anisotropic damage growth and the initial anisotropy resulting from a forming process, for instance, rolling. Strain rate constitutive equations and anisotropic damage growth equations are then represented by expressions such as:

$$\mathbf{d}^p = \mathbf{f}(\boldsymbol{\sigma}, \boldsymbol{\omega}; \mathbf{A}) \quad (1.36)$$

$$\check{\boldsymbol{\omega}} = \mathbf{g}(\boldsymbol{\sigma}, \boldsymbol{\omega}; \mathbf{A}), \quad (1.37)$$

where \mathbf{A} is a fourth order constitutive tensor characterizing the anisotropy due to, for example, rolling, i.e. the anisotropy of the material in its undamaged state.

A general representation of and similarly of is given through a linear combination

$$\mathbf{d}^p = \sum_{\alpha} \varphi_{\alpha} \mathbf{G}_{\alpha} \quad (1.38)$$

Where \mathbf{G} are symmetric tensor generators of rank two involving the argument tensors $\boldsymbol{\sigma}, \boldsymbol{\omega}, \mathbf{A}$.

1.2.2 Orthotropic creep damage

Damage anisotropy in creep conditions under nonproportional high temperature loadings requires a modification of the simple scalar description of the damage growth rule and the creep-damage coupling in constitutive equations. The complexity of the description depends on the question whether the principal direction of the stress tensor are constant or rotate with respect to material particles, as examined for example by [71].

Consider first a simpler case when principal directions of the stress and damage tensors $\boldsymbol{\sigma}, \mathbf{D}$ coincide and do not change with time. In such case the orthotropic theory of brittle damage coupled with the similarity of deviators of principal creep strain rates $\dot{\boldsymbol{\epsilon}}^c$ and either the principal stress deviator \mathbf{s} or the principal effective stress deviator $\tilde{\mathbf{s}}$ are applicable [60] [125]. When formulated in the material axes of an orthotropic material, there is no coupling effect between normal stress and shear strain. Therefore, in their principal direction the stress and damage tensors are:

$$[\boldsymbol{\sigma}] = \begin{bmatrix} \sigma_1 & 0 & 0 \\ 0 & \sigma_2 & 0 \\ 0 & 0 & \sigma_3 \end{bmatrix} \quad (1.39)$$

$$[\mathbf{D}] = \begin{bmatrix} D_1 & 0 & 0 \\ 0 & D_2 & 0 \\ 0 & 0 & D_3 \end{bmatrix} \quad (1.40)$$

and the orthotropic creep-damage growth rule holds [125]:

$$\dot{D}_i = \left(\frac{\sigma_i}{A_i} \right)^{r_i} (1 - D_i)^{-k_i} \quad (1.41)$$

The damage effective stress is given by:

$$\tilde{\boldsymbol{\sigma}} = \frac{1}{2} [\boldsymbol{\sigma} \cdot (1 - \mathbf{D})^{-1} + (1 - \mathbf{D})^{-1} \cdot \boldsymbol{\sigma}] \quad (1.42)$$

Hence, when principal stress and damage axes coincide and $D_{12} = D_{23} = D_{31} = 0$, $\sigma_{12} = \sigma_{23} = \sigma_{31} = 0$, $\tilde{\sigma}_{12} = \tilde{\sigma}_{23} = \tilde{\sigma}_{31} = 0$, the general matrix representation of the transformation:

$$\tilde{\sigma}_{ij} = M_{ijkl}(\hat{D}_{ijkl})\sigma_{kl} \quad (1.43)$$

reduces to the form:

$$\begin{Bmatrix} \tilde{\sigma}_1 \\ \tilde{\sigma}_2 \\ \tilde{\sigma}_3 \end{Bmatrix} = \begin{bmatrix} \frac{1}{1-D_1} & 0 & 0 \\ 0 & \frac{1}{1-D_2} & 0 \\ 0 & 0 & \frac{1}{1-D_3} \end{bmatrix} \begin{Bmatrix} \sigma_1 \\ \sigma_2 \\ \sigma_3 \end{Bmatrix} \quad (1.44)$$

Note that when $\boldsymbol{\sigma}$, $\tilde{\boldsymbol{\sigma}}$ and \mathbf{D} are coaxial in their principal direction, all different matrix representations of the damage effect tensor $\mathbf{M}(D_1, D_2, D_3)$, coincide as well [126]. Creep damage model for transversally isotropic materials was also introduced in [93], [94].

1.3 Experimental investigation of creep and damage of welded joints

Welded components in power plants and chemical plants often operate at temperatures that are high enough for creep deformation to occur. Under these conditions, the rate of accumulation of damage may be significantly higher in the weld region than elsewhere. A typical weld in a component consists of parent material, heat-affected zone and weld metal. The variety of them in terms of heat sources, geometry types and even types of environment where they can be performed made welding the most commonly used type of joining engineering elements made of metals. However even welding processes themselves may affect the joined or "base" materials when forming melted metal region during laying the weld pass. This will lead to changes in the microstructure of base metals and create so called heat-affected zones. Non trivial geometry of welded joints and different number of weld passes can make heat-affected zone (HAZ) even more complicated. A typical weld in a component consists of parent material, heat affected zone and a weld metal. The weld and parent material can have the same or different composition. But even for welds joined by the weld metals with the same composition as the parent materials, the creep properties in parent, heat-affected zone and weld materials will be different. Thus, the weldments are highly complex heterogeneous structures (Fig.1.6).

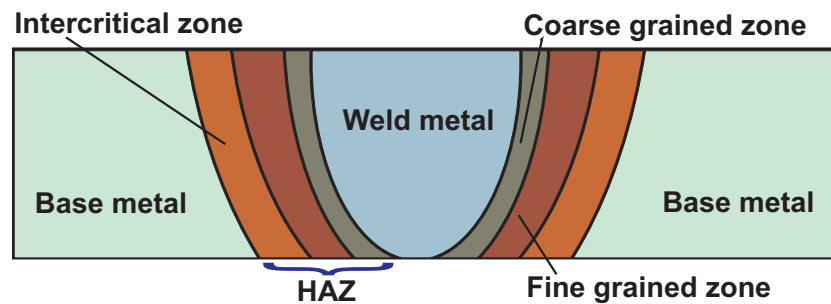


Figure 1.6 Typical structure of the welded joint. After [34]

Experimental study of the P91 steel and microstructure of the weld regions, used in the current work, is made in [32]. On figure 1.7 one can see the optical micrographs of the different welded joint zones.

Moreover, in the case of multipass welds, the weld material is also inhomogeneous. It consists of overlapping weld beads that will create specific heat affected zones within the weld metal because of cooling and heating from the next pass. A single weld bead generally consists of a columnar solidification structure. However in multipass weld when the further bed is laid over the previous one, part of it will be recrystallized and will create coarse and fine grained structure [34].

Complexity of the structure of welded joints makes it useful to consider their properties with complementary methods. The combination of mechanical testing of samples with macroscopic metallographic microstructure research gives an opportunity to develop more adequate models of creep and damage of welded joints. A typical example of this experimental study is the work [140].

Microstructural changes that take place in during the process of welding are in a direct dependence to the macroscopic properties of the metal [23] [130]. Influence of the grain size of the martensitic steels on the creep properties is investigated in [115]. It was observed, that the coarser the microstructure is, the longer the time to rupture, Fig. 1.8.

High temperature creep flow and damage properties of 9Cr1MoNbV steel and weldment are investigated on a circumferentially welded joint of two pipes of 295mm in outer diameter and 55mm in thickness. Both creep tests on specimens containing only base metal (far from the welding area) and on cross-weld specimens with all microstructural states: weld metal, base metal and heat-affected zone in the gauge area were performed.

To separately determine the steady-state creep flow properties of the weld metal, creep tests were also carried out on a plate specimen. This specimen

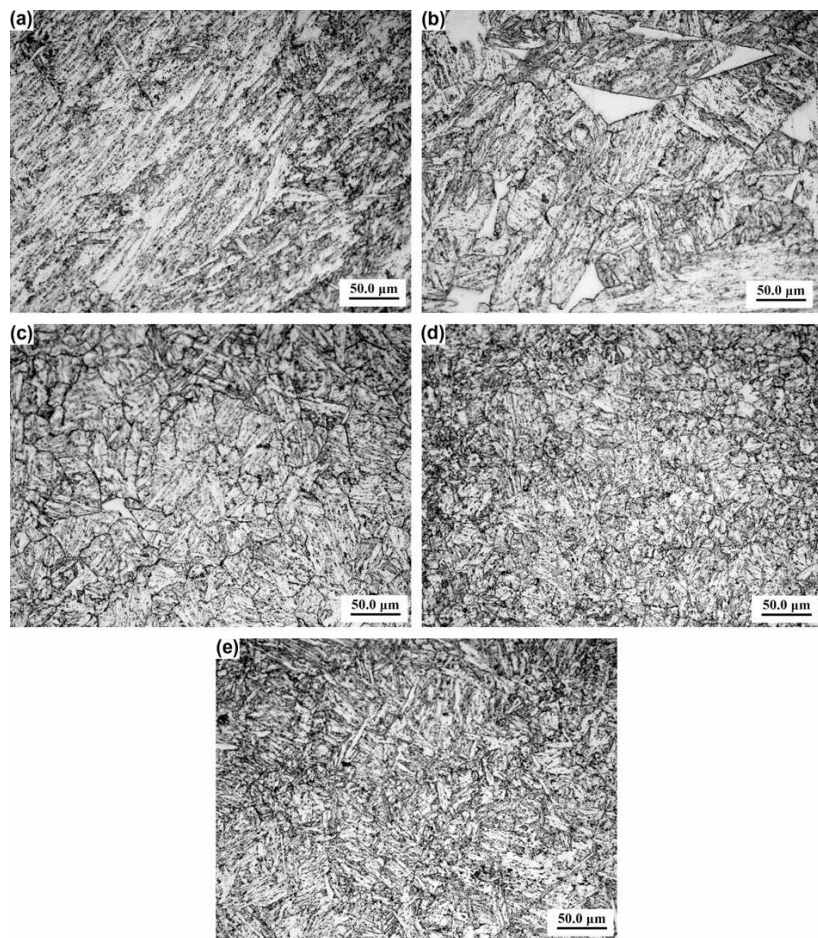


Figure 1.7 Optical micrographs of the pre-creep welded joint (a) welded metal, (b) ICHAZ, (c) CGHAZ, (d) FGHAZ, and (e) base metal. After [32]

was machined from the weldment in the largest welded area so that all the gauge length was made of weld metal. Experimental results indicate that the steady-state creep rate substantially different in different areas of the joint. The steady-state strain rate, $\dot{\epsilon}$ was represented by simple regression analysis of the steady-state creep strain rate data as a function of stress, using a Norton power law

$$\dot{\epsilon} = B\sigma^n \quad (1.45)$$

Parameters for different creep zones are presented in Table 1.2.

HAZ dimensions were established by metallographic observations. Microstructures were examined by light optical and scanning electron microscope. The base metal is a tempered martensitic stainless steel. After the part

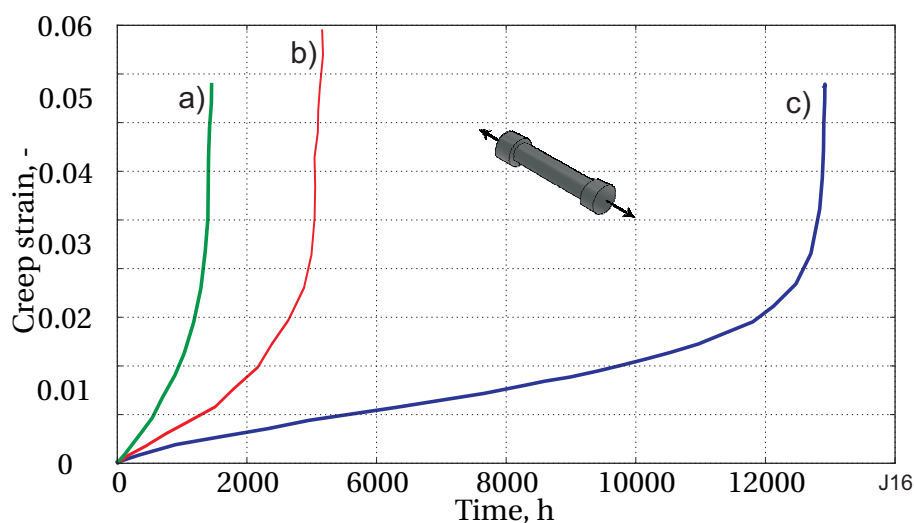


Figure 1.8 Creep curves for martensitic steel with grain size of (a) $0.58 \mu\text{m}$, (b) $0.90 \mu\text{m}$, (c) $1.46 \mu\text{m}$. After [115]

Table 1.2 Norton power law parameters for base metal and HAZ at 625 C. After [84]

	$B(\text{h}^{-1}\text{MPa}^{-n})$	n
Base metal	$3.03 \cdot 10^{-22}$	8.1
Weldment	$2.08 \cdot 10^{-17}$	6
HAZ	$3.23 \cdot 10^{-16}$	5.8

weld heat treatment, the weld metal exhibits a microstructure very similar to that of the base metal. Major microstructural changes were evidenced in the HAZ as local heating of the base metal led to phase transformations. The HAZ is approximately a 4-5mm wide area that is usually divided into three main areas from the weld to the base metal (the coarse grained heat-affected zone, The coarse grained heat-affected zone, the intercritical heat-affected zone). The typical picture of the changes in the microstructure of HAZ is shown in Fig.1.9

Metallurgical investigations have shown that the loss of creep strength can be attributed to microstructural changes such as carbide coarsening and extensive lath recovery that occur in the HAZ during welding. A similar method for the experimental study of creep and long-term strength for various steels used in [6],[31],[56], [103],[116],[117],[140]. To develop methods of non-destructive testing of welded joints the correlation between the hardness of the different zones of the welded joint and the characteristics of creep and

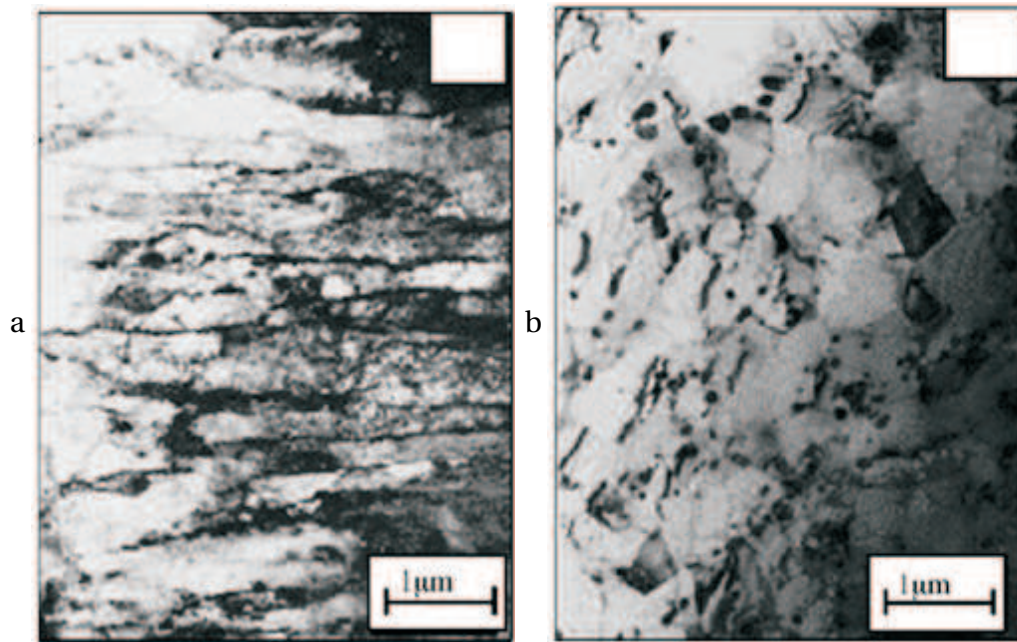


Figure 1.9 Microstructural changes in the heat-affected zone of the welded joint: a) observation of base metal; b) observation of the HAZ. After [116]

long-term strength is investigated in [22],[85]. For a more detailed analysis of the creep properties the HAZ and special specimens are used [37],[84]. Notch area is chosen sufficiently small to ensure that it is entirely within the HAZ.

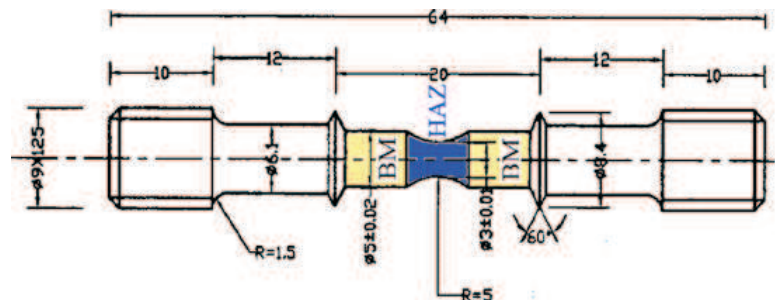


Figure 1.10 U-notched creep specimen for the identification of the HAZ parameters. After [37]

Making different samples for creep tests of individual zones of the welded joint is very complicated task, especially for a detailed study of HAZ. To overcome these difficulties in [136] a local deformation measuring technique is developed to determine the creep properties of weldment constituents in light of optical fiber marking and remote monitoring technique. The measuring

system consists from quartz optical fibers, advanced long distant microscope and computer image analysis techniques.

The selected quartz optical fiber has an outer diameter of 140 μm and a core diameter of 110 μm . It is possible to arrange 3-4 fibers in a region as small as 1 mm. The fibers can thus be attached to the narrow regions of weld metal and HAZ of a weldment. This method is applied to the creep deformation measurement of cross-weld specimens [135]. For thick cross sections multi-pass welding is usually performed, where many stringer beads are deposited in a defined sequence. As a result of heating and cooling cycles during the welding process, the complex microstructure of the weld metal is formed. One of the consequences of these processes is that in addition to heterogeneity, anisotropy of material mechanical properties shows itself. Experimental study of the anisotropy of the material requires experiments on samples cut in different directions. Whilst there are a number of studies of the creep behavior of weldments, there are very few concerning the anisotropy of the creep behavior of the weld metal itself. In [149] creep tests on welds of 308 stainless steel deposited on a 304 stainless steel parent were conducted. Samples were taken with the stress axis both longitudinal and transverse to the welding direction. They were able to show clear differences between the creep behavior in the two orientations, with the longitudinal specimens exhibiting a higher creep strain rate and larger strain to failure than the transverse specimens.

Consistent study of the anisotropy of the properties of creep and long-term strength for the weld metal 9CrMoNbV are performed in [54]. Uniaxial creep, creep rupture and Bridgman notched bar creep rupture tests were performed at 650°C, using test specimens removed from two directions, i.e. in the longitudinal and transverse directions, with respect to the welding direction, from a weld pad. From the test results obtained, the differences in the creep ductility, minimum creep strain rate, rupture strength and notch strength sensitivity behavior of the material, in the two directions, are identified. Material constants, in creep and damage constitutive equations, were obtained from the test data. Metallurgical studies were conducted with the aim of gaining an understanding of the difference in the mechanisms in the two directions which cause the anisotropy. The results obtained clearly indicate that anisotropy of the weld metal exists and this will need to be considered in numerical modeling.

The uniaxial creep curves obtained from the tests in the transverse and longitudinal directions are presented in Fig.1.11 a and Fig.1.11 b, respectively, from which it can be seen that there are significant differences in the creep deformation behavior.

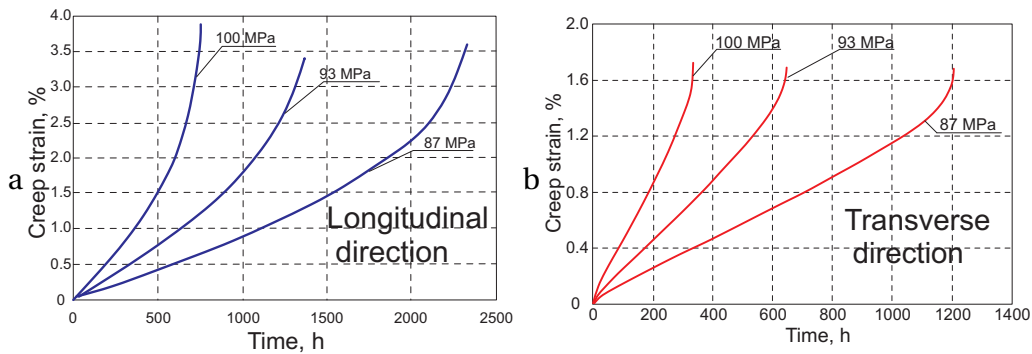


Figure 1.11 Uniaxial creep strain curves of the 9CrMoNbV weld metal at 650°C. After [93]

Results show that the creep strain vs. time curves significantly differ for specimens removed from the weld metal in the longitudinal (welding) direction and the transverse direction. Furthermore, different types of damage were observed for the longitudinal and the transverse specimen. Similar experiments have been performed in [131] on the directionally-solidified Ni-based superalloy commonly used for first and second row blades and vanes of gas turbines. During the process of directed crystallization in the manufacturing of blanks the anisotropy of mechanical properties is formed in them. This situation is similar in its effects to the processes occurring in manufacturing multipass welds.

The process of fusion welding is necessary for the construction and repair of steel pipelines in power plants. Welding involves high thermal cycles which are responsible for the microstructural evolution of the different metallurgical zones within the weld and heat affected zone and the mechanical properties which are related to its temperature history during welding. Let us consider possible failure modes in welded pipes under typical operating conditions. The cracking of welded joints is usually classified according to the position of the crack. Type I and Type II cracking occur within the weld metal, either growing outside the weld metal to HAZ or staying within. Type III cracking occurs in the coarse grained region of the HAZ. Type IV form of cracking stands for an enhanced rate of creep void formation in the fine grained and intercritically HAZ of the weld, leading to failure before the lifetime prediction of the welded component [32]. A schematic representation of the long term failure modes in ferritic welds is shown in Fig.1.12 for CrMoV welds; similar results would be expected for other ferritic steels [56].

The microstructure at each location of the heat affected zone is closely related to the temperature-time characteristics of the welding process. In ad-

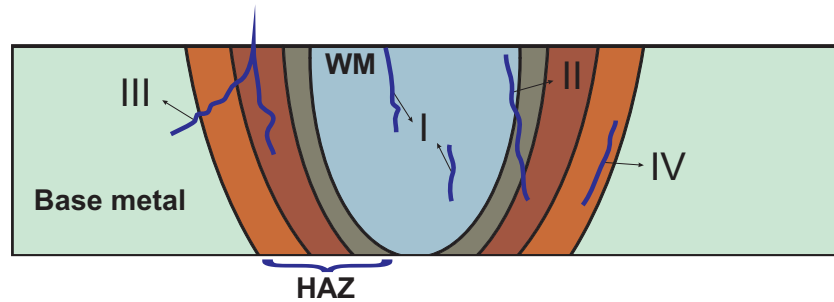


Figure 1.12 Cracking types in welds. After [54]

dition, geometrical changes occur due to the difference in temperature and the generated residual stresses during welding. Furthermore, residual stresses and microstructural changes influence the reduction in corrosion resistance of the material. Various chemical and physical processes also occur especially in the melted zone region during welding.

1.4 Modeling of welded structures operating at high temperatures

Mathematical modeling of welded joints is caused by the necessity of designing welded structures with guaranteed parameters of long durability and reliability.

The first step in such a simulation is the development of equations of state for the different zones of the weld. Because the weld structure is inhomogeneous, and some have small area size, difficulties arise in the procedure of experiments. It is practically impossible to make samples of the weld zone with homogeneous mechanical properties. In particular this applies to HAZ, which, despite its small size, may significantly affect the creep and rupture strength of welded joints. This features of the welds leads to the necessity to promote methods of mathematical modeling in the early stages of analysis of experimental results. In [34] to identify the creep parameters in the Norton law for HAZ, physical experiments for the base metal, weld metal and welded joint are combined with finite-element modeling of creep specimen. Respectively, Fig.1.13 shows comparison of specimen creep deformation between experiment, and bi-material FE calculations with the width of HAZ= 4 and 2mm.

Bimaterial FE calculations gave useful information about constraint effects and especially allowed to determine the value of HAZ length well representing constraining effects in 9Cr1MoNbV steel weldments. It was also

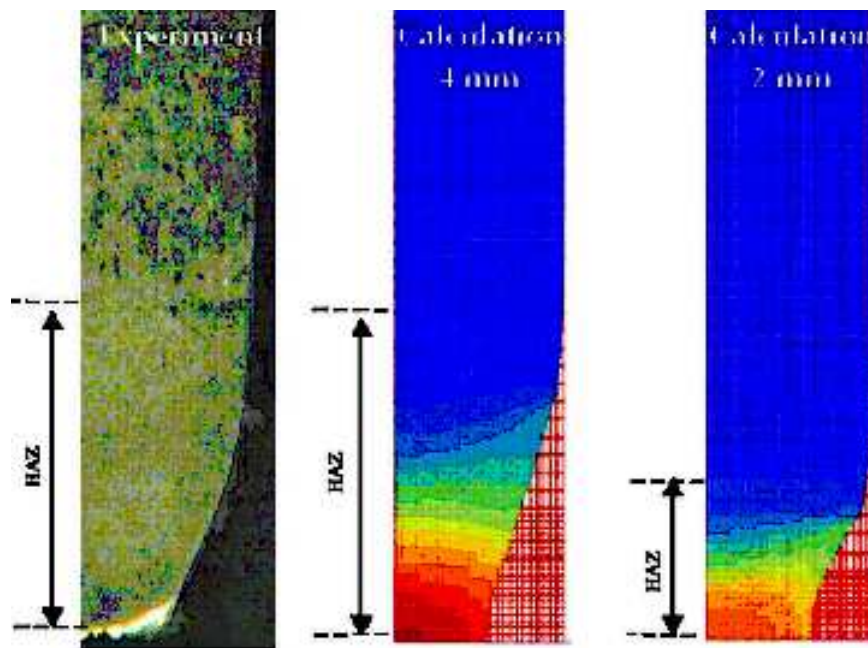


Figure 1.13 Weldment cut outs. After [34]

shown that the lower creep strength of the HAZ can mainly be attributed to its creep flow properties, whereas its intrinsic ductility is similar to that of the base metal.

A similar combination of physical experiments with numerical simulations used in [84]. CAST3M finite element modeling (FEM) software is used to model the creep behavior and damage mechanisms of modified 9Cr1Mo steel weldments. Experimental creep results are used to identify parameters for a three-phase (base metal, welded metal and heat affected zone) creep models that includes the effect of damage. The influence of the thickness of the HAZ has been investigated, as it may vary according to the welding process. Three values of the thickness of the HAZ have been computed for a wide range of stresses.

Finite element modeling is applied in [13], [134] for the numerical analysis of creep and damage for Bridgman notch specimen.

Mathematical modeling of creep and damage of welded elements of real structures is reduced to the formulation of nonlinear initial- boundary value problems for bodies of complex shapes in a variety of boundary conditions. For these tasks, there are different methods for finding approximate solutions.

Using analytical solutions often requires significant simplifications in the problem statement. Among the numerical methods finite element method is widely used due to its flexibility and create a large number of commercial software systems with user-friendly interface.

Much attention is paid to the typical elements of the design which are widely used in steam and gas turbines, chemical engineering and nuclear power. Among these elements should first be noted welds walled tubes loaded with internal pressure.

One of the earliest publications on this issue is an article [134]. Finite element analysis is used by Tu and Sanstrom for the creep analysis of butt-welded joint in pressurised tubes with creep soft weld. On the basis of the predicted structural response, the rupture time was calculated and subsequently the weldment creep reduction factors were evaluated for different lifetimes. These reduction factors were also compared with those defined by the ASME Code Case N47-29.

The original semi-analytical method for calculating the butt weld pipe joints developed in [122] with the following assumptions. The idealized material behavior having the secondary creep stage was only considered. In this case the steady state solution of creep in the pipe exists, for which the stresses do not depend on time. It was assumed that the difference between the material properties of constituents is not great. The governing equations can be summarized as Norton's creep law. The proposed technique allows to obtain solutions by means of perturbation method. The unperturbed solution corresponds to the stress field in a homogeneous pipe. Authors used the Kantorovich method to reduce the 2-D variational problem to 1-D variational problem. The results obtained by perturbation method were compared with solution, obtained by the Ritz method, and numerical solution obtained with the help of ANSYS finite element code. The error of the perturbation method becomes substantial when the creep properties differ from one another by one order of magnitude.

Numerical analysis is used in [42], [43] to predict long-term strength of the butt welded joint in thick-walled pipes. Preliminary metallographic studies of welded seam showed that in the area of the junction there is a large number of zones with different structures. Thus, in [129] separate material structures were identified in the heat-affected zone. Many of these microstructures have not been prepared in sufficient volumes, to enable creep test to be performed. Hence limited uni-axial data is available. Therefore, the finite element model was constructed without such detailization. The weld model contains the three main microstructural regions of the weldment, namely: the

parent metal, the heat-affected zone and the weld metal.

Finite element modeling was used in [5], [101] for numerical analysis of multi-pass welding and post-weld heat treatment of a pipe specimen. 3D finite element models have been developed to simulate the welding process and residual stresses, using uncoupled thermal mechanical analysis. Short-term creep tests have been conducted to reach to the required creep properties. Norton's primary creep model was used to fit the creep test data. The relaxation process has been simulated using this creep model.

During the manufacture of large cylindrical containers longitudinal welds are often used. In such cases, the weld seams are exposed to larger tensile forces than in butt joints. In [100],[101], [129] three-dimensional finite element creep analysis of the longitudinal welded tube specimen was performed. The longitudinal welded tube specimen model consists of a base metal, a weld metal and a HAZ. Boundaries of the HAZ in the actual specimen were traced in the model. Norton law was adopted as a creep constitutive equation. The coefficients and the index in Norton law of each material were determined [129]. For determination of rupture time the criteria of accumulated maximum creep strain in the circumferential direction at the mid-thickness of the HAZ was used. Rupture time is defined as the "limited strain" which is calculated by product of the steady state creep strain rate and the rupture time.

Detailed analysis of creep and long-term strength requires a large amount of experimental data for the different zones of the welded joint. In the absence of a complete set of the required parameters some assumptions have to be made and they must be used for verification of numerical modeling. An example of this approach is the work [70]. Due to the small number of test results the special procedure for generating creep modeling data was used for analysis of the creep behavior of longitudinal weld in a reheat header. In particular, some of the needed parameters for the different zones and temperature levels in Norton law are calculated using averaging procedure. The same procedure was used to develop the creep rupture law. A two-dimensional FE model of the weld was generated based on drawings supplied by the manufacturer. Results of modeling show that point of maximum damage is predicted to occur at the mid-wall position. Shortened life is due to raised stresses in the HAZ. These in turn are due to the higher creep rate in the parent material and the resulting greater mismatch between the parent and weld materials.

T-shaped (branched pipe) welded assemblies of thick-walled pipes are the examples with more complex geometries. Numerical analysis of such elements requires design of 3-D models with complex geometry of feature zones of the welded joint. In [151] three - dimensional creep damage analysis was

conducted on a medium bore welded branched pressure vessel, under a constant inner pressure and an axial loading at a uniform temperature of 630°C. Due to the symmetry of the pressure vessel, only one quarter of it was modeled and symmetric boundary conditions were assigned on the two cross sections in the computation.

Typical continuum damage mechanics constitutive equations of creep damage with a single damage variable was used in multi-axial form:

$$\dot{\boldsymbol{\epsilon}}^{cr} = \frac{3\mathbf{S}}{2\sigma_{eq}} \frac{A\sigma_{eq}^n}{(1-\omega)^n} \quad (1.46)$$

Some experimental results of a multi-material cross-weld specimen were used from [104]. The joint part of the specimen contained four kinds of material: base metal, weld metal, coarse grained HAZ and fine-grained HAZ. A new constitutive model, which combines phenomenological CDM equations with the micromechanism-based void growth model, is presented to analyze the creep damage development in HAZ of weldments. FE analysis shows that stress is redistributed from the weak fine-grained HAZ to the stronger coarse-grained HAZ and base material, leading to a relatively high stress state surrounding the HAZ.

Several studies [46],[47],[96] dedicated to CDM analysis of t-shaped welds for cylindrical and spherical vessels. To describe the creep behavior of the materials of the weld using CDM, the following equations can be used for multi-axial creep strain rate $\dot{\epsilon}_{ij}$ and the damage rate $\dot{\omega}$.

$$\frac{d\epsilon_{ij}}{dt} = \frac{3}{2}G \frac{\sigma_{eq}^{n-1}}{(1-\omega)^n} S_{ij} t^m \quad (1.47)$$

$$\frac{d\omega}{dt} = M \frac{[\alpha\sigma_1 + (1-\alpha)\sigma_{eq}]^\tau}{(1+\varphi)(1-\omega)^\varphi} S_{ij} t^m \quad (1.48)$$

where σ_{eq} is the effective stress, σ_1 is the maximum principal tension stress, m , n , G , M , φ , τ are constants over particular stress ranges, and α is the multi-axial creep rupture criterion.

The ability of these constitutive equations to predict the results of the uni-axial tests carried out in the laboratory on the parent, Type IV, HAZ and the weld metal has been demonstrated in [39].

To cover the whole range of stress, two groups of the constants can be identified for some materials: one for low stress, and the other for high stress levels. The break stress $\hat{\sigma}$ represents the transition point between levels. This results

in a bilinear approximation to the true behavior which is sufficiently accurate for most practical purposes. In finite element modeling T-junction tubes of different diameters, larger diameter cylinder was replaced by sphere that allowed to build two-dimensional axisymmetric model. Estimation of errors associated with such simplification is made.

In the further work [47] 3-D computer software DAMAGE XXX was used to analyse the initiation and growth of creep damage and subsequent failure in the branch weld. CDM analysis was development for a five-material model that includes: parent, Type IV, refined heat affected zone, coarse grained heat affected zone and weld materials. The set of constitutive equation developed in [106],[107] was used under numerical analysis:

$$\dot{\epsilon}_{ij} = \frac{3s_{ij}}{2\sigma_{eq}} A \sinh \left[\frac{B\sigma_{eq}(1-H)}{(1-\Phi)(1-\omega)} \right], \quad (1.49)$$

$$\dot{H} = (h\dot{\epsilon}_{eq}/\sigma_{eq})(1 - (H/H^*)), \quad (1.50)$$

$$\dot{\Phi} = (K_c/3)(1 - \Phi)^4, \quad (1.51)$$

$$\dot{\omega} = CN\dot{\epsilon}_{eq}(\sigma_1/\sigma_{eq})^\nu, \quad (1.52)$$

where H, Φ and ω are three internal state variables. Finite element model of single quadrant of the branch figure was created using the FEMSYS software. Different weld zones are simulated with a high detailization.

A three-dimensional CDM FE solver, DAMAGE XXX [109] was used for the numerical computations. The authors conducted a detailed numerical analysis of creep and damage by varying the number and size of the zones of the welded joint. Comparison of damage predictions with the results of micro-structural examinations of tested vessel was executed.

Some studies investigated the properties of weld joint on the models of plates with longitudinal seams. In [28] a longitudinal weld which has a single 'V' and double-faced 'X' configuration was analyzed. Finite element analysis was performed using an in-house code developed for the inelastic analysis of plane strain structures with various constitutive models, including the Chaboche viscoplastic model. The stress concentrations developed at the weldments during the long time operation at high temperature due to the mismatch in the creep properties of weldment constituents were estimated using finite element analysis.

Three-dimensional elastic creep FEM analysis was carried [141] out for longitudinal multipass welding of plate specimens using the mechanical properties of the weld metal, fine grained HAZ, and base metal.

Much less papers were published in which creep and damage of welded structures is investigated. Such calculations require significant computing power. This is due to the fact that zones of welds require a very fine discretization, and the overall size of construction can significantly exceed dimensions of the individual zones of the welds. In the work [32] the uniaxial and multiaxial creep behavior of 9CR1Mo steel was considered and the finite element calculations of a pressured welded vessel were performed. Properties of the weld metal zones were obtained as a result of metallographic studies and uniaxial tests data. The microstructure of the welded joint was analyzed using optical microscopy and hardness measurements. A significant difference between the subgrain size was observed for base metal, weld metal and the intercritical HAZ. A united constitutive model of Robinson model was used to describe the creep behavior of P91 steel alloy. Finite element calculations were performed using the commercial finite element code ABAQUS.

The review [138], presents results of the investigation of the beltline welding seam from the VVER-440/V-213 reactor pressure vessel of the German nuclear power plant Greifswald. The main focus of the paper is the application of the master curve approach and the "VERLIFE" procedure on the VVER-440 weld metal.

1.5 A micro-macro approach to continuum mechanics

Consideration of the phenomena surrounding us with varying degrees of detailization is a common method of research. Micro-macro approaches are widely used in all branches of science, from fundamental physics to economic theories. These approaches vary significantly even within a relatively narrow fields of science. In the mechanics of deformable bodies micro-macro (or even micro-meso-macro) approaches are used to solve a number of different tasks.

Such approaches are widely used to describe the mechanics of composite materials, where the homogenization procedure is almost impossible to avoid the design of actual composite structures. Homogenization consists in replacing the heterogeneous composite with the equivalent (in some sense) homogeneous, often anisotropic material. Vast amount of literature was devoted to methods for determining the averaged elastic properties of composites. For periodic structures, the basic method is to allocate the minimum representative volume and analysis its stress state. Characteristic dimensions

of such representative cells, for example such as carbon fibre, are in the range 10^{-3} - 10^{-4} m. Almost the entire range of mathematical methods of the theory of elasticity is being used in determining of average elastic characteristics. Much more difficult is the problem of homogenization for physically nonlinear problems of the plasticity theory and creep. Lets also note some works related to damage and creep of composites. In paper [30] the relationships for an isotropic a single-parameter Kelvin-Voigt material was used later to determine the effective anisotropic relationship for general three-dimensional composites. Due to the infinite variations in the shape of the microstructure among composites no closed form expressions can be derived here for the anisotropic material property matrices. Therefore asymptotic expansion homogenization methods [2] were used in the context of the finite element method. Through a numerical technique, general composites with complex microstructures can be homogenized.

The papers [75],[154] investigate the creep behavior, extrapolation method and damage mechanism of the hybrid glass/carbon short-fibre-reinforced composite with a random fibre distribution. The rupture strength and creep limit for this short hybrid fibre material were determined experimentally, relating both to stress and time. The data have been used for the current valve maintenance and are able to be applied to the design of composite components that are in service at elevated temperature. Two existing theoretical approaches for creep failure criteria of viscoelastic polymer-matrix composites were reviewed in [38]. One criterion is based on the continuum damage mechanics and the other is based on the fracture mechanics extended to viscoelastic materials. The method based upon Eshelby's approach was used in [118] for determining the stress/strain fields in a single-fibre model composite subjected to creep loading conditions. The non-linear viscoelastic behavior was modelled through an incremental stress/strain formulation. A model based on the average field theory was developed to study creep behavior and predict transverse creep deformation in a unidirectional metal matrix composite in [29]. The material investigated was unidirectional silicon carbide/aluminium (SiC/Al). The creep model of the composite is based on Eshelby's solution for representative volume of the composite consists of a number of fibres embedded in a block of matrix. Combined micromechanical approach was used in [152] for yield limit analysis of periodic composite. On the microscopic level, a representative volume element was selected to reflect the microstructures of the composite materials. Based on the homogenization theory and the static limit theorem the macroscopic strength domain of the representative volume element was obtained [79].

The computational micro-to-macro transition approach that couples heterogeneities on the microscopic scale to the macroscopic response of a continuum was developed in [86]. The nonlinear microscopic boundary value problem for heterogeneities with a spherical stiff inclusion and a void was approximated using the finite element method. The macroscopic constitutive response of the macroscopic material was determined using an energetic interface directly from a simulation that captures the heterogeneous microstructure. Interface homogeneities have also been considered in the context of contact problems [114],[146].

Modern continuum damage mechanics [57],[73], [89] is widespread and has achieved significant success through the systematic use of the results of the analysis at the microscopic level for modeling of materials at the macroscale level. Metallographic studies allow us to establish mechanisms of damage and destruction at various external loadings. Thus microscopic damage is found in micro cavities, micro cracks, or in the decohesion in microstructures of materials. Research at the microscopic level allows establishing the physical picture of ductile and brittle damage, creep damage as well as low and high cycle fatigue damage. Particularly under creep conditions thermal activation plays an important role. When polycrystalline metals are subject to static load at high temperature for long time, diffusion of vacancies takes place and leads to an increase of number of cavities mainly on grain boundaries perpendicular to the tensile stress. The growth of these cavities leads to microscopic decohesion. Examination of the physical picture of various kinds of rupture gives the opportunity to develop adequate phenomenological models.

The internal structure of the welds is of high complexity. This is due to many reasons. Difference in chemical compositions of joined metals, electrodes and welding wires, used flux and gas medium, leads to the fact that the weld zones can appear with variable chemical composition. It becomes more complicating because during the welding and cooling temperature change rates may vary for different areas of the weld. This leads to uneven structural transformations for both metal of weld and base metal. Additional factors appear when considering multipass welds, when heterogeneity is combined with the material anisotropy.

It should be noted that the boundaries between the different zones of the weld are suppositive, because changes in the spatial coordinates of the material properties occur continuously. Some areas particularly HAZ, have very small size, but effect significantly on the creep and long term strength welded joints and the entire structure. Investigation of the material properties of

welded joints on macroscopic samples may not provide complete information to create models of creep and damage of various zones. Metallographic examination on a microscopic level, allow determining the structure, size and shape of the various zones of the weld. The combination of mechanical tests on macro samples and micro-structure study provides the opportunity to develop mathematical models of creep and damage of the joint.

In [141] microstructural changes of multi-pass welding with 39 passes joint of P91 steel were examined by conducting long term creep rupture tests. The relationships between changes in microstructure and nucleation and propagation of creep damage of the welded joint specimen during creep were studied. Microstructural observations were conducted using an optical microscope, a scanning electron microscope (SEM), and a transmission electron microscope (TEM). Thin foils and carbon extraction replicas were used for the TEM observation. Figure 1.14 shows the cross-sectional view of the welded joint.

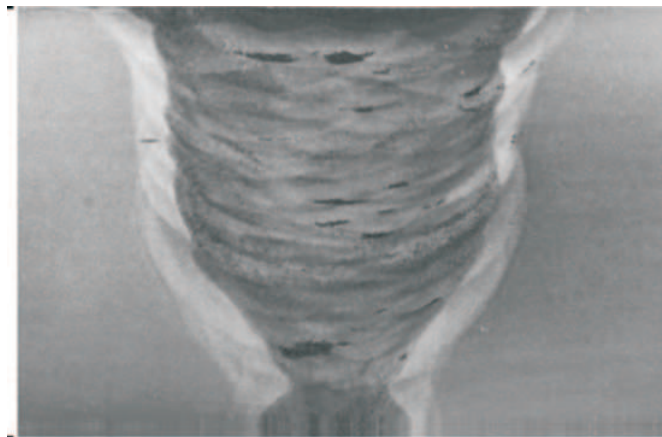


Figure 1.14 Weldment microstructure. After [141]

TEM micrographs of thin foils cut out from the weld metal, the HAZ and the base metal of a welded joint are shown in Fig.1.15

The microstructure of a base metal, the heat-affected zone and weld metal of a 9Cr steel longitudinal welded tube was studied [100], [147] by transmission electron microscopy and energy dispersive X-ray spectroscopy. The results indicate that the recovery of the microstructure is faster in HAZ than in other portions, and thus creep deformation preferentially occurs in HAZ.

Correlation between microstructure and mechanical properties including residual stress of welded steel specimen was investigated in [58],[59] by neutron strain scanning. Tensile properties of the weld metal were measured on macro specimens. It was determined that residual stress state in the weld

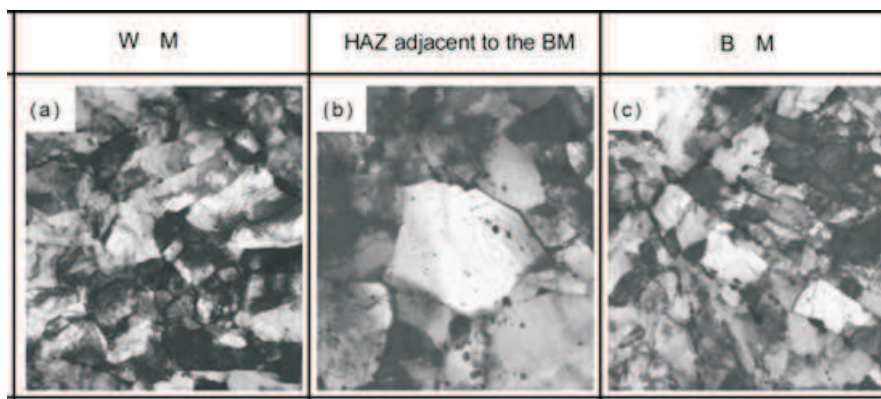


Figure 1.15 Microstructure of weldment zones. After [141]

metal and HAZ is strongly tensile. The transverse and through-thickness stress components vary from tensile to compressive in the weld region as a function of depth into the plate.

When applying multipass welds, metal is subjected to cyclic thermal stresses that cause changes in microstructure and macroscopic thermal stresses. The paper [103] is devoted to results of a study on the microstructural and micro chemical variations in a multipass welding of 9Cr-1Mo steel. The changes produced in the steel due to the heating and cooling cycles during welding were investigated by optical microscopy and scanning electron microscopy.

Using results of metallographic analysis in combination with macroscopic experiments to simulate creep and damage welds systematically applied in the many publications [6],[11],[34],[64], [116],[117],[129].

1.6 Scope and Motivation

Currently the world's leaders in the production of power plant equipment, steam and gas turbines, nuclear reactors (Siemens, Alstom, General Electric, Toshiba, Mitsubishi, Turboatom et al.), widely use welded elements of heavily loaded structures operating at high temperatures. In the welded joints of these structures creep deformation occurs and creep rupture strength of welded joints often determines the strength of the assembly. Fracture of welded joints of turbine units and nuclear reactors can lead to disasters with huge economic losses, loss of life and long-term contamination of the environment. This leads to considerable interest in the study of various aspects of the strength and reliability of welded structures worldwide.

Study of the processes occurring in the welded joints at high temperatures, is given a lot of attention in the last decade from the leading manufacturers of power equipment. Work in this direction is carried out at university research centers, such as The University of Manchester [43],[109] , Swedish Institute for Metals Research [120],[136] , University of Nottingham [13],[56] , Central Research Institute of Electric Power Industry, Japan [101],[147], Materialprüfungsanstalt Stuttgart, Germany [65],[142] and others.

International research foundations and organizations are funding special research projects on welds. European Commission supports Brite-EuRam project LICON [120], Project Programme of Brite/EuRam HIDA [48], Project SOTA- Programme of Standards, Measurements and Testing [128], National scientific organizations such as the National Research Institute for Metals (Japan) [3],[148], Electricité de France, Framatome and Le Commissariat 'a l'Energie Atomique [35] [84], Oak Ridge National Laboratory (USA) [116], Engineering and Physical Sciences Research Council (UK) [51], German Academic Exchange Service [122], Australian Institute for Nuclear Science and Engineering [70], German Science Foundation (DFG) [86] etc., support research on various aspects of this problem. Experimental studies on the micro level, including metallographic analysis using optical microscopes, electron microscopes, a scanning and a transmission electron microscope [6],[12], [35] [103],[116],[117], and even Neutron diffraction strain scanning on beam line accelerator [58], [59] have established the structure of the individual zones in a weld with high detail. Mechanical tests on macro level became a basis for constructing creep-damage models for individual zones and the welded joint as a whole. Construction of phenomenological models proceeded in parallel with experimental studies and using their results. Desire to improve the accuracy of theoretical models leads to their complexity. The simplest model described only the stage of steady creep of the weld as a whole and used classical long-term strength criteria [28],[31],[32],[70],[84],[101]. Including of the CDM approaches allowed building sophisticated creep-damage model for welds. Isotropic creep model built with one [13],[39],[151],[44], [56] or more scalar internal parameters [47],[50]. Development of models for the directed nature of damage started with the introduction of measures of damage tensor for isotropic materials in the initial state [10],[88],[89],[91],[93], [94] [108], [126]. To take into account the initial anisotropy of the different zones of the weld models were designed only for the case of transverse anisotropy [88],[94]. Logic of theoretical studies of welded joints, the latest experimental results and practical needs of power engineering necessitate the creation of creep-damage model based on the weld material anisotropy and directional nature

of damage. Developing of such a model suitable for practical use in predicting the long-term strength of welded structures is the aim of the present work. For multi-pass welds it is advisable to develop an averaging technique for the mechanical properties of the welded joint. Such homogenization is effective in creep-damage analysis of welded structures at the macro level. The present thesis focuses on numerical simulation of steel weldments subjected to creep. A continuum damage mechanics approach is used for a better understanding of weldment performance in high temperature application. The scientific objective with this work is to increase the physical understanding of the response of weldments subjected to creep. The technical objective with this work is to improve the basis for further development of present high temperature design codes and life assessment procedures. This will contribute to an increased safety in high temperature energy equipment. To achieve this goal in the dissertation the following main tasks were set and solved:

- Development of anisotropic creep constitutive relations taking into account the directional nature of the material damage of the weld. o Formulation of kinetic equations describing the process of damage accumulation that can determine the time to failure in a welded joint.
- Analysis of particular cases of a model: orthotropy, transverse isotropy and cubic isotropy.
- Development of methods for the model parameters identification on the basis of the experimental results and micromechanics simulations.
- Development of methods and procedures for homogenization in multi-pass welds
- Implementation of constitutive equations for creep damage models into the ABAQUS finite element code.
- Numerical analysis of some practical cases in high temperature weldment design and life assessment.

Consequently, within the framework of the dissertation an anisotropic creep-damage model based on continuum mechanics approach and applicable to analysis of weldment has to be developed. The model must be based on results of micro-macro investigations of weldments. As far as it is possible, the model must contain a minimum of creep material parameters, which can be easily identified from the standard procedures for creep and rupture uniaxial testing. For the purpose of effective application to numerical structural

analysis in ABAQUS software the model should be presented in the form of a user-defined subroutine.

Constitutive equations

2.1 Creep and damage of isotropic weld zones

In modern literature, a large number of diverse creep-damage models for isotropic materials are presented [71],[133],[61],[94],[111],[106],[119],[40],[145],[19], most of which are based on the concepts of Rabotnov - Kachanov [9], [20]. These models differ in the number of material constants (or functions) to be determined through experiments, as well as the amount of damage internal parameters. In the creep and damage study of the individual zones of the welded joint it is advisable to stay with the model, requiring minimum number of basic experiments. This is due to the fact that the sizes of the individual zones can be small and the selection of samples for testing is a complicated technical problem. The dimensions of the samples for inhomogeneous material make use of very sophisticated versions of the model unfavorable.

Below creep-damage model that will be used for separate areas of the weld is considered. It is a generalization of the Norton steady stage creep law with the effective stress introduced according to the concept of equivalent strain [21]. Thus both structures which use multipass welds are sufficiently massive, in the operation process they are exposed to a non-uniform temperature field. Therefore, this model provides the opportunity to be used in cases with variable temperature.

2.1.1 Coupled creep-damage governing equations

Creep-damage constitutive equations of an isotropic material with isotropic damage are assumed in form:

$$\dot{\epsilon}^{cr} = A_c \exp\left(-\frac{Q_c}{RT}\right) \frac{3}{2} \frac{\sigma_{vM}^{n-1}}{(1-\omega)^n} \mathbf{S} \quad (2.1)$$

$$\dot{\omega} = A_d \exp\left(-\frac{Q_d}{RT}\right) \frac{\sigma_{eq}^k}{(1-\omega)^l} \quad (2.2)$$

In Equations (2.1) and (2.2) $\dot{\epsilon}^{cr}$ represents the creep strain rate tensor; $\sigma_{vM} = \sqrt{\frac{3}{2} \mathbf{S} \cdot \mathbf{S}}$ is the von Mises equivalent stress; \mathbf{S} is the stress deviator; A_c , A_d , n , k , l are creep material parameters; ω is an isotropic damage parameter ($0 < \omega < \omega^*$), σ_{eq} is the damage equivalent stress, used in the form proposed by [94].

$$\sigma_{eq} = \alpha \sigma_{max} + (1 - \alpha) \sigma_{vM} \quad (2.3)$$

$$\sigma_{max} = \frac{|\sigma_I| + \sigma_I}{2} \quad (2.4)$$

By varying the parameter α one can generate different versions of the equivalent stress for better matching the predictions of theoretical models with experimental results on the long-term strength under complex stress state [40], [50],[51],[53].

To specify the different temperature effects on the creep and damage, we use two different functional relations: the first one is entered into the constitutive equation for creep strain rate and the second one into the evolution equation that determines the damage rate. The temperature dependence in relations (2.1),(2.2) is described by the Arrhenius function [57]. Here R - universal gas constant, Q_c and Q_d -the activation energies of creep and damage process, T - the absolute temperature, A_c , A_d - the material constants in temperature dependencies.

The most common methods of experimental investigation of the mechanical properties of materials at high temperatures are creep tests and long-term strength in uniaxial tension at constant stress and temperature. For such conditions system (2.1),(2.2) can be integrated. Taking notation $\sigma_{11} = \sigma$ integrate the kinetic equation (2.2) with the initial condition $\omega = 0$ at $t = 0$.

$$\omega(t) = 1 - [1 - A_d \exp\left(-\frac{Q_d}{RT}\right) (l+1) \sigma^k t]^{\frac{1}{l+1}} \quad (2.5)$$

The time to rupture t_* can be defined with assumption $\omega^* = 1$ in the following form:

$$t_* = \frac{1}{A_d \exp(-\frac{Q_d}{RT})(l+1)\sigma^k} \quad (2.6)$$

By taking into account equation (2.5), the creep constitutive equation (2.1) is integrated for $\varepsilon_{11}^{cr} = \varepsilon^{cr}$ with the initial condition $\varepsilon^{cr} = 0$ for $t = 0$ as follows:

$$\varepsilon^{cr} = \frac{A_c}{A_d} \exp-\frac{Q_d - Q_c}{RT} \frac{\sigma^{n-k}}{l-n+1} \times \left[1 - \left[1 - A_d \exp-\frac{Q_d}{RT} (l+1)\sigma^k t \right]^{\frac{l-n+1}{l+1}} \right] \quad (2.7)$$

In the study of creep processes in the case of constant temperature, without loss of generality, we assume $Q_c = Q_d = 0$, and the constants A_c , A_d should be determined by the results of experiments at a given temperature. Then, Equations (2.5) and (2.7) take the form:

$$\omega(t) = 1 - [1 - A_d(l+1)\sigma^k t]^{\frac{1}{l+1}} \quad (2.8)$$

$$\varepsilon^{cr} = \frac{A_c}{A_d} \frac{\sigma^{n-k}}{l-n+1} \times \left[1 - \left[1 - A_d(l+1)\sigma^k t \right]^{\frac{l-n+1}{l+1}} \right] \quad (2.9)$$

The time to rupture at constant temperature is determined by the dependence:

$$t_* = \frac{1}{A_d(l+1)\sigma^k} \quad (2.10)$$

2.1.2 Parameter identification technique

Mathematical correlations between basic variables in governing equations of creep-damage model can be formulated by different ways. The large number of material constants in governing equations allows to model the behavior of material better. However it results in the necessity of conducting many expensive experiments and complicates procedures of material constants identification. Finding successful compromise between these tendencies defines the quality of governing equations.

Let's consider the basic steps of parameter identification of creep-damage model (2.1), (2.2) based on the results of experiments on the creep under uniaxial stress state at a constant stress and temperature. For most metals at stresses and temperatures typical for actual operating conditions on the creep curves one can mark the area with a constant rate of creep strain. This suggests that at the steady stage of creep the influence of damage is small and the

parameter ω in the creep law can be neglected in (2.1). Then the equation for the steady stage of the creep curve takes the form:

$$\dot{\varepsilon}^{cr} = A_c \sigma^n \quad (2.11)$$

It comprises two material constants A_c and n . To define them, one must hold at least two experiments for different stresses at the same temperature. Possessing data from N experiments ε^{cr} and σ_i ($i = 1, 2, \dots, N$) it is possible using approximation methods, find the values of the constants A_c and n . For convenient usage of the least squares method, equation (2.11) can be logarithmed.

$$\lg \dot{\varepsilon}_i = \lg A_c + n \lg \sigma_i \quad (2.12)$$

Procedure of least squares [16], provides a constant values that best approximate the experimental results:

$$n = \frac{N \sum_{i=1}^N (\lg \dot{\varepsilon}_i \cdot \lg \sigma_i) - (\sum_{i=1}^N \lg \dot{\varepsilon}_i) (\sum_{i=1}^N \lg \sigma_i)}{N \sum_{i=1}^N \lg \sigma_i^2 - (\sum_{i=1}^N \lg \sigma_i)^2} \quad (2.13)$$

$$\lg A_c = \frac{(\sum_{i=1}^N \lg \dot{\varepsilon}_i) (\lg \sigma_i^2) - (\sum_{i=1}^N \lg \dot{\varepsilon}_i \cdot \lg \sigma_i) (\sum_{i=1}^N \lg \sigma_i)}{N \sum_{i=1}^N \lg \sigma_i^2 - (\sum_{i=1}^N \lg \sigma_i)^2} \quad (2.14)$$

2.1.3 Parameters in damage evolution equations

For identification of the material parameters in the kinetic equation of damage accumulation (2.2) one must have a series of creep curves for different values of the stress with a strong tertiary stage. Finding A_d , k and l , that provide the best fit with Equation (2.9), is in principle possible with the help of the non-linear method of least squares [145]. This procedure is sensitive to the form of the creep curve in the third stage. For practical purposes it is more important how you can more accurately predict the time to rupture t_* . Therefore, creep experiments were carried out until fracture, measuring limit creep strain ε_*^{cr} . Relation (2.9), (2.10) predict a value for ε_*^{cr} , independent of A_d , k :

$$\dot{\varepsilon}_*^{cr} = A_c + \sigma^n t_* \frac{l+1}{l-n+1} \quad (2.15)$$

This allows us to determine the average value of constant l on the results of N experiments:

$$l = \frac{1}{N} \sum_{i=1}^N \frac{\dot{\varepsilon}_{*i}^{cr} \cdot n}{\dot{\varepsilon}_{*i}^{cr} - A_c + \sigma_i^n t_{*i}} \quad (2.16)$$

To identify A_d and k value for the time to rupture Equation (2.10) is conveniently to logarithm:

$$\lg t_* = -\lg[A_d(l+1)] - k \lg \sigma \quad (2.17)$$

The constants A_d , and k can be estimated using approximation function (2.17) from following relations, produced by the least squares regression method [145]:

$$\begin{aligned} k &= \frac{N \sum_{i=1}^N (\lg t_i^* \cdot \lg \sigma_i) - (\sum_{i=1}^N \lg t_i^*)(\sum_{i=1}^N \lg \sigma_i)}{N \sum_{i=1}^N \lg \sigma_i^2 - (\sum_{i=1}^N \lg \sigma_i)^2} \\ \lg A_d &= \frac{(\sum_{i=1}^N \lg t_i^*)(\lg \sigma_i^2) - (\sum_{i=1}^N \lg t_i^* \cdot \lg \sigma_i)(\sum_{i=1}^N \lg \sigma_i)}{N \sum_{i=1}^N \lg \sigma_i^2 - (\sum_{i=1}^N \lg \sigma_i)^2} - \lg(l+1) \end{aligned} \quad (2.18)$$

For heat-resistant steels numerous experimental data on long-term strength at high temperatures [73],[87], [88],[94],[105] were collected. There is a positive experience in parameter identification for creep-damage models for different metals and alloys [47],[68],[74], [126]. Often experimental data on the time to rupture t_{*i} for different stress levels σ_i under uniaxial tension without limiting values of creep deformation. In addition, before the fraction a sample necks down and the strain ε_*^{cr} becomes non-uniform along the length of the sample. In such cases it is advisable to apply the concept of effective stress and the kinetic equation (2.2), for $l = k$. Identification of the constants k and A_d is performed by (2.18).

2.2 Anisotropic creep damage model for multipass welds

Multipass welds used in the design of many critical elements of structures operating at high temperatures. These include housing nuclear of reactors, rotors of steam and gas turbines, chemical engineering machines.

Quite often welded structures are found ruptured before the expected resource of components [120]. One reason for this is the difference in creep properties of the weld and the base metal, the unfavorable shape of the weld, that causes a stress concentration in the weld. Creep and damage in form of voids and microcracks lead to the failure of the material. Typical weld metal consists of the base metal of the designed element, the heat affected zone and weld metal. Construction elements connected by weld seam can be made of

the same or different material. Materials of welded joints and the base material can also be from the same or different composition. But even for welds where welded metals are the same creep behavior in the base metal, heat affected zone in (GR) and the weld material will be different [52]. Thus, welded structures are very complex heterogeneous structures. In addition, in the case of multipass welding weld metal the structure is also heterogeneous. It consists of welds, overlapping each other, which leads to the creation of HAZ in the weld metal through the processes of heating and cooling during the imposition of the next pass to the previous. Single-pass welds usually consist of a columnar structure occurring during solidification. However in multipass weld where next layer is applied on top of the previous one, it will be partly recrystallized and it will create a coarse and fine-grained structure [121].

As a result of heating and cooling cycles during the welding process, the complex bead type microstructure of the weld metal is formed, where every single bead consists of columnar, coarse-grained, and fine-grained regions, e.g., [55]. The results of uniaxial creep tests for the weld metal 9CrMoNbV are reported in [50]. They show that the creep strain vs. time curves significantly differ for specimens removed from the weld metal in the longitudinal (welding) direction and the transverse direction. Furthermore, different types of damage were observed for the longitudinal and the transverse specimens.

It should be noted that the rules for design of welded structures under pressure based only on data on time to the rupture of the welded materials under uniaxial loading. However, in reality these structures operate at multi-axial loading conditions. All these factors make it important to take anisotropy into account in modeling of creep in multipass welds.

The number of passes in welding of thick-walled components can reach tens or even hundreds. In such cases, it is advisable to consider melted metal as a homogenous material, and whole weld as a heterogeneous structure composed of at least three constituents - the weld metal, the heat-affected zone, and the parent material with different creep properties [32],[39],[93],[94],[109],[144].

In the majority of works the weld metal is regarded as isotropic. Firstly anisotropy of the weld metal in the welded joint was considered in [93],[94]. A model of a transversely isotropic material is used, where the normal to the isotropy plane is aligned with the direction of the pass laying. Discussed below weld metal model is a continuation of these studies. The proposed model takes into account the initial orthotropic creep properties of the deposited material and the dependence of the rate of damage evolution to the orientation of the principal axes of the stress tensor with respect to the principal

directions of the initial orthotropy. Thermodynamic bases in models of this type are presented in [57],[97]. Principles of construction of anisotropic creep constitutive relations in the invariant form based on the concept of the symmetry group of the fourth rank tensor are given in [8],[94].

2.2.1 Constitutive equations of anisotropic creep

The strain rate - stress relations for creep of anisotropic materials are based on the assumption of the existence of the creep potential. The creep potential hypothesis is widely used for continuum mechanics modeling of isotropic and anisotropic creep [8],[66],[79],[82], [110],[94]. During the secondary creep stage the strain rate tensor is defined by the scalar valued potential and the flow rule:

$$\dot{\boldsymbol{\epsilon}} = \frac{\partial W}{\partial \boldsymbol{\sigma}} \quad (2.19)$$

For simple determination of creep potential on basis of uni-axial creep tests, the equivalent stress σ_{eq} is introduced as intermediate scalar argument $W(\sigma_{eq}(\boldsymbol{\sigma}))$. The Norton-Bailey's power law is used below for the approximation of the strain rate-stress relations:

$$W = \frac{A_c}{n+1} \sigma_{eq}^{n+1} \quad (2.20)$$

where the material parameters A_c and n depend on the temperature.

To model the microstructure of the multi-pass weld as equivalent continuum on the macroscopic scale, the representative volume element (RVE) was considered. The macroscopic creep properties of equivalent continuum are anisotropic in general case. The symmetry type of equivalent media is determined by geometric structure of multi-pass weld and the creep properties of the microstructure components. For modeling anisotropic creep behavior the equivalent stress is assumed in the general quadratic form [94],[110]:

$$\sigma_{eq}^2 = \boldsymbol{\sigma} \cdot \cdot^{(4)} \mathbf{B} \cdot \cdot \boldsymbol{\sigma} \quad (2.21)$$

The symmetric positively definite fourth rank tensor ${}^4\mathbf{B}$ must satisfy the following restrictions:

$$\begin{aligned}
\mathbf{a} \cdot \cdot {}^4\mathbf{B} \cdot \cdot \mathbf{a} &\geq 0 \\
\mathbf{a} \cdot \cdot {}^4\mathbf{B} &= {}^4\mathbf{B} \cdot \cdot \mathbf{a} \\
\mathbf{c} \cdot \cdot {}^4\mathbf{B} &= \mathbf{0} \\
\mathbf{a} &= \mathbf{a}^T \\
\mathbf{c} &= -\mathbf{c}^T
\end{aligned} \tag{2.22}$$

where \mathbf{a} and \mathbf{c} are second rank tensors.

The number of independent tensor components depends on symmetry class of equivalent continuum. For most multi-pass weld geometric structure one can assume equivalent continuum as an orthotropic solid. In this case tensor ${}^4\mathbf{B}$ can be presented in the base of orthonormal vectors $\mathbf{n}_1, \mathbf{n}_2, \mathbf{n}_3$, which are perpendicular to symmetry planes of orthotropic solid:

$${}^4\mathbf{B} = b_{ijkl} \mathbf{n}_i \otimes \mathbf{n}_j \otimes \mathbf{n}_k \otimes \mathbf{n}_l \tag{2.23}$$

In this case tensor ${}^4\mathbf{B}$ includes 9 nonzero independent components b_{ijkl} (including A_c in power law). With equivalent stress (2.21) the secondary creep equations for orthotropic solid can be written as follows:

$$\dot{\boldsymbol{\varepsilon}} = A_c \sigma_{eq}^{n-1} ({}^4\mathbf{B} \cdot \cdot \boldsymbol{\sigma}) \tag{2.24}$$

For a representation of the structure of the tensor ${}^4\mathbf{B}$ in the case of orthotropy, relation (2.24) can be represented in the matrix form:

$$\begin{vmatrix} \dot{\varepsilon}_{11} \\ \dot{\varepsilon}_{22} \\ \dot{\varepsilon}_{33} \\ \dot{\varepsilon}_{12} \\ \dot{\varepsilon}_{23} \\ \dot{\varepsilon}_{31} \end{vmatrix} = A_c \sigma_{eq}^n \begin{vmatrix} 1 & b_{1122} & b_{1133} & 0 & 0 & 0 \\ & b_{2222} & b_{2233} & 0 & 0 & 0 \\ & & b_{3333} & 0 & 0 & 0 \\ & & & b_{4444} & 0 & 0 \\ & & & & b_{5555} & 0 \\ & & & & & b_{6666} \end{vmatrix} \times \begin{vmatrix} \sigma_{11} \\ \sigma_{22} \\ \sigma_{33} \\ \sigma_{12} \\ \sigma_{23} \\ \sigma_{31} \end{vmatrix} \tag{2.25}$$

In a case where the creep strain occurs without volume change $\varepsilon_{ij}, \delta_{ij} = 0$ coordinates of tensor ${}^4\mathbf{B}$ must meet additional constraints:

$$\begin{aligned}
1 + b_{2211} + b_{3311} &= 0, \\
b_{1122} + b_{2222} + b_{3322} &= 0, \\
b_{1133} + b_{2233} + b_{3333} &= 0.
\end{aligned} \tag{2.26}$$

The number of independent components for incompressible orthotropic materials is reduced to six. For compressible transversely isotropic materials

(vector \mathbf{n}_1 perpendicular to the plane of isotropy) the number of independent components of the tensor ${}^4\mathbf{B}$ with A_c is reduced to five by the relations

$$\begin{aligned} b_{2211} &= b_{3311}, \\ b_{2222} &= b_{3333}, \\ b_{5555} &= \frac{1}{2}(b_{2222} - b_{2233}) \end{aligned} \quad (2.27)$$

For incompressible transversely isotropic bodies from three conditions (2.26) two remain independent. In this case, the number of independent components of the tensor ${}^4\mathbf{B}$ together with the A_c is reduced to three. In the case of an isotropic material in the initial state components of the tensor ${}^4\mathbf{B}$ satisfy:

$$\begin{aligned} b_{1111} &= b_{2222} = b_{3333} = 1, \\ b_{1122} &= b_{2233} = b_{1133}, \\ b_{4444} &= b_{5555} = b_{6666} = \frac{1}{2}(1 - b_{1122}). \end{aligned} \quad (2.28)$$

The number of independent constants is reduced to two. For isotropic incompressible material due to (2.26), one gets:

$$b_{1122} = b_{2233} = b_{1133} = -\frac{1}{2} \quad (2.29)$$

And the equivalent stress (2.20) coincides with the equivalent of von Mises type $\sigma_{eq} = \sigma_{vM}$.

2.2.2 Parameter identification technique

Depending on the anisotropy type, to identify the parameters of the model (2.24) it is required to perform a different number of independent steady-state creep experiments at various kinds of stresses. Test specimens should be cut in different directions with respect to the symmetry planes of the material. Let us set for multipass welds direction \mathbf{n}_1 as a direction along the passes of the seam. Under uniaxial tension for sample cut in the direction of \mathbf{n}_1 , with constant stress σ_{11} , creep strain rate at steady state is defined by relation:

$$\dot{\epsilon}_{11}^{cr} = A_c \sigma_{11}^n \quad (2.30)$$

Identification of parameters A_c and n is similar to the above mentioned isotropic model. It requires a minimum of two experiments at different levels of stress σ_{11} . Exponent in the Norton law (2.24) is assumed the same for all directions. This assumption is used in many papers on anisotropic creep and has satisfactory agreement with experimental data [50], [93], [94], [97],

[110], [112], [127]. Steady-state creep strain rates under uniaxial tension in the direction of \mathbf{n}_2 and \mathbf{n}_3 according to (2.24) are given by

$$\dot{\epsilon}_{22}^{cr} = A_c b_{2222}^{\frac{n+1}{2}} \sigma_{22}^n \quad (2.31)$$

$$\dot{\epsilon}_{22}^{cr} = A_c b_{2222}^{\frac{n+1}{2}} \sigma_{22}^n \quad (2.32)$$

Once one has experimental data on the steady-state creep specimens cut in the direction of \mathbf{n}_2 and \mathbf{n}_3 it is possible to find two components of the tensor ${}^4\mathbf{B}$.

$$b_{2222} = \left(\frac{\dot{\epsilon}_{22}^{cr}}{A_c \sigma_{22}^n} \right)^{\frac{2}{n+1}} \quad (2.33)$$

$$b_{3333} = \left(\frac{\dot{\epsilon}_{33}^{cr}}{A_c \sigma_{33}^n} \right)^{\frac{2}{n+1}} \quad (2.34)$$

For incompressible orthotropic material based on the relations (2.26) one can find three components of tensor ${}^4\mathbf{B}$:

$$\begin{aligned} b_{1122} &= \frac{1}{2}(b_{3333} - 1 - b_{2222}) \\ b_{2233} &= \frac{1}{2}(1 - b_{2222} - b_{3333}) \\ b_{1133} &= \frac{1}{2}(b_{2222} - b_{3333} - 1) \end{aligned} \quad (2.35)$$

The remaining three components of the tensor ${}^4\mathbf{B}$ can be determined according to the steady-state creep shear in three planes

$$b_{ijkl} = \left(\frac{\dot{\epsilon}_{ijij}}{A_c \sigma_{klkl}^n} \right)^{\frac{2}{n+1}} \quad (2.36)$$

where $i \neq j$ or according to samples cut at different angles to the directions of the principal axes of orthotropic material. For many practical problems due to the nature of structures it may not be necessary to find the whole set of components of the tensor ${}^4\mathbf{B}$. This applies to calculations of plates and shells, where biaxial stress state is realized, the plane stress/strain problems and analysis of axisymmetric bodies.

2.2.3 Damage evolution equation

Thermal loading and melting-solidification cycles are not the only issue that influences material properties of the weld metal in case of the multi-pass welds. Welding process itself creates structural imperfections and cracks on the weld metal. This combined with voids and micro-cracks that nucleate

during creep process may lead to the failure of the welded components earlier than predicted during pure creep analysis. That is why it is necessary to include damage into account in modeling of the welding behavior.

The available experimental data on creep and fracture of multipass welds indicate that the anisotropy in them is manifested not in the same way to the steady state creep rate and time to rupture. Dependence on the applied load and material parameters may vary for different directions. This necessitates the development of creep damage model in which the initial anisotropy and the anisotropy of damage described by independent tensors. Creep-damage constitutive equations of an anisotropic material with anisotropic damage are assumed in form [80]:

$$\dot{\boldsymbol{\epsilon}}^{cr} = A_c \frac{\sigma_{eq}^{n-1}}{(1-\omega)^n} {}^4\mathbf{B} \cdot \cdot \boldsymbol{\sigma} \quad (2.37)$$

$$\dot{\omega} = A_d^* \frac{\sigma_{eq}^{k-1}}{(1-\omega)^k} {}^4\mathbf{D} \cdot \cdot \boldsymbol{\sigma} \quad (2.38)$$

Where the tensor ${}^4\mathbf{D}$ reflects the anisotropy of material properties with respect to damage, which is characterized by a second-rank tensor $\boldsymbol{\omega}$. Equivalent stresses, with respect to damage, are introduced as:

$$\sigma_{eq}^2 = \boldsymbol{\sigma} \cdot \cdot {}^4\mathbf{D} \cdot \cdot \boldsymbol{\sigma} \quad (2.39)$$

and the scalar measure of damage:

$$\dot{\omega} = A_d \frac{\sigma_{eqd}^{k-1}}{(1-\omega)^k} \quad (2.40)$$

Anisotropy of material properties occur due to multipass weld laying direction, shape and location of individual passes. This allows to suggest that the main axis of symmetry of the tensor ${}^4\mathbf{B}$ and ${}^4\mathbf{D}$ are collinear and all the considerations about the number of independent components of these tensors for different types of anisotropy are identical. In particular, for an orthotropic material tensor representation ${}^4\mathbf{D}$ in matrix form as in (2.25).

2.2.4 Parameters of the anisotropic damage model

In uniaxial tension along the principal directions of orthotropy or pure shear in the planes of symmetry at a constant stress level constitutive relations (2.37) can be integrated. Theoretical view of the creep curve for each basic experiment has the form (do not summarize by i, j):

$$\varepsilon_{ij}(t) = \frac{A_c}{A_d(\sqrt{d_{ijij}})^{k+1}} \frac{\sigma_{ij}^{n-k}}{k-n+1} \times \{1 - [1 - A_d(\sqrt{d_{ijij}})^{k+1} (k+1)\sigma_{ij}^k t]^{\frac{k-n+1}{k+1}}\} \quad (2.41)$$

where d_{ijij} are parameters of tensor ${}^4\mathbf{D}$. At start time, $\omega = 0$, and the failure occurs at $\omega = 1$. The time dependence of the parameter ω for each experiment determined by the basic function:

$$\omega(t) = 1 - [1 - A_d(\sqrt{d_{ijij}})^{k+1} (k+1)\sigma_{ij}^k t]^{\frac{1}{k+1}} \quad (2.42)$$

At the stage of steady creep when the damage parameter ω is small its impact on creep strain rate can be neglected. Then parameters A_c , n , and the components of the ${}^4\mathbf{B}$ can be identified by the method described above in (2.24). To find the parameters k and A_d and components of tensor ${}^4\mathbf{D}$ it is necessary to have data on the long-term strength of one component loadings. Theoretical time to rupture for each of these loadings can be found using (2.42) with condition $\omega = 1$ at $t = t^*(\sigma_{ij})$:

$$t^*(\sigma_{ij}) = \frac{1}{A_d(\sqrt{d_{ijij}})^{k+1} (k+1)\sigma_{ij}^k} \quad (2.43)$$

Parameters A_d and k for the case of tension in the direction \mathbf{n}_1 , assuming $d_{1111} = 1$, can be found according to formulas (2.41) for $l = k$. The remaining components of the tensor ${}^4\mathbf{D}$ are defined by known times to rupture for the corresponding stresses (do not summarize i, j):

$$d_{ijij} = \frac{1}{[t^*(\sigma_{ij}) A_d (k+1)\sigma_{ij}^k]^{\frac{2}{k+1}}} \quad (2.44)$$

Physical performing of all basic experiments for multipass weld metal is technically complex, expensive and time-consuming procedure. It is more efficient to use numerical technique for parameter identification of creep-damage model (2.37)-(2.37) on the basis of data on the properties of individual zones and the geometry of the weld metal multipass weld. This technique was tested for problems of homogenization of composite materials [79]. The presentation of this technique for multipass welds will be given in the next chapter.

Numerical Procedure of Homogenization for Multipass Weld

3.1 Parameters of steady state creep equivalent continuum

To simulate the microstructure of multipass welding as an equivalent continuum at the macroscopic level considered representative volume element was assumed prismatic body with a cross section:

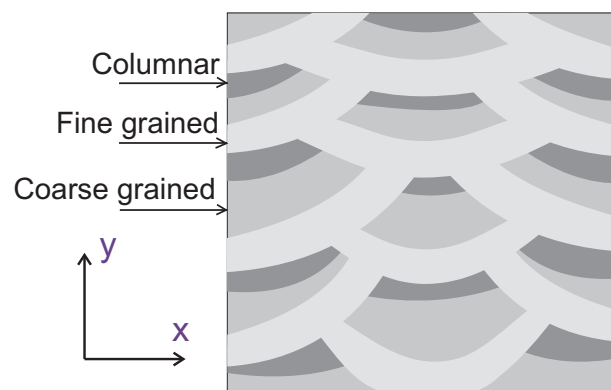


Figure 3.1 Volume Element

This section is considered as a repeating element is periodic in the plane OXY. Z axis is directed along the weld. Material properties of the weld metal zones are considered to be isotropic.

To describe the stationary creep of the weld metal zone Norton creep law for the incompressible material is used:

$$\dot{\boldsymbol{\epsilon}} = \frac{3}{2} A_c \sigma_{vM}^{n-1} \mathbf{S} \quad (3.1)$$

where \mathbf{S} is the stress deviator:

$$\begin{aligned} \mathbf{S} &= \boldsymbol{\sigma} - \sigma_0 \mathbf{I} \\ \sigma_0 &= \frac{1}{3} \text{tr} \boldsymbol{\sigma} \end{aligned} \quad (3.2)$$

Two material constants, included in Eq.(3.1) are defined according to procedure described in Sect.2.1. Nowadays significant amount of experimental data is available for different materials [34], [136],[84],[85], [140],[116],[51], [50],[94],[93]. Examples of defining material parameters for Norton creep law can be found in [34],[136], [140],[116] [50],[93].

Material parameters used for Eq.(3.1) are taken from [50] and are presented in Table 3.1. It should be noted that it is impossible to make the specimens directly from fine and coarse grained zones independently, that is why for these heat affected zones, material properties in them are assumed equal.

Table 3.1 Parameters of Norton law for weld metal zones. After [50]

Zone type	$K, \frac{\text{MPa}^{-n}}{\text{sec}}$	n
Columnar	$2.74 \cdot 10^{-21}$	7
Fine grained	$1.37 \cdot 10^{-20}$	7
Coarse grained	$1.37 \cdot 10^{-20}$	7

Section 2.2 outlined the sequence for determination of parameters characterizing the initial anisotropy of the weld metal, based on the basic physics experiments. Consider a procedure for performing numerical experiments for the theoretical finding these parameters.

The creep law for the homogenized continuum is presented by the averaged components in the volume V of the unit cell:

$$\langle \dot{\epsilon}_{ij} \rangle = A_c \langle \sigma_{vM} \rangle^{n-1} b_{ijkl} \cdot \langle \sigma_{kl} \rangle \quad (3.3)$$

$$\langle \sigma_{vM} \rangle = (\langle \boldsymbol{\sigma} \rangle \cdot \mathbf{B} \cdot \langle \boldsymbol{\sigma} \rangle)^{\frac{1}{2}}, \quad (3.4)$$

where $\langle \dot{\epsilon}_{ij} \rangle$ and $\langle \sigma_{kl} \rangle$ - averaged creep strain rates and stresses, which correspond to uniform macroscopic strain rate and stress:

$$\langle \boldsymbol{\sigma} \rangle = \frac{1}{V} \iiint_V \boldsymbol{\sigma} dV \quad (3.5)$$

$$\langle \dot{\boldsymbol{\epsilon}} \rangle = \frac{1}{V} \iiint_V \dot{\boldsymbol{\epsilon}} dV \quad (3.6)$$

For identification of 7 material constants in Eq.(3.3) 7 independent numerical tests should be executed. For these purposes 3-D finite element model of VE are created in the finite element code ABAQUS 3.2.

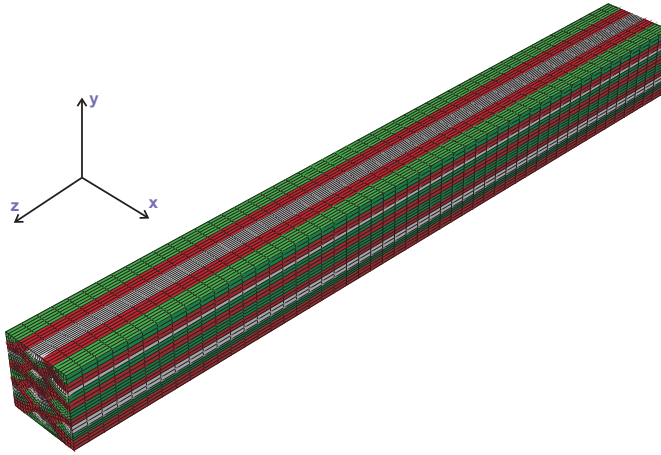


Figure 3.2 Finite element model of Volume Element

Finite element model of volume element consists of 43500 8-node linear brick elements, extruded from the meshed cross section 3.3 OXY that contained 4479 elements. Numerical experiments were performed using Static and Visco steps, with controlled time stepping.

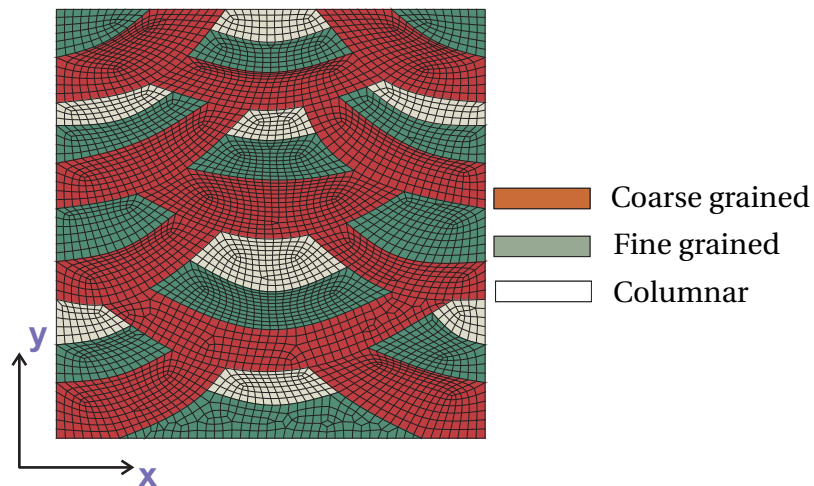


Figure 3.3 Cross section of finite element model of Volume Element

Three types of volume are created - a reference one (8 passes), the realization with twice more passes and realization with a half of the number of

passes. Due to the fact that in different zones on microscale level creep behavior is described by the different relations numerical experiments should be carried out to define the possibility to how Equation (3.3) approximates the creep behavior on the macroscopic level.

3.1.1 Numerical experiments for in-plane tension

Let us consider numerical experiment performed on an VE of uniaxial tension in the 11 direction. VE was subjected to the loading via Pressure on the boundaries orthogonal to the 11 direction [1]. Boundary conditions applied: symmetry boundary conditions on one of the planes orthogonal to 22 direction, and free boundary on the opposite plane Fig.3.4.

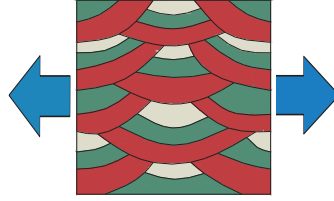


Figure 3.4 Boundary conditions for uniaxial tension in 11 direction

Average creep strain rate $\langle \dot{\epsilon}_{11} \rangle$ in case of uniaxial tension is related with average stress $\langle \sigma_{11} \rangle$ through the following equation (if $b_{1111} = 1$):

$$\langle \dot{\epsilon}_{11} \rangle = K \langle \sigma_{11} \rangle^n \quad (3.7)$$

Averaging by volume of stresses and strains can be reduced to averaging by area of VE's cross-section. To reduce the computational costs in calculation of average strains one can use the Green theorem:

$$\langle \dot{\epsilon}_{11} \rangle = \frac{1}{S} \iint_S \dot{\epsilon}_{11} ds = \frac{1}{S} \iint_S \frac{\partial \dot{U}}{\partial x} ds = \frac{1}{S} \oint_L \dot{U} dy = \frac{1}{ab} \int_0^b \dot{U} dy \quad (3.8)$$

where $x = 0, a, y = 0, b$ are the coordinates of VE's boundaries, U is a displacement in direction 11, S and L are the area and perimeter of VE correspondingly. Similar simplifications can be made to obtain stresses:

$$\langle \sigma_{11} \rangle = \frac{1}{S} \iint_S \sigma_{11} ds = \frac{1}{ab} \int_0^a dx \int_0^b \sigma_{11} dy = \frac{1}{b} \int_0^b \sigma_{11} dy \quad (3.9)$$

At first it is necessary to determine the conditions of reaching steady state stage for the strain rate. Series of creep analysis of VE were performed under the constant uniform stress $\langle \sigma_{11} \rangle$ for different time levels. From the results of numerical experiments one can extract the set of strain rate $\dot{\epsilon}_{11}$ values for the different moments of time t_i ($i = 1, \dots, N$). In Figure 3.5 we can observe the creep strain redistribution during creep, with a visible first stage and the ongoing second stage.

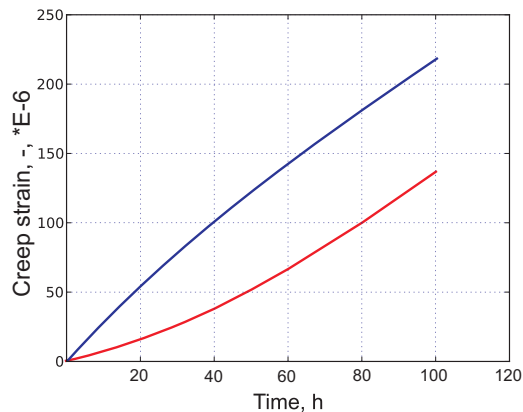


Figure 3.5 Creep strain in columnar zone and HAZ

On the figure 3.6 one can observe stress redistribution process under different stress levels in the different zones of the VE. It is clear that the higher the applied stress is, the more significant is the stress redistribution. We can observe the stress concentrating in the columnar zones and the HAZ is relaxing.

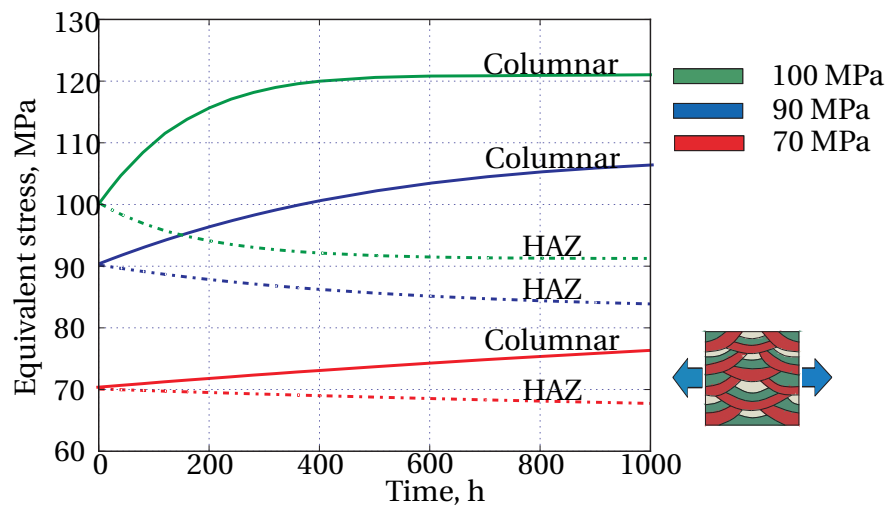


Figure 3.6 Equivalent stress redistribution in time for different zones

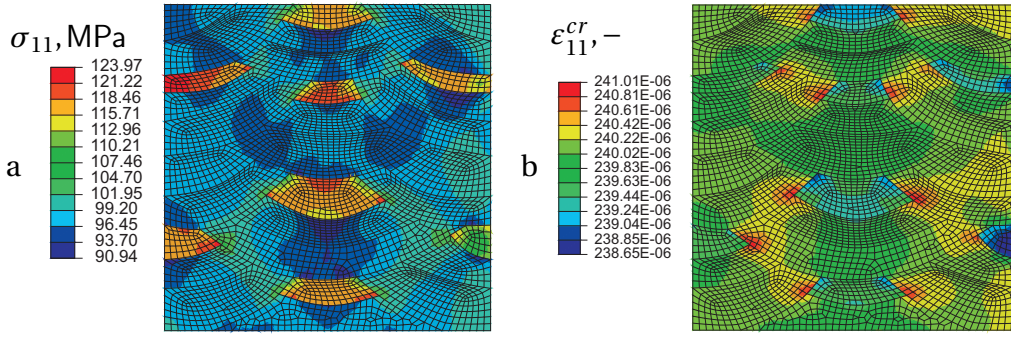


Figure 3.7 Stress σ_{11} , MPa (a) and creeps strain ε_{11}^{cr} , – (b) redistribution for tension test in 11 direction

Strain rate values on macroscopic level can be obtained by the following way:

$$\langle \dot{\varepsilon}_{11} \rangle = \frac{\sum_{i=1}^N \langle \varepsilon_{11} \rangle_i \cdot t_i}{\sum_{i=1}^N \cdot t_i^2} \quad (3.10)$$

To derive the exponent in creep law, set of numerical experiments under different macro-stress $\langle \sigma_{11} \rangle$ levels were made. Result of this series of M experiments is the set of $\langle \varepsilon_{11} \rangle_i$ for different stress values $\langle \sigma_{11} \rangle_i$, ($i = 1, \dots, M$).

To process the results of numerical experiments, relation (3.7) was rewritten in logarithmic form:

$$\ln \langle \dot{\varepsilon}_{11} \rangle = \ln K + n \ln \langle \sigma_{11} \rangle \quad (3.11)$$

Material constants for creep law of homogenized material are defined by processing results of numerical experiments using the least squares method:

$$n = \frac{\sum_{i=1}^M \ln \langle \dot{\varepsilon}_{11} \rangle_i \cdot \ln \langle \sigma_{11} \rangle_i - N \sum_{i=1}^M \ln \langle \dot{\varepsilon}_{11} \rangle_i \cdot \ln \langle \sigma_{11} \rangle_i}{\sum_{i=1}^N \ln \langle \sigma_{11} \rangle_i^2 - N \sum_{i=1}^N \ln \langle \sigma_{11} \rangle_i^2} \quad (3.12)$$

$$\ln K = \frac{1}{N} \left(\sum_{i=1}^M \ln \langle \dot{\varepsilon}_{11} \rangle_i - n \sum_{i=1}^M \ln \langle \sigma_{11} \rangle_i \right) \quad (3.13)$$

For the second in-plane direction 22, the numerical test is performed by the example of the tension in 11 direction. Now the load is applied on the faces orthogonal to the 22 direction and the symmetry and free boundary conditions applied on the opposite boundary faces orthogonal to 11 direction Fig. 3.8.

Relation between average creep strain rate and average stress in this numerical experiment turns the following way:

$$\langle \dot{\varepsilon}_{22} \rangle = K b_{2222} \langle \sigma_{22} \rangle^n \quad (3.14)$$

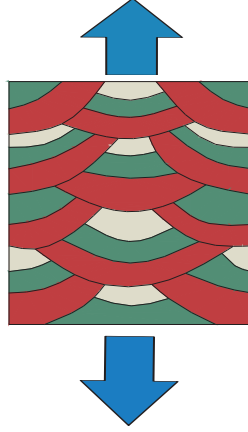


Figure 3.8 Boundary conditions for uniaxial tension in 22 direction

Since the parameter K was found in the previous numerical experiment, we still have 2 parameters to be found by performing 2 numerical experiments of this type. As well as for the first numerical test, averaging by volume can be reduced to averaging by area of VE's cross-section. Using the Green theorem in a same way as in Eq.(3.8) we get:

$$\langle \dot{\epsilon}_{22} \rangle = \frac{1}{S} \iint_S \dot{\epsilon}_{22} ds = \frac{1}{S} \iint_S \frac{\partial \dot{V}}{\partial y} ds = \frac{1}{S} \oint_L \dot{V} dy = \frac{1}{ab} \int_0^b \dot{V} dy, \quad (3.15)$$

and for stresses:

$$\langle \sigma_{22} \rangle = \frac{1}{S} \iint_S \sigma_{22} ds = \frac{1}{ab} \int_0^a dx \int_0^b \sigma_{22} dy = \frac{1}{b} \int_0^b \sigma_{22} dy \quad (3.16)$$

where $x = 0, a, y = 0, b$ are the coordinates of VE's boundaries, V is a displacement in direction 22, S and L are the area and perimeter of VE correspondingly.

Next step is extracting the set of strain rate $\dot{\epsilon}_{22}$ values for the different moments of time t_i ($i = 1, \dots, N$) from the series of creep analysis of VE under the constant uniform stress $\langle \sigma_{22} \rangle$. It is as well important to make sure that creep strain data points used for extraction lay on the steady stage of the creep curves.

Equation (3.10) for the numerical test for tension in 22 direction can be written as follows:

$$\langle \dot{\epsilon}_{22} \rangle = \frac{\sum_{i=1}^N \langle \epsilon_{22} \rangle_i \cdot t_i}{\sum_{i=1}^N t_i^2} \quad (3.17)$$

Assuming that the power coefficient n is equal for every direction, one can avoid making the set of numerical experiments under different macro-stress $\langle \sigma_{22} \rangle$ levels.

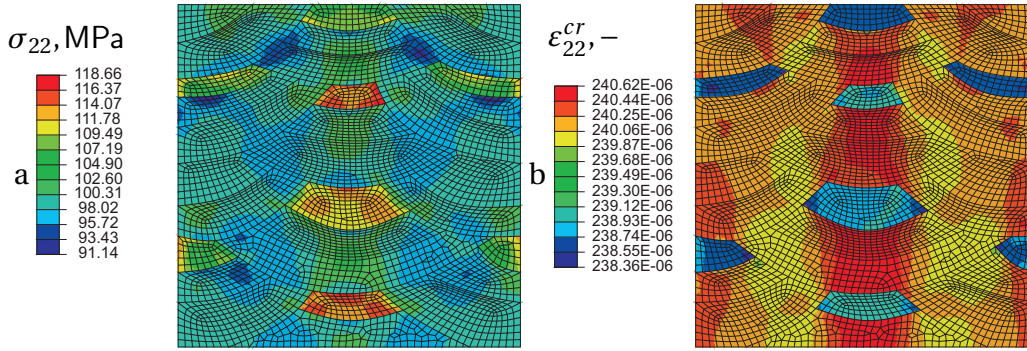


Figure 3.9 Stress σ_{22} , MPa (a) and creeps strain ϵ_{22}^{cr} , - (b) redistribution for tension test in 22 direction

To define the parameter b_{2222} relation (3.14) was rewritten interpreted in logarithmic form:

$$\ln\langle\dot{\epsilon}_{22}\rangle = \ln K + \ln b_{2222} + n \ln\langle\sigma_{22}\rangle \quad (3.18)$$

Using the least squares method one can form the resulting equation for b_{2222} :

$$\ln b_{2222} = \frac{1}{N} \left(\sum_{i=1}^M \ln\langle\dot{\epsilon}_{22}\rangle_i - n \sum_{i=1}^M \ln\langle\sigma_{22}\rangle_i \right) - \ln K \quad (3.19)$$

It is also possible to avoid simplifications regarding the equal power coefficient for every direction, then:

$$n(22) = \frac{\sum_{i=1}^M \ln\langle\dot{\epsilon}_{22}\rangle_i \cdot \ln\langle\sigma_{22}\rangle_i - N \sum_{i=1}^M \ln\langle\dot{\epsilon}_{22}\rangle_i \cdot \ln\langle\sigma_{22}\rangle_i}{\sum_{i=1}^N \ln\langle\sigma_{22}\rangle_i^2 - N \sum_{i=1}^N \ln\langle\sigma_{22}\rangle_i^2} \quad (3.20)$$

3.1.2 Numerical experiments for in-plane shear

For the numerical experiment on the in-plane shear FE model of VE was subjected to the loading via "Face traction" on the boundary faces [1]. No supplementary boundary conditions applied 3.10.

Equations (3.7) for this case will be formulated as follows:

$$\langle\dot{\gamma}_{12}\rangle = K b_{1212} \langle\tau_{12}\rangle^n \quad (3.21)$$

The Green theorem for shear strains:

$$\begin{aligned} \langle\dot{\gamma}_{12}\rangle &= \frac{1}{S} \iint_S \dot{\gamma}_{12} ds = \frac{1}{S} \iint_S \frac{\partial \dot{u}}{\partial y} + \frac{\partial \dot{v}}{\partial x} ds = \\ &= \frac{1}{ab} \oint_L \dot{V} dy - \frac{1}{ab} \oint_L \dot{U} dx = \frac{1}{ab} (\int_0^b V dy + \int_b^0 V dy) - \frac{1}{ab} (\int_0^a U dx + \int_a^0 U dx) \end{aligned} \quad (3.22)$$

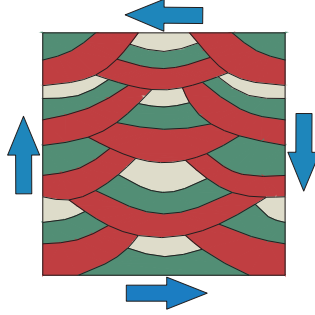


Figure 3.10 Boundary conditions for in plane shear

and for the stresses stresses one needs to perform averaging by the whole area of the VE.

As a result of the numerical experiment we can obtain stress and creep strain redistribution on the VE and extract the averaged values of creep shear strain rates $\dot{\gamma}_{12}$ for different stress levels and different moments of time t_i ($i = 1, \dots, N$).

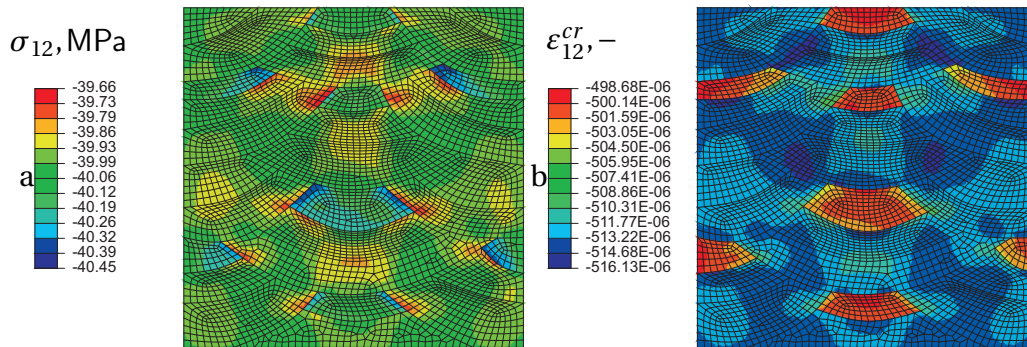


Figure 3.11 Shear stress σ_{12} , MPa (a) and shear creep strain ϵ_{12}^{cr} , - (b)

Strain rate values on macroscopic level can be obtained by the following way:

$$\langle \dot{\gamma}_{12} \rangle = \frac{\sum_{i=1}^N \langle \gamma_{12} \rangle_i \cdot t_i}{\sum_{i=1}^N \cdot t_i^2} \quad (3.23)$$

The logarithmic form of the relation (3.21):

$$\ln \langle \dot{\gamma}_{12} \rangle = \ln K + \ln b_{1212} n \ln \langle \tau_{12} \rangle \quad (3.24)$$

Material constant b_{1212} for homogenized material is defined using the least squares method as follows:

$$\ln b_{1212} = \frac{1}{N} \left(\sum_{i=1}^M \ln \langle \dot{\gamma}_{12} \rangle_i - n \sum_{i=1}^M \ln \langle \tau_{12} \rangle_i \right) - \ln K \quad (3.25)$$

3.1.3 Numerical experiments for longitudinal tension

Let us consider numerical experiment of uniaxial tension in the 33 direction. Instead of 2D models applied in the previous sections, to perform numerical experiments in the longitudinal direction it is necessary to use full 3D model of the VE.

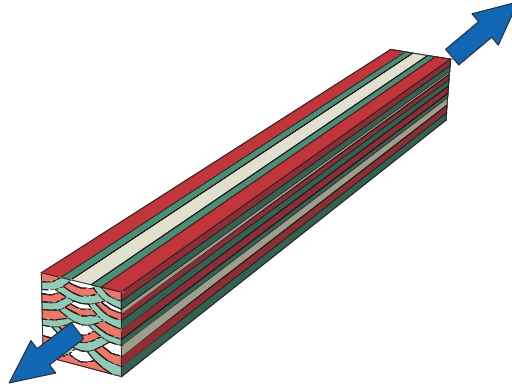


Figure 3.12 Loading and boundary conditions for uniaxial tension in 33 direction

Finite element model of the volume element was subjected to the loading via "Pressure" on the boundaries orthogonal to the 33 direction. And the following boundary conditions were applied: symmetry boundary conditions on one of the planes orthogonal to 22 and 11 direction, and free boundary on the opposite planes correspondingly, Fig.3.12.

Averaging creeps strain and stress acting on VE yields:

$$\langle \dot{\epsilon}_{33} \rangle = K b_{3333} \langle \sigma_{33} \rangle^n \quad (3.26)$$

It is important to note, that before using the standard procedure of simplification using the Green theorem for stresses and strains, one needs to avoid boundary effects that may occur in 3D VE near the areas of applied load. To do it, one can take to consideration a cut out volume from the 3D VE equally distanced from planes where load is applied, and substitute averaging on the

whole volume of a 3D VE with the averaging on this cut off volume. Then using the Green theorem once again we obtain:

$$\langle \dot{\epsilon}_{33} \rangle = \frac{1}{S} \iint_S \dot{\epsilon}_{33} dx = \frac{1}{ab} \int_0^b \dot{W} dx \quad (3.27)$$

$$\langle \sigma_{33} \rangle = \frac{1}{S} \iint_S \sigma_{33} ds = \frac{1}{ab} \int_0^a dx \int_0^b \sigma_{33} dy = \frac{1}{b} \int_0^b \sigma_{22} dy \quad (3.28)$$

where $x = 0, a, y = 0, b$ are the coordinates of cross section boundaries, W is a displacement in direction 33, S and L are the area and perimeter of cross section, respectively.

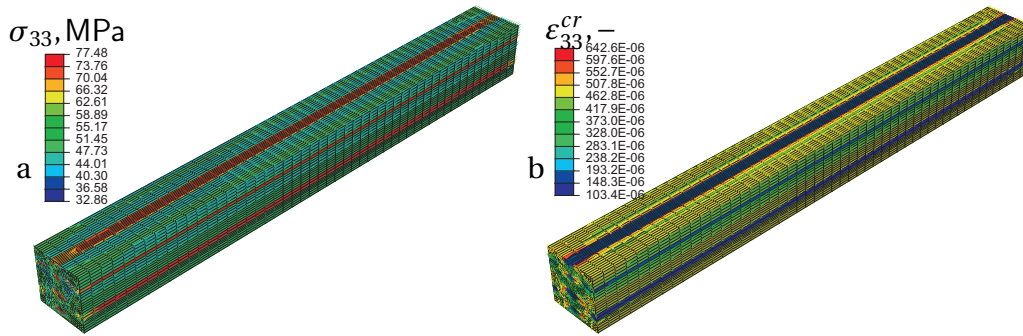


Figure 3.13 Stress σ_{33} , MPa (a) and creeps strain ϵ_{33}^{cr} , – (b) redistribution for tension test in longitudinal direction

For better visual representation, the cross section view of the VE is presented on 3.14.

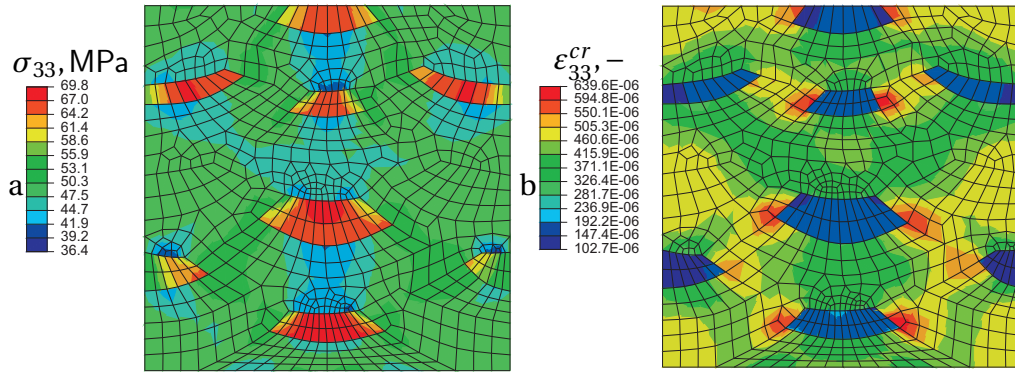


Figure 3.14 Cross-sectional view of stress and creep strain redistribution for tension test in longitudinal direction

Equation (3.10) for the numerical test for tension in 33 turns to:

$$\langle \dot{\epsilon}_{33} \rangle = \frac{\sum_{i=1}^N \langle \epsilon_{33} \rangle_i \cdot t_i}{\sum_{i=1}^N \cdot t_i^2} \quad (3.29)$$

To define the parameter b_{3333} logarithmic form of relation (3.26) is used:

$$\ln\langle\dot{\epsilon}_{22}\rangle = \ln K + \ln b_{2222} + n \ln\langle\sigma_{22}\rangle \quad (3.30)$$

the resulting equation for b_{3333} is:

$$\ln b_{3333} = \frac{1}{N} \left(\sum_{i=1}^M \ln\langle\dot{\epsilon}_{33}\rangle_i - n \sum_{i=1}^M \ln\langle\sigma_{33}\rangle_i \right) - \ln K \quad (3.31)$$

3.1.4 Numerical experiments for longitudinal shear

The numerical experiment on longitudinal shear, both for 23 and 13 directions performed by the similar way. For example, let's consider the numerical experiment to define b_{2323} . In this case VE should be subjected to the loading via "Face traction" on the boundaries orthogonal to the 33 direction in the 22 direction and the opposite, also it should be applied on the faces orthogonal to 22 direction in the direction 33 and opposite. The boundary conditions applied are: symmetry boundary conditions on one of the plane orthogonal to 11 direction, and free boundary on the opposite plane Fig.3.15.

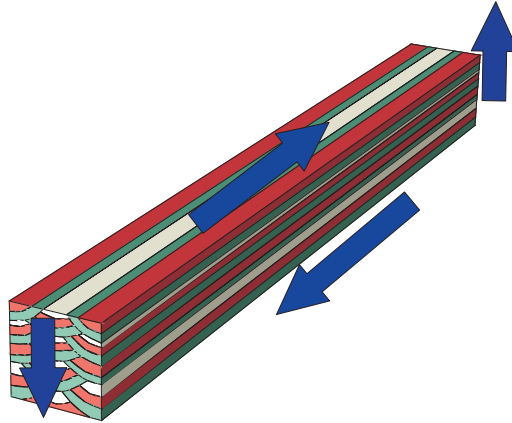


Figure 3.15 Boundary conditions for shear in 23 direction

Average creep strain rate $\langle\dot{\gamma}_{23}\rangle$ in case of longitudinal shear is related with average stress $\langle\tau_{23}\rangle$ by:

$$\langle\dot{\gamma}_{23}\rangle = K b_{2323} \langle\tau_{23}\rangle^n \quad (3.32)$$

Since this numerical test is performed also on the 3D VE, we must follow the procedure of the previous numerical experiment 3.1.3 in order to avoid boundary effects. Then applying Green theorem:

$$\langle\dot{\gamma}_{23}\rangle = \frac{1}{S} \iint_S \dot{\gamma}_{23} ds = \frac{1}{S} \iint_S \frac{\partial \dot{W}}{\partial x} ds = \frac{1}{S} \oint_L \dot{W} dy = \frac{1}{ab} \int_0^b \dot{W} dy \quad (3.33)$$

The distribution of the stresses and strains in the volume of the VE is presented in Fig.3.16 and 3.17.

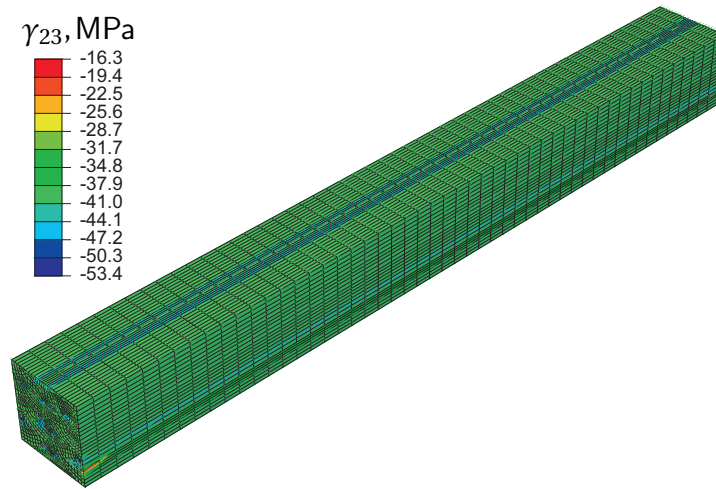


Figure 3.16 Shear stress γ_{23} , MPa

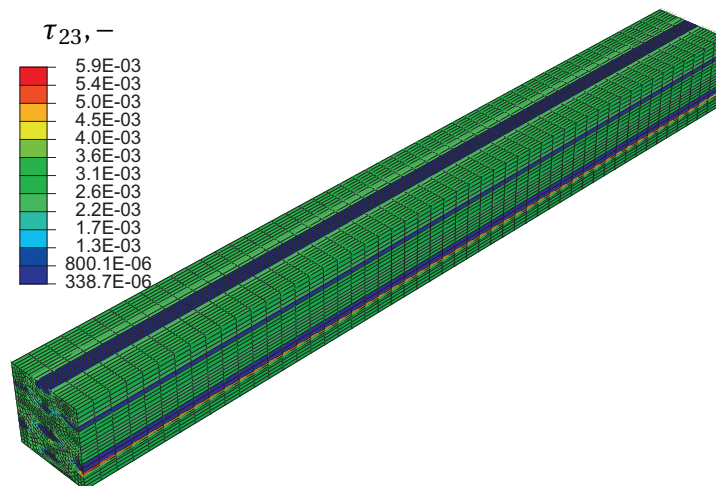


Figure 3.17 Shear creep strain τ_{23} , -

For the better visual representation, focus on the cross section of the VE in the area equally distanced from loading faces Fig. 3.18(a) and Fig. 3.18(b).

Strain rate values on macroscopic level:

$$\langle \dot{\gamma}_{23} \rangle = \frac{\sum_{i=1}^N \langle \gamma_{23} \rangle_i \cdot t_i}{\sum_{i=1}^N \cdot t_i^2} \quad (3.34)$$

Following the process described in previous numerical experiments:

$$\ln \langle \dot{\gamma}_{23} \rangle = \ln K + \ln b_{2323} + n \ln \langle \tau_{23} \rangle \quad (3.35)$$

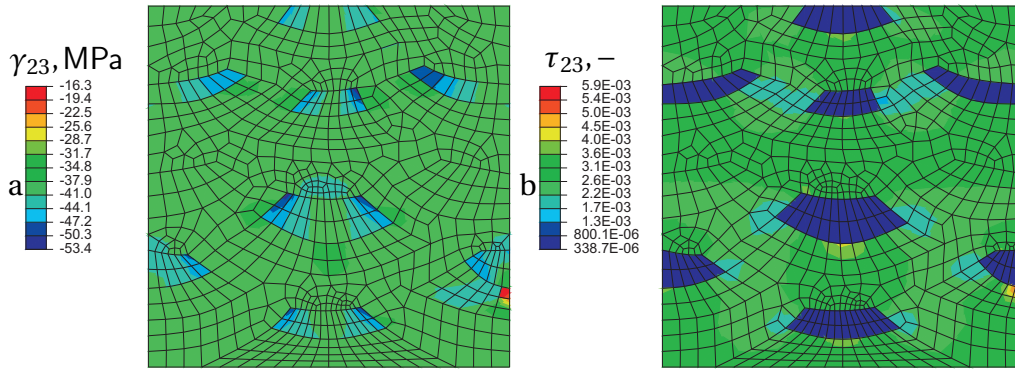


Figure 3.18 Shear stress γ_{23} , MPa(a) and shear creep strain τ_{23} , –(b)

The resulting equation to define the parameters responsible for longitudinal shear behavior description:

$$\ln b_{2323} = \frac{1}{N} \left(\sum_{i=1}^M \ln \langle \dot{\epsilon}_{11} \rangle_i - n \sum_{i=1}^M \ln \langle \sigma_{11} \rangle_i \right) - \ln K \quad (3.36)$$

Performing the similar analysis to define the last parameter b_{1313} we can complete the list of components of tensor 4B in Eq.(2.23), 3.2. Table 3.2 summarizes all values of tensor 4B .

Table 3.2 Parameters of tensor 4B , $\frac{\text{MPa}^{-\frac{2n}{n+1}}}{\text{sec}}$

-	16-pass	8-pass	4-pass
b_{1111}	9.05	9.22	9.33
b_{2222}	8.82	8.88	8.66
b_{3333}	6.86	6.91	6.97
b_{1212}	8.21	8.04	8.15
b_{1313}	8.26	8.21	8.26

$\times 10^{-6}, \frac{\text{MPa}^{-\frac{2n}{n+1}}}{\text{s}}$

3.2 Parameters of creep damage equivalent continuum

Thermal loading and melting-solidification cycles are not the only issue that influences material properties of the weld metal and HAZ in case of the multi-pass welds. Welding process itself creates structural imperfections and cracks

on the weld metal. This combined with voids and micro-cracks that nucleate during creep process may lead to the failure of the welded components earlier than predicted during pure creep analysis. That is why it is necessary to include damage into account in modeling of the weldings behavior. As we assumed previously, weld metal constituents are isotropic so to implement damage in modeling behavior of the weld metal during creep, isotropic creep damage model described in Sect. 1.2.1 was used. Creep and damage constitutive equation for isotropic materials can be written as follows:

$$\dot{\varepsilon}^{cr} = a \frac{\sigma^n}{(1-\omega)^m} \quad (3.37)$$

with damage rate formulated as:

$$\dot{\omega} = b \frac{\sigma^k}{(1-\omega)^l} \quad (3.38)$$

where t^* - time to rupture, and ω^* is the critical value of the damage parameter.

Similar to pure creep analysis, it is not possible to define parameters C , D , n , m , k and l for all weld metal zones. However to perform qualitative evaluation of the influence from the inhomogeneity of the weld metal, we can take creep curves Fig. 3.19 of the columnar zone and fine-grained zone in HAZ of the base metal from [150], and assume that the relation between time to rupture would be the same as for the columnar and HAZ of the weld metal. Processing the data from the creep curves and assuming that $n = m$, and $k = l$,

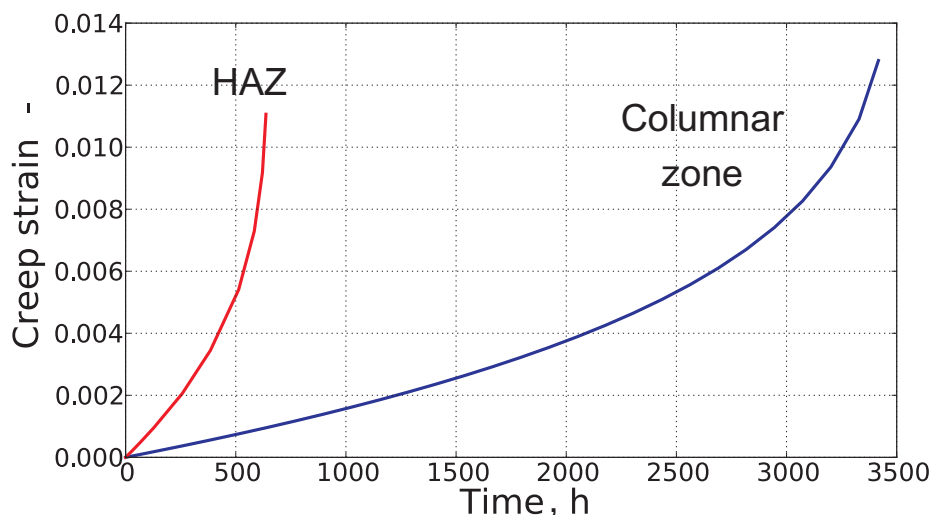


Figure 3.19 Creep curves assumed for columnar zone and HAZ

the relation between time to rupture of the weld metal constituents $t_h^*/t_c^* = 2.5$, where indexes h and c are for HAZ and columnar zone respectively. Power indexes were set $n = 3, k = 4$ for both materials.

To model the creep damage behavior of the equivalent homogenous material for weld metal, VE from the previous analysis was used and the same set of numerical experiments was performed. As results of this numerical experiments damage parameter distribution on the VE and its evolution during time was obtained. In Figure 3.20 one can see the difference in the damage

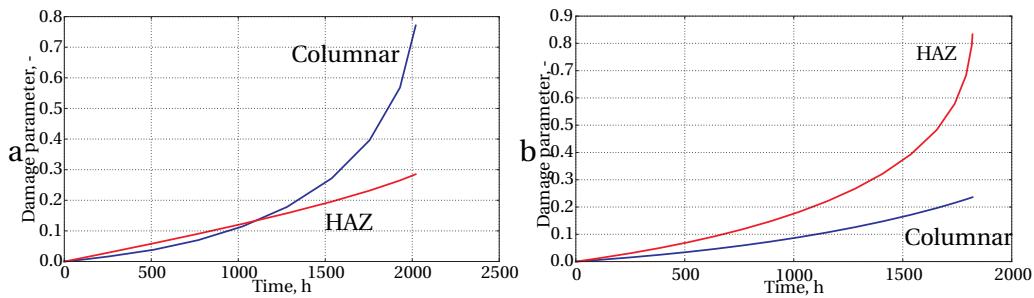


Figure 3.20 Damage parameter ω in tests on longitudinal (a) and transverse (b) directions, -

parameter evolution between a) longitudinal tension test and b) test in the transverse direction. In case of the longitudinal direction damage parameter increases faster on the columnar zone, despite the fact that HAZ is more prone to damage according to the material parameters. This happens because of the stress redistribution due to creep in the longitudinal tension test. In Figure 3.21 a) one can see that stress in this numerical experiment concentrates in the columnar zone, and in some time points equivalent stress in columnar zone may reach twice the value compared to HAZ. On the other hand, in nu-

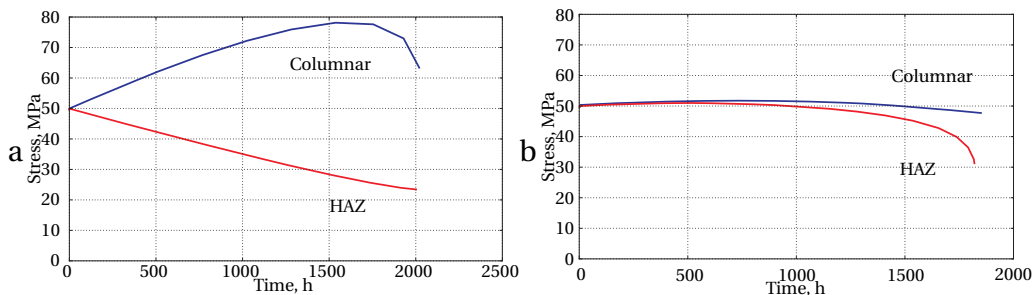


Figure 3.21 Stress redistribution in time for tension tests in 33 and 11 directions

merical experiments on tension in one of the cross-section directions, stress

redistribution between the zones not so essential, however still been higher in columnar zone. This is why damage parameter in these tests reflects material parameters better, and increases faster in more damage prone zone - HAZ.

Damage parameter distribution over the VE for numerical experiment on longitudinal tension at the moment for failure is shown In Figure 3.22.

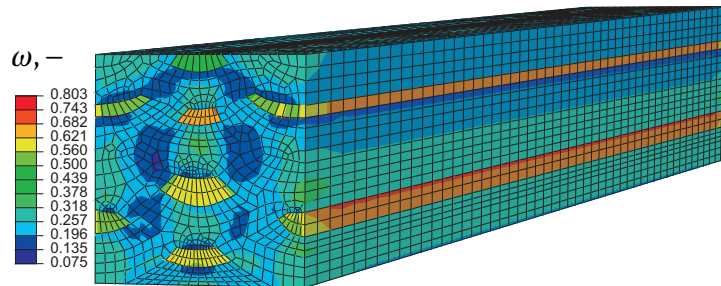


Figure 3.22 Damage parameter redistribution in longitudinal tension test

In Fig.3.22 one can see the averaged equivalent creep strain redistribution over time for three numerical experiments on uniaxial tension in longitudinal, and two cross-section directions. As one can see, curves that reflect the behav-

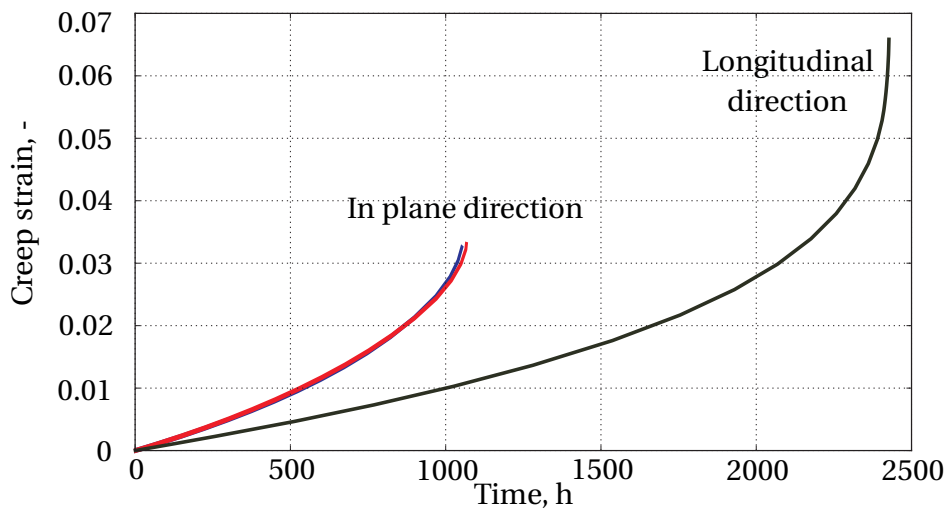


Figure 3.23 Equivalent creep strain in tension tests for different directions

ior of the VE in tension tests on the cross-section directions almost coincide, and the longitudinal tension test curve has lower creep rate and has higher time to rupture value. Based on this result one can assume that creep damage material properties of the equivalent material for multi-pass weld metal are transversely isotropic. To describe such anisotropy in the equivalent material response, the model of creep with damage for transversally isotropic material described in 2.2.3 was used.

Table 3.3 Time to rupture, h

-	16-pass	8-pass	4-pass
$t^*(1111)$	1740	1821	1899
$t^*(2222)$	1735	1837	1926
$t^*(3333)$	2342	2493	2614
$t^*(1212)$	891	956	1001
$t^*(1313)$	989	1032	1103

Creep-damage evolution equations for anisotropic material are assumed following:

$$\dot{\boldsymbol{\epsilon}} = A_c \frac{\sigma_{vM}^{n-1}}{(1-\omega)^n} {}^4\mathbf{B} \cdot \boldsymbol{\sigma} \quad (3.39)$$

$$\dot{\boldsymbol{\omega}} = A_d^* \frac{\sigma_{eq}^{k-1}}{(1-\omega)^k} {}^4\mathbf{D} \cdot \boldsymbol{\sigma} \quad (3.40)$$

By the similar way as in 3.1 one can define the parameters of damage evolution equation. Extracting the data from numerical experiments we can get the set of time to rupture values t^* for different one-component loading tests 3.3. Parameters A_d and k for the case of tension in the direction \mathbf{n}_1 , assuming $d_{1111} = 1$, can be found according to formulas (2.41) for $l = k$. The remaining components of the tensor ${}^4\mathbf{D}$ are defined by known times to rupture for the corresponding stresses (do not summarize i, j):

$$d_{ijij} = \frac{1}{[t^*(\sigma_{ij}) A_d (k+1) \sigma_{ij}^k]^{\frac{2}{k+1}}} \quad (3.41)$$

CHAPTER

4

Macroscale

Multi-pass welds are commonly used when it is necessary to make a joint of thick-walled constructional elements, for example thick-walled tubes. To make such welding joints operators usually make an angle cut on the joining surface [123]. This leads to difference in number of passes between the areas close to the top and bottom surface of the constructional elements. As a result, this will cause the difference in the properties of top and bottom layers of weld metal. One of the ways to take this kind of operational features into account in modeling a real construction is to create a model with the each and every pass including the heat affected zones. However this will lead to non-reasonable computational costs. The way that is proposed in this work is to substitute this kind of complex inhomogeneous structure with three layers of homogeneous equivalent materials, the properties of which will differ accordingly to number of passes.

Typical microstructure of the welded joint consists of base metal, weld metal and the heat affected zone (HAZ) that is formed from a part of a base metal as a result of a heating and cooling processes appearing during welding. In figure 4.1 one can see two model types of welded joint - one with the passes and one with the equivalent material layers. The material properties of the base metal and the HAZ used for analysis are taken from , and the properties for the equivalent material layers are taken from the analysis of VE's on a microscale - top layer corresponds to VE with 16 number of passes, middle layer corresponds to VE with 8 passes, and bottom layer corresponds to the VE with 4 passes. To analyze whether it is possible to make such a substitution series of numerical experiments on uniaxial tension were performed in three

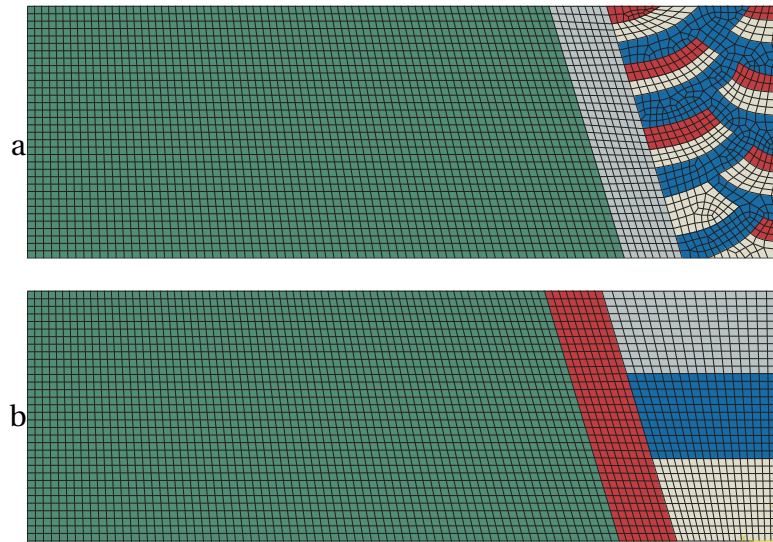


Figure 4.1 Finite Element Model of a welded joint (a) with passes and (b) with equivalent material layers

Table 4.1 Equivalent stress and creep strain response difference between models

-	σ_{eq} (in plane)	σ_{eq} (longitud.)	ε_{eq} (in plane)	ε_{eq} (longitud.)
Top layer	2.4%	1.82%	1.7%	0.92%
Middle layer	0.83%	0.76%	0.69%	0.54%
Bottom layer	1.85%	1.3%	1.5%	1.47%

directions: welding direction, and two orthogonal directions.

Comparing average equivalent stress response of each layer with the corresponding area of the model with passes one can see that the difference in response between two models is at maximum less than 2.5% (Table 4.1).

It should be noticed that to make an accurate comparison and to define the possibility to substitute complex model with passes with the layer model it is necessary to perform statistical analysis.

As an example of an analysis in the macroscale level, typical benchmark for welded constructional elements - T-type joined pressure vessel was used, with the additional welding on one of the T-side pipes. This was made to avoid possible undistinguished influence on results from geometrical features of T-type vessel. Geometrical model of the pressure vessel, designed in ANSYS Software is shown on figure 4.3. Only a quarter was taken for modeling due to the symmetry of the pressurized unit.

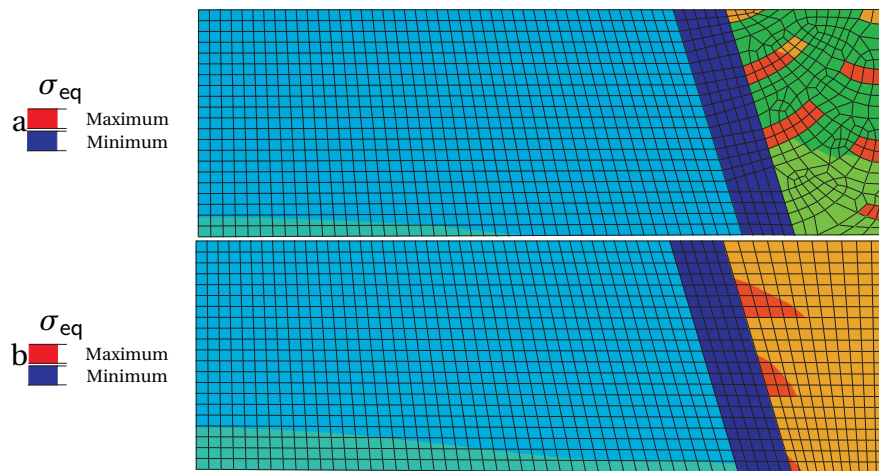


Figure 4.2 Equivalent stress redistribution after 1000 hours of creep (a) model with passes (b) model with equivalent material layers

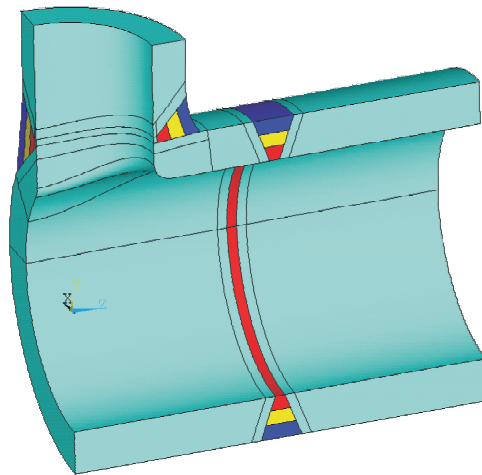


Figure 4.3 Geometrical model of the pressured vessel

Material properties for welded pressure vessel were taken from the results in a mesoscale, so that properties of the base metal were used for both pipes, heat affected zone of the welded joint correspondingly was taken for HAZ in the joints of the vessel. And to describe the behaviour of the weld metal, 3-layer model was used and properties that were found as a result in a microscale level were used.

The applied load for the model was inner pressure of 30MPa, and symmetry boundary conditions were used on every face of the vessel pipes. Damage parameter redistribution on the VE is shown on figure 4.5a. As one can see, damage accumulates on the heat affected zone of the welded pipe, this corre-

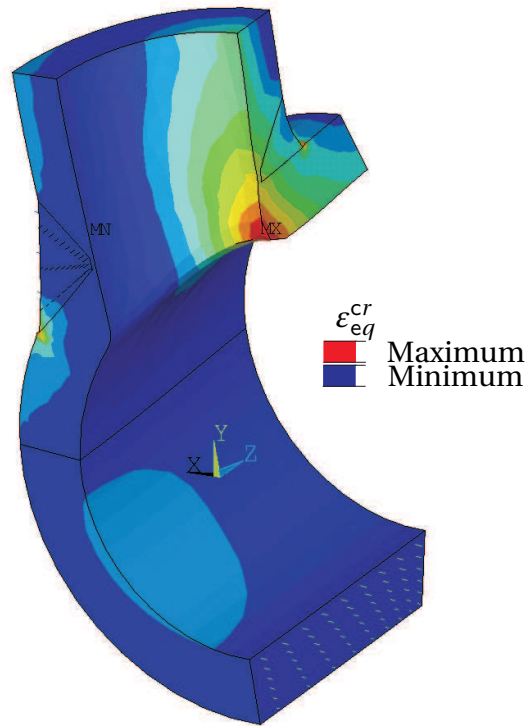


Figure 4.4 Equivalent creep strain at the moment of failure

sponds to the Type IV cracks in real constructions, and is the most common reason for failure of welds. In figure 4.4 one can see the creep strain redistribution of the pressured vessel, and notice the significant concentration of creep strain on the geometrical feature of the vessel - the joining area.

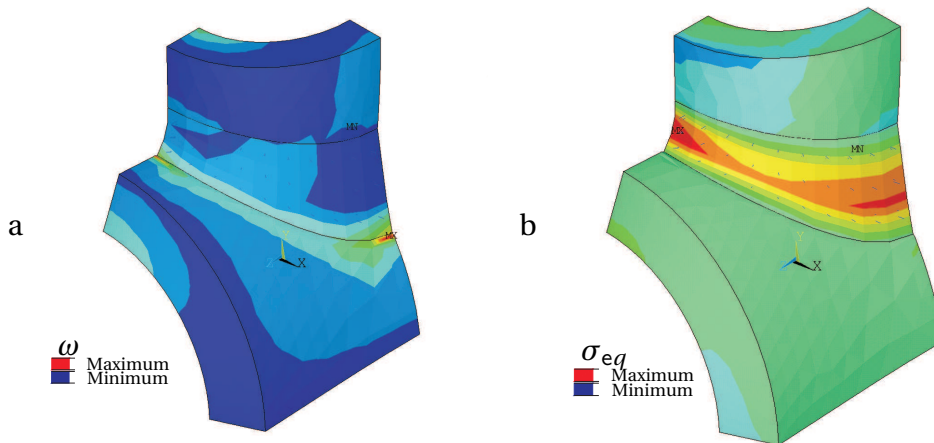


Figure 4.5 Damage parameter and equivalent stress redistribution

And of figure 4.6, one can see contour plots of stress redistribution after 1

hour of loading (a) and after 1000 hours of creep loading (b). What is clearly observed is that at the beginning of loading, when the influence of creep processes is neglectable, stress mainly concentrates on the geometrical feature area - T-joint of pipes. However, during time, stress redistributes due to creep, and now concentrates on weld metal, on both weld joints. This can be also observed from another angle on figure 4.5b.

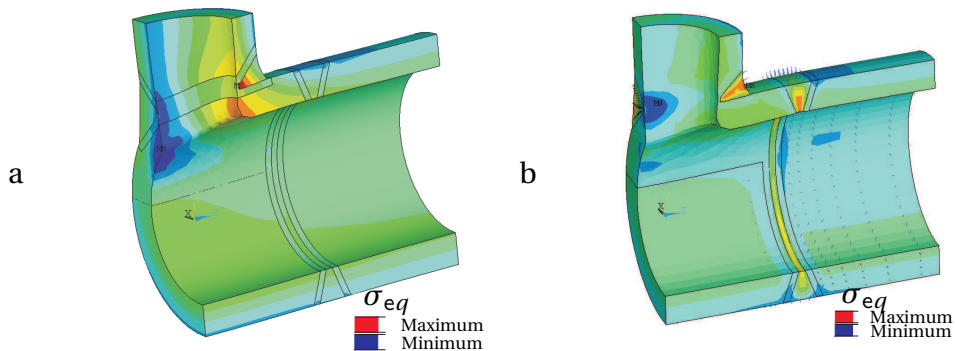


Figure 4.6 Equivalent stress redistribution in elasticity (a) and after 1000 hours of creep (b)

Dependence of the stress level on the time to rupture is shown by the dependence of 1st Principal stress vs time 4.7 in the region of failure. Even

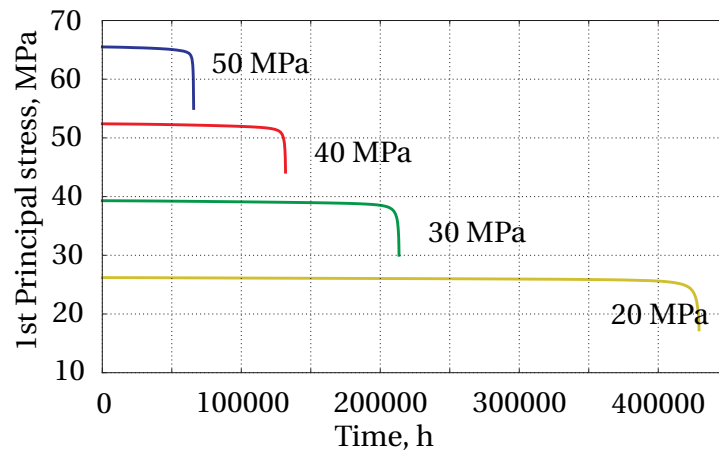


Figure 4.7 Maximum principal stress vs time diagram

though Type IV cracks in HAZ of the welded joint are the most common problem in welded constructions, in some particular cases of loading damage and crack nucleation and propagation may appear in the weld metal, especially in case of inhomogeneity of its microstructure. To model this kind of phenomena, we neglected the influence of HAZ, setting the material properties of its

area to those of the base metal and performed exact same numerical experiment. Neglecting the influence of HAZ does not effect the redistribution of

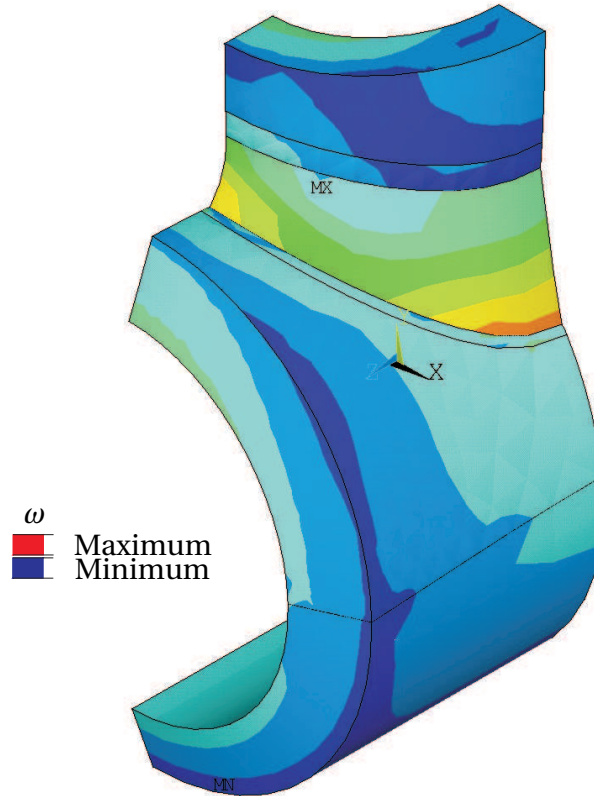


Figure 4.8 Damage parameter redistribution in experiment neglecting HAZ

equivalent creep strain and equivalent stress in sufficient amount, because the main factor remains to be the geometrical feature of the vessel, and properties of the weld metal in comparison to base metal. However damage parameter evolution takes another form, as can be seen on figure 4.8. It is now concentrating in the weld metal. Zooming the cross-sectional view of the weld metal 4.9, one can observe that damage is redistributed with a certain gradient, which corresponds to the different number of passes in bottom and on the top of the weld cut. This effects the density of the columnar zone part in the relative volume of the weld metal.

To analyze possible influence of input material properties on the creep damage response of the welded pressure vessel, a series of numerical experiments were repeated varying the A_c parameters for different welded joints zones. In particular of fig. 4.10 one can observe the dependencies between ratio of A_c parameters for columnar and HAZ of weld metal and time to rup-

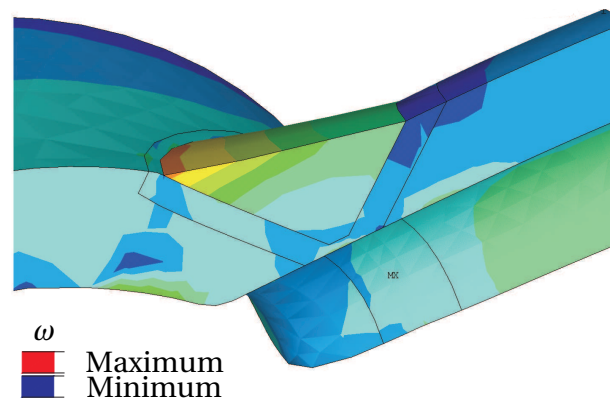


Figure 4.9 Damage parameter redistribution in weld metal in experiment neglecting HAZ

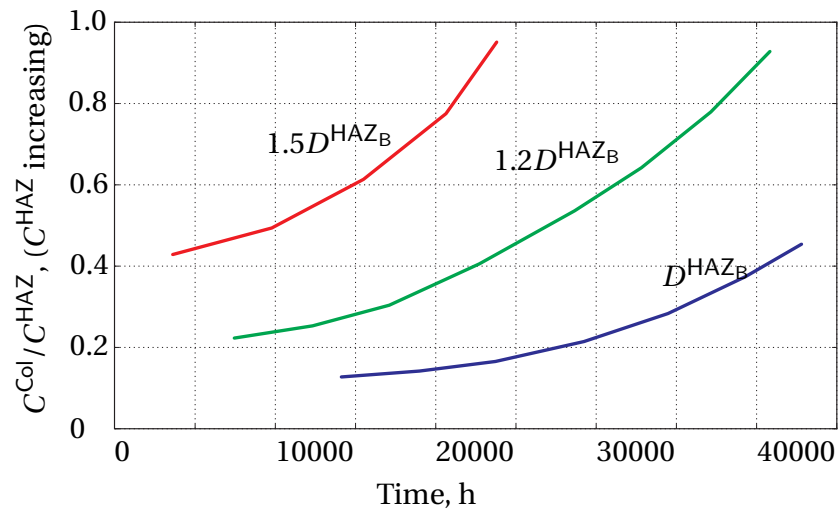


Figure 4.10 Parameter sensitivity

ture. Three lines represent 3 different values of A_d for heat affected zone of the whole weldment.

As we vary the value of A_c for columnar zone with respect to the A_c for HAZ of the weld metal, and performed bottom-to-top analysis defining the material properties of the equivalent material of weld metal for 3 types of VE, and then inputting this parameters to the 3 layered model of the weld metal in the macroscale analysis, and extracting time to rupture values from numerical experiments on pressure vessel tests, one can form the dependence between the material properties of the microstructural zones and time to rupture of the macro model of the vessel. As one can see from the graph, taking into account that the higher the time to rupture is - the better, the the recommended structure of the weld metal is homogeneous. And on opposite side, the bigger the

difference between creep properties between microscale zones is, the lower the time to rupture value.

Comparing three curves, one can also notice the significant dependence of time to rupture value from the A_d parameter of welded joint HAZ. As it represent the intensity of Type IV cracking, the higher the value of the damage material parameter is, the lower time to rupture is.

Conclusions

A new micro - macro approach to the analysis of creep and creep rupture of structures with multi-pass welds is introduced. Theoretical basis of this approach is the modern advances in the theory of creep and continuum mechanics of damage. The proposed approach uses the results of metallographic examination of the microstructure of the welded joint. Essential novelty of the proposed approach is the consideration of the anisotropy of the creep properties and the development rate of damage in multipass welds. Practical implementation of the micro- macro approach required the use of known numerical methods in mechanics of deformable bodies and the development of new special algorithms. Main stages of a multi-level approach, the elements of scientific novelty and features that are essential for the structural analysis of structural elements are as follows:

- Decomposition of the studied design element highlighting areas for micro -, meso- and macro - analysis. At the micro level Columnar, Fine grained and Coarse grained zone of weld metal are considered. Meso level analysis considers welded joint consisting of homogenized weld metal, HAZ and Base metal.
- Presented in 2.1 model based on the concepts Rabotnov-Kachanov, used to describe isotropic zones of multipass weld. Defining relations of this model are chosen in a form suitable for use in homogenization procedures at the meso level.
- Described in paragraph 2.2 procedure of identification of material parameters of an isotropic creep-damage model based on the results of

physical experiments, allows to use it also for the main stages of processing the results of computational experiments on identification of anisotropic creep-damage model.

- Main practical difficulty of using creep models of anisotropic materials in the initial state is a large number of material parameters. Introduced in 2.2 version of this model uses experimentally confirmed hypothesis about the same value of the exponent in the Norton law for different directions. Introduction of the anisotropy tensor in dimensionless form facilitates the analysis of its structure for different types of anisotropy and identification procedure of the model parameters.
- Long-term strength anisotropy of properties may vary significantly from the initial anisotropy on the stage of steady creep. To adequately reflect this in 2.2 a new creep-damage model was introduced in which a special fourth-rank tensor was formulated with the components that are associated with long-term strength limits in different directions.
- Conducting all required physical experiments to identify the material parameters of creep-damage model of a multipass weld - is very complicated, costly and time-consuming task. In 3 a technique of numerical modeling of creep and damage in multipass weld was proposed, which theoretically allows to find the parameters of creep-damage model of the equivalent homogeneous material. A significant advantage of this approach is the possibility of modeling the joints with different amounts and diverse forms of individual passes.
- To use the proposed approach in the structural analysis of design elements the user-subroutine was developed and implemented in the software package ABACUS. Numerical experiments were performed on structural elements of power machinery, which confirmed the suitability of the proposed approach in design practice.

Investigation of creep and fracture of welded structural elements approach proposed in the work has a potential for the development and improvement. This applies to modifications of creep-damage model for orthotropic materials, as well as to developing more effective ways of homogenization of structurally inhomogeneous media. To achieve these objectives, the following tasks are planned:

- Defining relations for the creep strain rate (2.23) can be improved to reflect the process of hardening in the first stage of creep. Various

forms of such ratios for the isotropic material are known. In the case of anisotropic models its necessary to overcome the problem of ensuring the continuity of theoretical creep curves for different directions.

- For structural elements of nuclear plant it is relevant to incorporate effect of radiation on the creep processes. In such operating conditions one can observe swelling of the material over time. Account of such phenomena in anisotropic materials creep models is a promising task.
- Reduction of computational cost in defining material parameters of equivalent homogeneous materials is possible by the development of algorithms that use dual periodicity conditions of representative volume.
- For typical forms of multipass welds it would be suitable to develop software of computer-aided design and analysis of the welds oriented for use in commercial software products.



Bibliography

- [1] SIMULIA ABAQUS 6.9. *ABAQUS Analysis User's Manual*. Dassault Systèmes Simulia Corp., USA, 2009.
- [2] Bensoussan A., Lions J.L., and Papanicolaou G. *Asymptotic analysis for periodic structures*. North-Holland, New York, 1978.
- [3] F. Abe and M. Tabuchi. Microstructure and creep strength of welds in advanced ferritic power plant steels. *Science and Technology of Welding and Joining*, 9(1):22–30, 2004.
- [4] Siemens AG. Welding on rotors for power plant turbo sets. State of the Art. <http://www.energy.siemens.com>, 2005.
- [5] I. Akbarzadeh, I. Sattari-Far, and M. Salehi. Numerical and experimental study of the effect of short-term and long-term creep modeling in stress relaxation of a multi-pass welded austenitic stainless steel pipe. *Materials Science and Engineering A*, 528(4-5):2118–2127, 2011.
- [6] S.K. Albert, M. Matsui, T. Watanabe, H. Hongo, K. Kubo, and M. Tabuchi. Microstructural investigations on type iv cracking in a high Cr steel. *ISIJ International*, 42(12 SPEC.):1497–1504, 2002.
- [7] Alstom. Thermal power plant solutions. <http://www.alstom.com>, 2013.
- [8] H. Altenbach. Classical and nonclassical creep models. In Altenbach H. and Skrzypek J., editors, *Creep and Damage in Materials and Structures*, pages 45 – 95. Springer, Wien, New York, 1999.

- [9] H. Altenbach, O. Morachkovsky, K. Naumenko, and A. Sychov. Geometrically nonlinear bending of thin-walled shells and plates under creep-damage conditions. *Archive of Applied Mechanics*, 67(5):339–352, 1997.
- [10] H. Altenbach, C. Huang, and K. Naumenko. Creep damage predictions in thinwalled structures by use of isotropic and anisotropic damage models. *J. Strain Anal.*, 37:265–275, 2002.
- [11] B. Arivazhagan, S. Sundaresan, and M. Kamaraj. A study on influence of shielding gas composition on toughness of flux-cored arc weld of modified 9Cr-1Mo (P91) steel. *Journal of Materials Processing Technology*, 209(12-13):5245–5253, 2009.
- [12] M.H. Avazkonandeh-Gharavol, M. Haddad-Sabzevar, and A. Haerian. Effect of chromium content on the microstructure and mechanical properties of multipass mma, low alloy steel weld metal. *Journal of Materials Science*, 44(1):186–197, 2009.
- [13] A.A. Becker, T.H. Hyde, and L. Xia. Numerical analysis of creep in components. *Journal of Strain Analysis for Engineering Design*, 29(3):185–192, 1994.
- [14] J. Betten. *Kontinuumsmechanik*. Springer, Berlin, 1993.
- [15] J. Betten. Creep damage and life analysis of anisotropic materials. *Archive of Applied Mechanics*, 71(2-3):78–88, 2001.
- [16] J. Betten. *Creep Mechanics*. Springer, Berlin, 2005.
- [17] J. Betten, A. Sklepus, and A. Zolochovsky. A constitutive theory for creep behavior of initially isotropic materials sustaining unilateral damage. *Mechanics Research Communications*, 30:251 – 256, 1998.
- [18] J. Betten, S. Sklepus, and A. Zolochovsky. A creep damage model for initially isotropic materials with different properties in tension and compression. *Eng. Fracture. Mech*, 59:623–641, 1998.
- [19] A. Bjorck, P. Heggernes, and P. Matstoms. Methods for large scale total least squares problems. *SIAM Journal on Matrix Analysis and Applications*, 22(2):413–429, 2001.
- [20] A. Bodnar and M. Chrzanowski. A non-unilateral damage in creeping plates. In M. Zyczkowski, editor, *Creep in Structures*, pages 287–292. Springer, Berlin, 1991.

- [21] J.T. Boyle and J. Spence. *Stress Analysis for Creep*. Butterworth London, 1983.
- [22] J. Brozda and M. Zeman. Wrong heat treatment of martensitic steel welded tubes caused major cracking during assembly of resuperheaters in a fossil fuel power plant. *Engineering Failure Analysis*, 10(5):569–579, 2003.
- [23] S. Bxsrauser, C. Schwenk, M. Rethmeier, T. Noack, and S. Juttner. Influence of welding-induced cracks on the fatigue strength of resistance-spot-welded joints made of high-strength austenitic steel. *Welding and Cutting*, 11(4):232–235, 2012.
- [24] J.L. Chaboche. Continuous damage mechanics. A tool to describe phenomena before crack initiation. *Nuclear Engineering and Design*, 64(2): 233 – 247, 1981.
- [25] J.L. Chaboche. Le concept de contrainte effective applique a lelasticite et a la viscoplasticite en presence dun endommagement anisotrope. In Jean-Paul Boehler, editor, *Mechanical Behavior of Anisotropic Solids / Comportment Mechanique des Solides Anisotropes*, pages 737–760. Springer Netherlands, 1982. doi: 10.1007/978-94-009-6827-1_43.
- [26] J.L. Chaboche. Anisotropic creep damage in the framework of continuum damage mechanics. *Nuclear Engineering and Design*, 79(3):309 – 319, 1984.
- [27] J.L. Chaboche and G. Rousselier. On the plastic and viscoplastic constitutive equations. *J. Press. vess. technol.*, 105:105–164, 1983.
- [28] P. Chellapandi and S.C. Chetal. Influence of mis-match of weld and base material creep properties on elevated temperature design of pressure vessels and piping. *Nuclear Engineering and Design*, 195(2):189–196, 2000.
- [29] H.J. Chun and I.M. Daniel. Transverse creep behavior of a unidirectional metal matrix composite. *Mechanics of Materials*, 25(1):37–46, 1997.
- [30] P.W. Chung, K.K. Tamma, and R.R. Namburu. A micro/macro homogenization approach for viscoelastic creep analysis with dissipative correctors for heterogeneous woven-fabric layered media. *Composites Science and Technology*, 60(12-13):2233–2253, 2000.

- [31] A.H. Daei Sorkhabi and F. Vakili-Tahami. Experimental study of the creep behavior of parent, simulated HAZ and weld materials for cold-drawn 304L stainless steel. *Engineering Failure Analysis*, 21:78–90, 2012.
- [32] G. Eggeler, A. Ramteke, M. Coleman, B. Chew, G. Peter, A. Burblies, J. Hald, C. Jefferey, J. Rantala, M. deWitte, and R. Mohrmann. Analysis of creep in a welded 'P91' pressure vessel. *International Journal of Pressure Vessels and Piping*, 60(3):237–257, 1994.
- [33] findpatent.ru. Welded rotor of turbomachinery. <http://www.findpatent.ru/patent/203/2033524.html>, 2009.
- [34] V. Gaffard, A.F. Gourgues-Lorenzon, and J. Besson. High temperature creep flow and damage properties of the weakest area of 9Cr1Mo-NbV martensitic steel weldments. *ISIJ International*, 45(12):1915–1924, 2005.
- [35] V. Gaffard, A.F. Gourgues-Lorenzon, and J. Besson. High temperature creep flow and damage properties of 9cr1monbv steels: Base metal and weldment. *Nuclear Engineering and Design*, 235(24):2547–2562, 2005.
- [36] F. Garofalo. *Fundamentals of creep and creep-rupture in metals*. Macmillan, New York, 1965.
- [37] V. Garrard. *Experimental study and modelling of high temperature creep flow and damage behaviour of 9Cr1Mo-NbV steel weldments*. Phd thesis, ENSMP, France, 2009.
- [38] R.M. Guedes. Relationship between lifetime under creep and constant stress rate for polymer-matrix composites. *Composites Science and Technology*, 69(7-8):1200–1205, 2009.
- [39] F.R. Hall and D.R. Hayhurst. Continuum damage mechanics modelling of high temperature deformation and failure in a pipe weldment. *Proc. R. Soc. Lond*, 433:383–403, 1994.
- [40] D. R. Hayhurst. Creep rupture under multi-axial states of stress. *J. Mech. Phys. Solids*, 20:381 – 390, 1972.
- [41] D.R. Hayhurst. Creep rupture under multiaxial states of stress. *J. Mech. Phy Solids*, 20:381 – 390, 1972.

- [42] D.R. Hayhurst. The use of computational creep continuum damage mechanics to optimize materials selection for high-temperature weldments. *Modelling and Simulation in Materials Science and Engineering*, 2(3 A):421–438, 1994.
- [43] D.R. Hayhurst. The use of Continuum Damage Mechanics in creep analysis for design. *J. Strain Anal.*, 25:233–241, 1994.
- [44] D.R. Hayhurst. Materials data bases and mechanisms-based constitutive equations for use in design. In Altenbach H. and Skrzypek J., editors, *Creep and Damage in Materials and Structures*, pages 285 – 348. Springer, Wien, New York, 1999.
- [45] D.R. Hayhurst. CDM mechanisms-based modelling of tertiary creep: ability to predict the life of engineering components. *Arch. Mech.*, 57: 103 – 132, 2005.
- [46] D.R. Hayhurst, P.R. Dimmer, and C.J. Morrison. Development of continuum damage in the creep rupture of notched bars. *Philosophical Transactions of the Royal Society of London (Series) A: Mathematical and Physical Sc*, 311(1516):103–129, 1984.
- [47] D.R. Hayhurst, R.J. Hayhurst, and F. Vakili-Tahami. Continuum damage mechanics predictions of creep damage initiation and growth in ferritic steel weldments in a medium bore branched pipe under constant pressure at 590 c using a five-material weld model. *Proceedings of the Royal Society A: Mathematical, Physical and Engineering Sciences*, 461(2060): 2303–2326, 2005.
- [48] HIDA. Validation, Expansion and Standardisation of Procedures for High Temperature Defect Assessment. <http://cordis.europa.eu/>, 1995.
- [49] J. Hult. Creep in continua and structures. pages 137–155, 1974.
- [50] T. H. Hyde, W. Sun, P. A. Agyakwa, P. H. Shipway, and J. A. Williams. Anisotropic creep and fracture behaviour of a 9CrMoNbV weld metal at 650C. In J. J. Skrzypek and A. Ganczarski, editors, *Anisotropic Behaviour of Damaged Materials*, Lecture Notes in Applied and Computational Mechanics Vol. 9, pages 295–316. Springer, Berlin, 2003.
- [51] T.H. Hyde, W. Sun, and J.A. Williams. Creep behaviour of parent, weld and haz materials of new, service-aged and repaired 1/2Cr1/2Mo1/4V:2

- 1/4Cr1Mo pipe welds at 640 C. *Materials at High Temperatures*, 16(3): 117–129, 1999.
- [52] T.H. Hyde, J.A. Williams, and W. Sun. Assessment of creep behaviour of a narrow gap weld. *International Journal of Pressure Vessels and Piping*, 76(8):515–525, 1999.
- [53] T.H. Hyde, W. Sun, and A.A. Becker. Failure prediction for multi-material creep test specimens using a steady-state creep rupture stress. *International Journal of Mechanical Sciences*, 42(3):401–423, 2000.
- [54] T.H. Hyde, W. Sun, P.A. Agyakwa, P.H. Shipway, and J.A. Williams. Anisotropic creep and fracture behaviour of a 9CrMoNbV Weld Metal at 650C. *Lecture Notes in Applied and Computational Mechanics*, 9:295–316, 2003.
- [55] T.H. Hyde, W. Sun, and J.A. Williams. Creep analysis of pressurized circumferential pipe weldments - a review. *Journal of Strain Analysis for Engineering Design*, 38(1):1–30, 2003.
- [56] T.H. Hyde, A.A. Becker, Y. Song, and W. Sun. Failure estimation of TIG butt-welded Inco718 sheets at 620 C under creep and plasticity conditions. *Computational Materials Science*, 35(1):35–41, 2006.
- [57] Lemaitre J. and Chaboche J.-L. *Mechanics of Solid Materials*. Cambridge University Press, Cambridge, 1990.
- [58] M.N. James, P.J. Webster, D.J. Hughes, Z. Chen, N. Ratel, S.-P. Ting, G. Bruno, and A. Steuwer. Correlating weld process conditions, residual strain and stress, microstructure and mechanical properties for high strength steel-the role of neutron diffraction strain scanning. *Materials Science and Engineering A*, 427(1-2):16–26, 2006.
- [59] M.N. James, S.-P. Ting, M. Bosi, H. Lombard, and D.G. Hattingh. Residual strain and hardness as predictors of the fatigue ranking of steel welds. *International Journal of Fatigue*, 31(8-9):1366–1377, 2009.
- [60] L. M. Kachanov. *Introduction to Continuum Damage Mechanics*. Kluwer Academic, Dordrecht, 1986.
- [61] L.M. Kachanov. O vremeni razrusheniya v usloviyakh polzuchesti (on the time to rupture under creep conditions, in russ.). *Izv. AN USSR. Otd. Tech. Nauk*, 8:26 – 31, 1958.

- [62] M.E. Kassner. Netherlands. In Michael E. Kassner, editor, *Fundamentals of Creep in Metals and Alloys (Second edition)*. Elsevier, Amsterdam, second edition edition, 2008.
- [63] P.I. Kattan. *Damage Mechanics with Finite Elements*. Springer, Berlin , 2002.
- [64] F. Kawashima, T. Igari, T. Tokiyoshi, A. Shiibashi, and N. Tada. Micro-macro combined simulation of the damage progress in low-alloy steel welds subject to type iv creep failure. *JSME International Journal, Series A: Solid Mechanics and Material Engineering*, 47(3):410–418, 2004.
- [65] A. Klenk, J. Schemmel, and K. Maile. Modelling deformation and damage of high temperature steels under creep-fatigue loading. *Transactions of the Indian Institute of Metals*, 58(2-3 SPEC. ISS.):481–487, 2005.
- [66] V.N. Konkin and O.K. Morachkovskii. Creep and long-term strength of light alloys with anisotropic properties. *Strength of Materials*, 19(5):626–631, 1988.
- [67] D. Krajcinovic. Constitutive equations for damaging materials. *J. Appl. Mech.*, 50:355 – 360, 1983.
- [68] D. Krajcinovic. Damage mechanics. *Mechanics of Materials*, 8(3):117 – 197, 1989.
- [69] R. Lagneborg. England. In Bressers J., editor, *Creep and fatigue in high temperature alloys*, pages 41 – 71. Applied Science Publishers, London, 1981.
- [70] M. Law, W. Payten, and R. Small. Modelling the creep behaviour of a re-heat header longitudinal weld. *International Journal of Pressure Vessels and Piping*, 77(2-3):99–103, 2000.
- [71] F.A. Leckie and D.R. Hayhurst. Constitutive equations for creep rupture. *Acta Metallurgica*, 25(9):1059 – 1070, 1977.
- [72] J. Lemaitre. A continuum damage mechanics model for ductile fracture. *ASME J. Eng. Mater. Technol.*, 107:83–89, 1985.
- [73] J. Lemaitre. *A Course on Damage Mechanics*. Springer, Berlin, 1996.
- [74] J. Lemaitre. Introduction to continuum damage mechanics. In O. Ailix and F. Hild, editors, *Continuum Damage Mechanics of Materials and Structures*, pages 235–258. Elsevier, 2002.

- [75] J. Li and G.J. Weng. Effective creep behavior and complex moduli of fiber- and ribbon-reinforced polymer-matrix composites. *Composites Science and Technology*, 52(4):615–629, 1994.
- [76] J. Lin, Y. Liu, and T. A. Dean. A review on damage mechanisms, models and calibration methods under various deformation conditions. *International Journal of Damage Mechanics*, 14(4):299–319, 2005.
- [77] R.F. Liu and C.C. Huang. Welding residual stress analysis for weld overlay on a BWR feedwater nozzle. *Nuclear Engineering and Design*, 256:291 – 303, 2013.
- [78] V. Lupinc. England. In Bressers J., editor, *Creep and fatigue in high temperature alloys*, pages 7 – 40. Applied Science Publishers, London, 1981.
- [79] I. Lvov and O. Morachkovsky. Anisotropic creep of composite plates under crosscut load. *NTU KHPI Per. Dynamichs and strength*, 42:111–118, 2009.
- [80] I. Lvov, K. Naumenko, and H. Altenbach. Homogenisation approach in analysis of creep behaviour in multipass weld. *Materials Science and Technology (United Kingdom)*, 30(1):50–53, 2014.
- [81] N.N. Malinin. *Prikladnaya teoriya plastichnosti i polzuchesti (Applied theory of plasticity and creep, in Russ.)*. Mashinostroenie, Moskva, 1975.
- [82] N.N. Malinin and G.M. Khadjinsky. Theory of creep with anisotropic hardening. *International Journal of Mechanical Sciences*, 14(4):235–246, 1972.
- [83] B.Z. Margolin, A.Ya. Varovi, and V.I.Kostilyov. Determination of residual stresses in the WWER vessels after multi-run welding, surfacing and high-temperature tempering. *Avtomaticheskaya Svarka*, 10:14 – 20, 2005.
- [84] T. Masse and Y. Lejeail. Creep mechanical behaviour of modified 9Cr1Mo steel weldments: Experimental analysis and modelling. *Nuclear Engineering and Design*, 254:97–110, 2013.
- [85] F. Masuyama. Creep degradation in welds of Mod.9Cr-1Mo steel. *International Journal of Pressure Vessels and Piping*, 83(11-12):819–825, 2006.

- [86] A. McBride, J. Mergheim, A. Javili, P. Steinmann, and S. Bargmann. Micro-to-macro transitions for heterogeneous material layers accounting for in-plane stretch. *Journal of the Mechanics and Physics of Solids*, 60(6):1221–1239, 2012.
- [87] S. Murakami and N. Ohno. A continuum theory of creep and creep damage. In *Proceedings of the Third IUTAM Symposium on Creep in Structures*, Springer, Berlin, 1980.
- [88] S. Murakami. Notion of continuum damage mechanics and its application to anisotropic creep damage theory. *J. Eng. Mater. Tech.*, 105:99–105, 1983.
- [89] S. Murakami. *Continuum Damage Mechanics – A Continuum Mechanics Approach to the Analysis of Damage and Fracture*. Springer, Dordrecht, Heidelberg, London, New York, 2012.
- [90] S. Murakami and T. Imaizumi. Mechanical description of creep damage state and its experimental verification. *Journal de Mecanique Theorique et Appliquee*, 1:743 – 761, 1982.
- [91] S. Murakami and N. Ohno. A continuum theory of creep and creep damage. In A. R. S. Ponter and D. R. Hayhurst, editors, *Creep in Structures*, pages 422 – 444. Springer, Berlin, 1981.
- [92] S. Murakami, M. Kawai, and H. Rong. Finite element analysis of creep crack growth by a local approach. *International Journal of Mechanical Sciences*, 30(7):491 – 502, 1988.
- [93] K. Naumenko and H. Altenbach. A phenomenological model for anisotropic creep in a multipass weld metal. *Archive of Applied Mechanics*, 74(11-12):808–819, 2005.
- [94] K. Naumenko and H. Altenbach. *Modeling of Creep for Structural Analysis*. Springer, Berlin, Heidelberg, 2007.
- [95] B. Neubauer and U. Wedel. Advances in life prediction methods. In *ASME Conference*, New York, 1983.
- [96] H. Nishida, H. Yamaguchi, I. Nonaka, and F. Takemasa. Refinement of the accuracy of residual life assessment based on the generation and growth behavior of creep voids for boiler welded zone. *Nihon Kikai Gakkai Ronbunshu, A Hen/Transactions of the Japan Society of Mechanical Engineers, Part A*, 66(649):1657–1665, 2000.

- [97] Morachkovsky O., Altenbach H., and Pasynok M. Computational modelling of creep damage evolution in transversally-isotropic structures. *NTU KHPI Per. Dynamichs and strengh*, 56:9–18, 1998.
- [98] F. K. G. Odqvist. *Mathematical Theory of Creep and Creep Rupture*. Oxford university press, Oxford, 1974.
- [99] F. K. G. Odqvist. Historical survey of the development of creep mechanics from its beginnings in the last century to 1970. In A. R. S. Ponter and D. R. Hayhurst, editors, *Creep in Structures*, pages 1 – 12. Springer, Berlin, 1981.
- [100] T. Ogata, T. Sakai, and M. Yaguchi. Damage characterization of a p91 steel weldment under uniaxial and multiaxial creep. *Materials Science and Engineering A*, 510-511(C):238–243, 2009.
- [101] T. Ogata, T. Sakai, and M. Yaguchi. Damage assessment method of P91 steel welded tube under internal pressure creep based on void growth simulation. *International Journal of Pressure Vessels and Piping*, 87(11): 611–616, 2010.
- [102] M. Pajnic, K. Markulin, A. Matokovic, and H. Franjic. Advanced approach of reactor pressure vessel in-service inspection. In *10th Euro-ean Conference on Non-Destructive Testing*, Moscow, Russia, 2010.
- [103] V.T. Paul, S. Saroja, P. Hariharan, A. Rajadurai, and M. Vijayalakshmi. Identification of microstructural zones and thermal cycles in a weldment of modified 9Cr-1Mo steel. *Journal of Materials Science*, 42(14): 5700–5713, 2007.
- [104] W. Payten. Large scale multi-zone creep finite element modelling of a main steam line branch intersection. *International Journal of Pressure Vessels and Piping*, 83(5):359–364, 2006.
- [105] R. K. Penny and D. L. Mariott. *Design for Creep*. Chapman & Hall London, 1995.
- [106] I.J. Perrin and D.R. Hayhurst. Creep constitutive equations for a 0.5Cr-0.5Mo-0.25V ferritic steel in the temperature range 600-675 C. *Journal of Strain Analysis for Engineering Design*, 31(4):299–314, 1996.
- [107] I.J. Perrin and D.R. Hayhurst. Continuum damage mechanics analyses of type iv creep failure in ferritic steel crossweld specimens. *International Journal of Pressure Vessels and Piping*, 76(9):599–617, 1999.

- [108] W. Qi, W. Brocks, and A. Bertram. An fe-analysis of anisotropic creep damage and deformation in the single crystal srr99 under multiaxial loads. *Computational Materials Science*, 19(1-4):292–297, 2000.
- [109] Hayhurst D. R., W.M. Tak, and V.-T. Farid. The use of cdm analysis techniques in high temperature creep failure of welded structures. *JSME International Journal, Series A: Solid Mechanics and Material Engineering*, 45(1):90–97, 2002.
- [110] Y. N. Rabotnov. *Creep Problems in Structural Members*. North Holland Publishing Co., Amsterdam, 1969.
- [111] Y.N. Rabotnov. O mechanizme dlitelnogo razrusheniya (a mechanism of the long term fracture, in russ.). *Voprosy prochnosti materialov i konstruktsii, AN SSSR*, 1:5 – 7, 1959.
- [112] D.N. Robinson, W.K. Binienda, and M.B. Ruggles. Creep of polymer matrix composites i: Norton/bailey creep law for transverse isotropy. *Journal of Engineering Mechanics*, 129(3):310–317, 2003.
- [113] Evans R.W. and Wilshire B. *Creep of metals and alloys*. Institute of Metals, London, 1985.
- [114] Stupkiewicz S. *Micromechanics of Contact and Interphase Layers*. Springer, Berlin, 2007.
- [115] T. Sakamoto, H. Kurishita, T. Furuno, T. Nagasaka, S. Kobayashi, K. Nakai, S. Matsuo, H. Arakawa, A. Nishimura, and T. Muroga. Uniaxial creep behavior of nanostructured, solution and dispersion hardened V1.4Y7W9Mo0.7TiC with different grain sizes. *Materials Science and Engineering: A*, 528(27):7843 – 7850, 2011.
- [116] M.L. Santella, R.W. Swindeman, R.W. Reed, and J.M. Tanzosh. Martensite transformation, microsegregation, and creep strength of 9 cr-1 mo-v steel weld metal. pages 713–718, 2002.
- [117] K. Sawada, M. Bauer, F. Kauffmann, P. Mayr, and A. Klenk. Microstructural change of 9creep. *Materials Science and Engineering A*, 527(6): 1417–1426, 2010.
- [118] J. Schjodt-Thomsen and R. Pyrz. Non-linear creep modelling of single-fibre model composites. *Composites Science and Technology*, 60(9): 1791–1800, 2000.

- [119] V.P. Sdobyrev. Kriterij dlitelnoj prochnosti dlya nekotorykh zharo-prochnykh splavov pri sloznom napryazhenom sostoyanii, (Criterion of long term strength of some high-temperature alloys under multiaxial stress state, in russ.). *Izv. AN SSSR. OTN. Mekh. i Mashinostroenie*, 6:93–99, 1959.
- [120] P. Segle. *Numerical simulation of weldment creep response*. Phd thesis, Royal Institute of Technology, Stockholm, Sweden, 2002.
- [121] P. Segle, S.-T. Tu, J. Storesund, and L.Å. . . Samuelson. Some issues in life assessment of longitudinal seam welds based on creep tests with cross-weld specimens. *International Journal of Pressure Vessels and Piping*, 66 (1-3):199–222, 1996.
- [122] A.V. Shutov, H. Altenbach, and K. Naumenko. Steady-state creep analysis of pressurized pipe weldments by perturbation method. *International Journal of Solids and Structures*, 43(22-23):6908–6920, 2006.
- [123] Ramesh Singh. Welding and joining processes. In Ramesh Singh, editor, *Applied Welding Engineering*, pages 147 – 170. Butterworth-Heinemann, Boston, 2012.
- [124] V. Sklenicka, K. Kucharova, M. Svoboda, L. Kloc, J. Burs, and A. Kroupa. Long-term creep behavior of 9-12%Cr power plant steels. *Materials Characterization*, 51(1):35 – 48, 2003.
- [125] J. Skrzypek and A. Ganczarski. Modeling of damage effect on heat transfer in time-dependent non-homogeneous solids. *J. Therm. Stresses*, 21: 205 – 231, 1998.
- [126] J.J. Skrzypek and A. Ganczarski. *Modeling of Material Damage and Failure of Structures*. Springer, Berlin, 1999.
- [127] O.V. Sosnin. Anisotropic creep of materials. *Journal of Applied Mechanics and Technical Physics*, 7(4):117–119, 1969.
- [128] SOTA. Development of creep crack growth testing and data analysis for welds. <https://odin.jrc.ec.europa.eu/>, 1995.
- [129] S. Spigarelli and E. Quadrini. Analysis of the creep behaviour of modified p91 (9Cr-1Mo-NbV) welds. *Materials and Design*, 23(6):547–552, 2002.

- [130] M. Staubach, R. Mueller, and S. Juettner. Measurement and minimisation of welding-induced distortions in t-joints between sections. *Welding and Cutting*, 6(1):41–44, 2007.
- [131] C.M. Stewart, A.P. Gordon, Y.W. Ma, and R.W. Neu. An anisotropic tertiary creep damage constitutive model for anisotropic materials. *International Journal of Pressure Vessels and Piping*, 88(8-9):356–364, 2011.
- [132] T. Takaichi and Y. Ando. Welding experience of the reactor pressure vessel for tokai nuclear power station. *Nuclear structural engineering*, 1:295–307, 1965.
- [133] I.I. Trunin. Kriterii prochnosti v usloviyakh polzuchesti pri slozhnom napryazhennom sostoyanii (failure criteria under creep conditions in multiaxial stress state, in russ.). *Prikl. Mekhanika*, 7:77–83, 1965.
- [134] S.-T. Tu and R. Sandstroem. The evaluation of weldment creep strength reduction factors by experimental and numerical simulations. *International Journal of Pressure Vessels and Piping*, 57(3):335–344, 1994.
- [135] S.-T. Tu, J.-M. Gong, X. Ling, and X.-Y. He. Measurement of local creep deformation in cross-weld specimen by optical fiber marking and remote monitoring. *Journal of Pressure Vessel Technology, Transactions of the ASME*, 124(1):54–58, 2002.
- [136] S.-T. Tu, P. Segle, and J.-M. Gong. Creep damage and fracture of weldments at high temperature. *International Journal of Pressure Vessels and Piping*, 81(2):199–209, 2004.
- [137] Turboatom. Turboatom ojsc. <http://www.turboatom.com.ua/en/>, 2000.
- [138] H.-W. Viehrig and J. Schuhknecht. Fracture mechanics characterisation of the wwer-440 reactor pressure vessel beltline welding seam. *International Journal of Pressure Vessels and Piping*, 86(4):239–245, 2009.
- [139] R. Viswanathan. *Damage mechanisms and life assessment of high temperature components*. ASM International, Metal Parks, Ohio, 1989.
- [140] X. Wang, Z. Shi, Q.-G. Pan, and H.-L. Wu. High-temperature creep properties of fine grained heat-affected zone in P92 weldment. *Transactions of Nonferrous Metals Society of China (English Edition)*, 19(SUPPL. 3): s772–s775, 2009.

- [141] T. Watanabe, M. Tabuchi, M. Yamazaki, H. Hongo, and T. Tanabe. Creep damage evaluation of 9Cr-1Mo-V-Nb steel welded joints showing Type iv fracture. *International Journal of Pressure Vessels and Piping*, 83(1): 63–71, 2006.
- [142] J. Weber, A. Klenk, and M. Rieke. A new method of strength calculation and lifetime prediction of pipe bends operating in the creep range. *International Journal of Pressure Vessels and Piping*, 82(2):77–84, 2005.
- [143] B. Wilshire and H. Burt. Damage evolution during creep of steels. *International Journal of Pressure Vessels and Piping*, 85(1-2):47 – 54, 2008. Special Issue: Creep and Fracture in High-Temperature Components-Design and Life Assessment Issues.
- [144] H. Wohlfahrt and D. Brinkmann. Consideration of inhomogeneties in application of deformation models, describing the inelastic behaviour of welded jointss. In E. Steck, R. Ritter, U. Peil, and A. Ziegenbein, editors, *Plasticity of Metals: Experiments, Models, Computation. Final Report of the Coll. Res. Centre 319*, pages 361–382. Wiley-VCH, 2001.
- [145] J. Wolberg. *Data analysis using the method of least squares: Extracting the most information from experiments*. Springer Berlin, 2006.
- [146] P. Wriggers and J. Reinelt. Multi-scale approach for frictional contact of elastomers on rough rigid surfaces. *Computer Methods in Applied Mechanics and Engineering*, 198(21-26):1996–2008, 2009.
- [147] S. Yamada, M. Yaguchi, and T. Ogata. Microstructural change of a 9Cr steel longitudinal welded tube under internal pressure creep loading. *Materials Science and Engineering A*, 560:450–457, 2013.
- [148] Koji Yamaguchi and Satoshi Nishijima. Prediction and evaluation of long-term creep-fatigue life. *Fatigue and Fracture of Engineering Materials and Structures*, 9(2):95–107, 1986.
- [149] M. Yamazaki, H. Hongo, T. Watanabe, J. Kinugawa, T. Tanabe, and Y. Monma. Heterogeneity of creep properties of welds in 304 stainless steel plate. *Zairyo/Journal of the Society of Materials Science, Japan*, 48 (2):110–115, 1999.
- [150] L. Yongkui. *Study on Creep Damage in Thick Welded Joint of Mod.9Cr-1Mo Steel Plates*. Phd thesis, Kochi University, Japan, 2009.

-
- [151] T. Yu, M. Yatomi, and H.-J. Shi. Numerical investigation on the creep damage induced by void growth in heat affected zone of weldments. *International Journal of Pressure Vessels and Piping*, 86(9):578–584, 2009.
- [152] H. Zhang, Y. Liu, and B. Xu. Plastic limit analysis of ductile composite structures from micro- to macro-mechanical analysis. *Acta Mechanica Solida Sinica*, 22(1):73–84, 2009.
- [153] T. Zhang, F. W. Brust, G. Wilkowski, H. Xu, A. A. Betervide, and O. Maz-zantin. Welding residual stress in a large diameter nuclear reactor pres-sure vessel nozzle. *J. Pressure Vessel Technol.*, 135:021208–1 – 021208–7, 2013.
- [154] X. Zhu, Z. Li, Y. Jin, and W.J.D. Shaw. Creep behaviour of a hybrid fi-bre (glass/carbon)-reinforced composite and its application. *Compos-ites Science and Technology*, 50(4):431–439, 1994.